AD-A053 766 TECHNOLOGY INC SAN ANTONIO TEX LIFE SCIENCES DIV F/G 6/18
OCULAR HAZARDS OF PICOSECOND AND REPETITIVE-PULSED LASERS. VOLU--ETC(U)
APR 78 J S CONNOLLY, H W HEMSTREET F41609-73-C-0016
UNCLASSIFIED TI-77-0564-03 SAM-TR-78-21 NL

| OF |
AD
A053 766

END
DATE
FILMED
6-78
DDC

Report SAM-TR-78-21

# OCULAR HAZARDS OF PICOSECOND AND REPETITIVE-PULSED LASERS

## Volume II: Argon-Ion Laser (514.5 nm)



J. S. Connolly, Ph.D.
H. W. Hemstreet, Jr., Ph.D.
D. E. Egbert, Captain, USAF (USAFSAM/RZL)
Technology Incorporated
511 West Rhapsody Drive
San Antonio, Texas 78216

April 1978

Final Report for Period 16 February 1973 - 15 February 1976



Approved for public release; distribution unlimited.

Prepared for
USAF SCHOOL OF AEROSPACE MEDICINE
Aerospace Medical Division (AFSC)
Brooks Air Force Base, Texas 78235

## NOTICES

This final report was submitted by Technology Incorporated, 511 West Rhapsody Drive, San Antonio, Texas 78216, under contract F41609-73-C-0016, job order 7757-02-33, with the USAF School of Aerospace Medicine, Aerospace Medical Division, AFSC, Brooks Air Force Base, Texas. Major Jack A. Labo (SAM/RZL) was the Laboratory Project Scientist-in-Charge.

When U.S. Government drawings, specifications, or other data are used for any purpose other than a definitely related Government procurement operation, the Government thereby incurs no responsibility nor any obligation whatsoever; and the fact that the Government may have formulated, furnished, or in any way supplied the said drawings, specifications, or other data is not to be regarded by implication or otherwise, as in any manner licensing the holder or any other person or corporation, or conveying any rights or permission to manufacture, use, or sell any patented invention that may in any way be related thereto.

The animals involved in this study were procured, maintained, and used in accordance with the Animal Welfare Act of 1970 and the "Guide for the Care and Use of Laboratory Animals" prepared by the Institute of Laboratory Animal Resources - National Research Council.

The views expressed herein do not necessarily reflect the views of the USAF School of Aerospace Medicine, the U.S. Air Force, or the Department of Defense.

This report has been reviewed by the Information Office (OI) and is releasable to the National Technical Information Service (NTIS). At NTIS, it will be available to the general public, including foreign nations.

This technical report has been reviewed and is approved for publication.

Jack A. Labo

JACK A LABO, Major, USAF
Project Scientist

Ralph G. Allen

Ralph G. Allen, Ph.D.
Supervisor

Robert G. McIver

ROBERT G. MCIVER
Brigadier General, USAF, MC
Commander

UNCLASSIFIED

SECURITY CLASSIFICATION OF THIS PAGE *(When Data Entered)*

**REPORT DOCUMENTATION PAGE**

READ INSTRUCTIONS BEFORE COMPLETING FORM

1. REPORT NUMBER: SAM-TR-78-21

2. GOVT ACCESSION NO.: AD-A053 564-03

3. RECIPIENT'S CATALOG NUMBER:

4. TITLE (and Subtitle): OCULAR HAZARDS OF PICOSECOND AND REPETITIVE-PULSED LASERS. VOLUME II. Argon-Ion Laser (514.5 nm).

5. TYPE OF REPORT & PERIOD COVERED: Final Report. 16 Feb 73 - 15 Feb 76.

6. PERFORMING ORG. REPORT NUMBER: 77-0564-03

7. AUTHOR(s): J.S. Connolly, H.W. Hemstreet, Jr., D.E. Egbert

8. CONTRACT OR GRANT NUMBER(s): F41609-73-C-0016

9. PERFORMING ORGANIZATION NAME AND ADDRESS: Technology Incorporated, Life Sciences Division, 511 West Rhapsody Drive, San Antonio, Texas 78216

10. PROGRAM ELEMENT, PROJECT, TASK AREA & WORK UNIT NUMBERS: 62202F; 7757-02-33

11. CONTROLLING OFFICE NAME AND ADDRESS: USAF School of Aerospace Medicine (RZL), Aerospace Medical Division (AFSC), Brooks Air Force Base, Texas 78235

12. REPORT DATE: Apr 78

13. NUMBER OF PAGES: 81

84 Pl

14. MONITORING AGENCY NAME & ADDRESS *(if different from Controlling Office)*

15. SECURITY CLASS. *(of this report)*: Unclassified

15a. DECLASSIFICATION/DOWNGRADING SCHEDULE

16. DISTRIBUTION STATEMENT *(of this Report)*

Approved for public release; distribution unlimited.



17. DISTRIBUTION STATEMENT *(of the abstract entered in Block 20, if different from Report)*

18. SUPPLEMENTARY NOTES

19. KEY WORDS *(Continue on reverse side if necessary and identify by block number)*

Laser-induced retinal damage/rhesus monkey
Argon-ion laser
Single-pulse thresholds
Repetitive-pulse thresholds
Photobiological damage mechanisms
Ocular damage thresholds
Thermal damage mechanisms
Mode-locked pulse trains

20. ABSTRACT *(Continue on reverse side if necessary and identify by block number)*

Retinal damage thresholds were determined for exposures of the maculae of rhesus monkeys to CW and repetitive-pulse trains of argon-ion laser radiation at 514.5 nm in the TEMoo mode. Single-pulse exposures were made at pulsewidths of 2, 10, 40, and 100 μsec and 1, 10, 100, and 500 msec. Repetitive-pulse exposures were made for 27 different combinations: train durations of 0.05, 0.5, 5, and 30 sec; pulse repetition frequencies from 0.10 Hz to 10 kHz and pulsewidths of 10, 40, and 100 μsec and 1 msec. Damage thresholds for mode-locked argon laser pulses at 104 MHz and 250 psec pulsewidth for pulse trains of 9.9-sec, 10-msec, and

DD FORM 1 JAN 73 1473 EDITION OF 1 NOV 65 IS OBSOLETE

UNCLASSIFIED

SECURITY CLASSIFICATION OF THIS PAGE *(When Data Entered)*

401 630

20. ABSTRACT (continued)

10-μsec duration were also measured.

For pulsewidths of 10 μsec, there is an apparent cumulative effect provided the repetition frequencies are in the range of ≃0.1 to ≃ 10 Hz. The retina is more sensitive to double-pulse exposures, by a factor of 2 to 3 relative to single-pulse thresholds, when the interpulse spacing is ≃ 2.5 sec.

Nonthermal damage mechanisms, involving a two-step, two-threshold process, may explain our results. Specifically, for double-pulse configurations, the first acts as a reversible photo-trigger which sensitizes the retina in preparation for the subsequent pulse. The elements of an empirical model have been assembled and appear to account satisfactorily for the observed double-pulse threshold data.

## SUMMARY

This volume discusses retinal damage thresholds for exposures of the maculae of rhesus monkeys (*Macaca mulatta*) to continuous-wave (CW) and repetitive-pulse trains of argon-ion laser radiation at 514.5 nm. The laser was operated in the $TEM_{00}$ mode with a full angle beam divergence of $\tilde{>}0.6$ mrad and a $1/e^2$ beam diameter of $\tilde{>}1.7$ mm at the corneal plane.

Single-pulse exposures were made at pulsewidths of 2, 10, 40, and 100 μsec and 1, 10, 100, and 500 msec. Repetitive-pulse exposures were made for 27 combinations of intracavity modulated pulses with train durations of 0.05, 0.5, 5 and 30 sec at pulse-repetition frequencies from 0.01 Hz to 10 kHz with pulsewidths of 10, 40, and 100 μsec and 1 msec. We also report here the first threshold data for mode-locked visible pulses. Repetition frequency and nominal pulsewidth were fixed at ∿104 MHz and 250 psec, respectively, for pulse trains of 9.9-sec, 10-msec, and 10-μsec duration.

For each threshold measurement, four to ten eyes were exposed at each of sixteen macular sites and were examined ophthalmoscopically at one hour postexposure. In some cases we also employed a 24-hour damage criterion. A simple lesion/no lesion determination was made and the damage thresholds (ED50) were calculated by the method of probits. Threshold powers are expressed in terms of peak pulse power at the cornea. For all single-pulse exposures and for repetitive pulses of greater than 40-μsec pulsewidth, retinal damage appears to be induced primarily by thermal mechanisms. That is, the observed data show good agreement with calculations made using the Illinois Institute of Technology Research Institute (IITRI) thermal model. Similarly, for all pulsewidths, agreement with thermal predictions is generally satisfactory for pulse repetition frequencies higher than 1 kHz.

In contrast, for shorter pulsewidths (10 μsec), there is an apparent cumulative effect of repetitive, Q-switched pulses when the repetition frequencies are in the range of ∿0.1 to ∿10 Hz. For example, the retina is more sensitive to double-pulse exposures, by a factor of 2 to 3 relative to single-pulse thresholds, when the interpulse spacing is ∿2.5 sec.

Non-thermal damage mechanisms appear to be involved, and we invoke a two-step, two-threshold process to explain our results. Specifically, for double-pulse configurations, the first acts as a reversible photo-trigger which sensitizes the retina in preparation for the subsequent pulse. The elements of an empirical model have been assembled and appear to account satisfactorily for the observed double-pulse threshold data.

However, this hypothesis of photochemical damage remains to be tested; other mechanisms, such as membrane disruption induced by acoustic shock or a combination of effects, including thermal processes, are not ruled out. For that matter, our present understanding of the fundamental biochemical and biophysical mechanisms involved in thermal damage of the retina can best be termed rudimentary. Thus, we likewise do not rule out strictly thermal damage processes of a type not previously encountered in laser ocular hazards research.

## PREFACE

The authors wish to recognize the superb technical assistance of Ms. Kathleen K. Altobelli, Mr. J. Michael Scott, and Mr. Charles C. Stevens throughout the course of this three-year study. We thank Mr. John E. McGlothan, III and Mr. Gregory L. Sweeney for preparing the figures, and Mrs. Maribeth Bains and Mrs. Sharon Johnson for typing the various drafts of the manuscript.

We also thank Mr. Richard C. NcNee, USAFSAM Biometrics Division, for carrying out the many probit analyses reported here and for his critical review of the manuscript. Very helpful discussions with Dr. Joseph A. Zuclich, Dr. J. Terry Yates, Major Jack A. Labo, and Lieutenant Colonel William D. Gibbons, are also gratefully acknowledged.

The Hewlett-Packard and Tektronix spectrum analyzers, used in the mode-locking experiments, were loaned to us by the respective local representatives; we are indeed grateful for their consideration and assistance.

Our highest praise and deepest gratitude are reserved for Mr. W. Robert Bruce, without whose expertise and assistance this program could not have been completed. Mr. Bruce evaluated all of the more than 12,000 retinal exposures made in this study. The precision of the data is an eloquent tribute to his remarkable skills, his long experience, and his professional objectivity.

TABLE OF CONTENTS



LIST OF FIGURES

LIST OF FIGURES (continued)



LIST OF TABLES

# OCULAR HAZARDS OF PICOSECOND AND REPETITIVE-PULSED LASERS

## VOLUME II: ARGON-ION LASER (514.5 nm)

## INTRODUCTION

Effects of laser radiation on retinal tissues were reviewed in Volume I. Briefly, it appears that retinal damage induced using a wide variety of laser exposure conditions may be understood in terms of irreversible thermal processes in the pigment epithelium and other chorioretinal layers. The absorbed optical radiation is converted to heat, and the resulting damage, centered about the region of maximum temperature increase, is thought to involve thermal denaturation of proteins or enzyme inactivation (1).

The theoretical model developed by Takata and co-workers (2) at the Illinois Institute of Technology Research Institute (IITRI) is based on assumptions of strictly thermal processes. This sophisticated computer routine, commonly referred to as the IITRI model, can make fairly accurate predictions of absolute damage thresholds (ED50) for a wide range of exposure conditions; calculated values of relative thresholds (e.g., scaled to one experimental value in a series of exposure conditions) are even more accurate.

In the near-infrared (IR) region of the spectrum, specifically at 1064 nm, thermal processes appear to predominate for single-pulse exposures ranging in duration from ∿30 nsec to 1000 sec. That is, the trend of the experimental data parallels IITRI model predictions (see Fig. 6, Vol. I). In addition, thermal model predictions are in general agreement with empirical damage thresholds for repetitive, 300-nsec pulses, at least for short (≤50 msec) pulse-train durations (Fig. 7, Vol. I). However, we found a pronounced cumulative effect of repetitive, Q-switched 1064-nm pulses for pulse-train durations of 0.5 sec or longer. When displayed for fixed numbers of pulses (Fig. 8, Vol. I), the threshold data show that the cumulative effect of successive pulses is maximal when the interpulse spacing is 0.5 sec. This behavior could not be predicted or even understood on the basis of strictly thermal effects; photobiological processes, discussed in greater detail in this volume, are invoked to explain the results.

Similarly, for visible wavelengths (∿400-700 nm), there is a growing body of evidence that processes other than strictly thermal are involved in laser damage to the primate retina. Single-pulse exposure durations from about 10 μsec to 10 sec appear to induce retinal damage that is primarily thermal in nature. Gibbons and Allen (3,4) have shown that even at exposure times of up to $10^3$ sec, damage thresholds, determined using a 1-hour evaluation criterion, follow a trend that appears to reflect thermal mechanisms. Using a 24-hour criterion, however, they found that the damage threshold (ED50) for 514.5 nm radiation is lower than the 1-hour ED50 by a factor of ∿15, an effect not observed using 1064 nm laser light. Unspecified photochemical processes in the photoreceptors were invoked to explain the long-term, low-level effects of visible laser radiation (4).

More recently, Ham et al. (5) observed a strong wavelength dependence of retinal damage thresholds for long-term (1-1000 sec), low-power exposures over the wavelength range 441.6 to 1064 nm. The results were compared with calculated temperature increases and the authors inferred that thermal mechanisms predominate in the case of near-IR exposures, with a gradual progression to unspecified photochemical processes with decreasing wavelength. Ham (6) has now concluded from histological studies that the latter mechanisms involve coagulation or aggregation of pigment granules in the pigment epithelium. As in the case of the minimal retinal image-size exposures of Gibbons and Allen (3,4), the "photochemical" lesions induced by Ham et al. on large retinal areas (~500-μm diameter) are not visible ophthalmoscopically until 24 hours post-exposure.

One way to distinguish between photochemical and thermal effects is the test of energy (i.e., dose) reciprocity. Thermal processes depend on the power density in the exposed medium; i.e., damage is related to the peak temperature, taking into consideration diffusion and conduction of heat out of the irradiated volume element (2). The rate of a simple photochemical reaction likewise depends on the absorbed light intensity (power), but the extent of overall damage (i.e., molecular alteration) is linear with total absorbed dose (energy). Thus, if the quantum efficiency is constant, a photochemical process, evaluated in terms of exposure required to achieve a given effect (analogous to threshold), will show reciprocity. In other words, the specified level of effect will be observed for any combination of power and exposure time resulting in the same absorbed energy dose.

In general, photobiological processes, as contrasted with simple photochemical reactions, can be expected to show deviations from this reciprocity relationship (7). The end-point of a photo-initiated process in a biological system may be reached only after a series of complex chemical and biochemical reactions, and the overall quantum efficiency may depend on the irradiation history of the specimen. For example, the quantum efficiency for bleaching of the photoreceptor pigment, rhodopsin, approaches zero as the fraction bleached approaches 0.5 and approaches unity in the limit of negligible bleaching (8).

Nevertheless, some photobiological processes do manifest photochemical reciprocity. Of direct interest to the present study is the observation of Zuclich and Connolly (9,10) that near-ultraviolet (UV) laser radiation induces single-photon photochemical damage in the corneal epithelium of the rhesus monkey. They showed that a constant energy relationship obtains over a wide range of exposure conditions, from modulated 250-μsec pulses to CW exposures of 120 sec. Although the molecular processes involved remain to be identified, close adherence to reciprocity suggests that the overall mechanism is relatively simple.

In more complex cases of photo-initiated biological processes, cumulative effects of successive exposures can be anticipated, but with significant deviations from reciprocity. Indeed, the visible-wavelength data of Ham et al. (5) show pronounced deviations from a constant energy relationship, especially at the shorter exposure times used (1 and 16 sec). Recent experiments (11), similar to those of Ham et al., have shown evidence of a cumulative effect of 465.8-nm laser radiation on large retinal areas (~750 μm diameter) for exposure times up to 120 sec; strict reciprocity, however, was not observed.

Although most studies of laser-induced retinal damage have been concerned with single-pulse exposures, some recent investigations have considered also the effects of repetitive-pulse exposures in the visible and near-IR regions.

Skeen et al. (12,13) measured macular thresholds under so-called worst-case conditions ($TEM_{00}$ mode, focused to a diffraction-limited retinal image), using repetitive pulses from an argon-ion laser (514.5 nm) and a Q-switched Nd:YAG laser (1064 nm). Expressing thresholds in terms of either energy per pulse or peak pulse power, they found evidence for cumulative effects at both wavelengths; i.e., the energy per pulse required to produce a threshold lesion decreased as the total number of pulses in the exposure train (0.5 sec duration) increased. Ebbers and Dunsky (14) noted a slight decrease in damage thresholds for repetitive, Q-switched Nd:YAG (~10-nsec pulsewidth, 1064 nm) exposures in the paramacula; however, no significant evidence for a cumulative effect could be inferred from their results.

In another early study, Gibbons (16) observed a pronounced cumulative effect in the rhesus macula for repetitive pulses from a Q-switched, frequency-doubled Nd:YAG laser (~15-nsec pulsewidth, 532 nm). Using a fixed repetition frequency of 5 Hz and pulse-train durations of 30 and 120 sec, he measured damage thresholds (ED50) at 1-hour and 24-hours post-exposure. For 30-sec trains, the 1-hour ED50 decreased from 3.02 μJ (single pulse to 0.51 μJ/pulse; the 24-hour ED50 was even lower at 0.29 μJ/pulse. The threshold energy for 120-sec pulse trains decreased to ~0.16 μJ/pulse using both evaluation criteria.

A similar effect was reported by Gibbons and Egbert (15), who exposed the maculae of rhesus monkeys to repetitive pulses of argon-ion laser radiation at 514.5 nm. Using a fixed pulsewidth of 4 μsec, they determined damage thresholds (1-hour ED50) for single pulses and for 0.1-, 0.5-, and 1-sec trains of repetitive pulses at repetition rates of 100 Hz and 1 kHz. They observed cumulative effects of successive laser pulses, and concluded that pulse-train duration has a greater effect on threshold levels than does the repetition rate for the range of parameters studied.

At the time these earlier repetitive pulse studies (12-16) were published, the results were considered controversial, primarily because they were not consistent with thermal concepts. Then-current thinking on mechanisms of laser-induced ocular damage concentrated heavily on thermal effects, and other processes--photochemical or photobiological--were not given a great deal of attention. One of the few aspects of these studies on which there was general agreement among workers in the laser-bioeffects field was that more data were urgently needed.

Accordingly, the present program was designed specifically to investigate repetitive-pulse damage thresholds in the rhesus macula for two widely different laser wavelengths (514.5 and 1064 nm), using worst-case conditions over a broad range of pulsewidths, pulse-repetition frequencies and pulse-train durations. Volume I of this report deals exclusively with the near-IR studies. This volume is concerned primarily with the effects of repetitive visible laser pulses. In general, our results are consistent with those of other investigators (12-16), and can be understood in terms of a two-step, two-threshold hypothesis in which quantum conversion of the incident laser radiation plays a major role.

## OBJECTIVES

The objectives of the program were three-fold: (1) to acquire additional experimental threshold data for retinal damage induced by trains of repetitive laser pulses; (2) to construct an empirical model of such damage; and (3) to validate and help define the limits of applicability of the IITRI thermal model (2) of retinal damage induced by repetitive-pulse exposures.

As in many previous investigations (3,4,12-31), all experiments reported here were performed *in vivo* on the eyes of young rhesus monkeys (*Macaca mulatta*). There is evidence (25) that threshold measurements based on paramacular exposures yield higher values than those based on macular exposures; therefore in this study, all test exposures were placed within the macula and generally away from the *fovea centralis*. The anatomy, physiology and optical properties of the rhesus eye are very similar to those of the human eye; thus, for purposes of ocular-hazard evaluations, the rhesus eye can be considered as a scaled-down version of the human eye. In addition, the detailed thermal and optical absorption coefficients of rhesus ocular media have been measured *in vitro* (2,32-38), and these measurements provide parameters for developing thermal models that can be tested against the rapidly accumulating ocular damage data obtained from *in vivo* experiments on the rhesus.

The damage threshold, ED50, is a statistically determined value calculated from exposure data generally taken from ten or more test eyes. This value represents the pulse power (or energy), incident on the cornea, that has a 50% probability of inducing macular damage in an eye selected at random from the subject population (see Appendix A). For a given set of laser optical parameters (wavelength, beam divergence, mode structure, etc.), the damage threshold of an eye focused at infinity is a function of pulsewidth, pulse-repetition rate and pulse-train duration. Therefore, threshold measurements were performed using selected values of the above variables over a range compatible with state-of-the-art commercial laser equipment.

Since a large body of retinal threshold data has been acquired in prior research at other laboratories, experiments in the present program were conducted in such a way that direct comparisons could be made with previous data and that the accumulated results could be compiled into a self-consistent empirical model. Insofar as possible, the experimental parameters and criteria used in much of the previous work were adopted in this program as follows:

(1) The subjects used were young rhesus monkeys (*Macaca mulatta*) ranging in age from two to four years and in weight from two to four kg. No distinction was made between male and female subjects.
(2) Only the macular region of the retina was irradiated for purposes of damage determination.
(3) Damage was defined as the appearance of a lesion at the exposed site within 1 hour after irradiation, although in some cases observations were also made at 24 hours post-exposure.
(4) A lesion was defined as an ophthalmoscopically visible, dark circular discoloration containing a white or light-gray center.
(5) Each macula was exposed at 16 different sites, with a range of intensities (laser power) varying over a log normal distribution above and below the estimated threshold intensity. (See Appendix A.)

(6) In all but a few cases, a minimum of 10 eyes was irradiated at a given set of laser parameters to determine the threshold under those conditions.
(7) The laser was operated in its lowest order Fabry-Perot mode ($TEM_{00}$) with a diffraction-limited beam divergence.
(8) The laser power was taken to be the total energy in the beam (measured at the corneal plane) divided by the pulsewidth.
(9) An ophthalmic lens was used if the subject eye had a refractive error greater than ±0.5 diopter in any meridian.
(10) All retinal examinations were made by the same person.

The data reported here are for an argon-ion laser operating at 514.5 nm either in the continuous-wave (CW) mode or acousto-optically shuttered to give pulsewidths ranging from 100 msec to 2 μsec. In the CW mode, single-pulse exposure times ranged from 0.05 to 30 sec. In the shuttered mode, pulse-repetition rates varied from DC (i.e., single pulse) to 100 kHz for pulse-train durations of 0.05, 0.5, 5, and 30 sec.

In addition, we report here the first known threshold studies of retinal damage induced by mode-locked visible laser pulses. These experiments were carried out at fixed pulsewidth (nominally 250-300 psec) and repetition frequency (∿104 mHz); pulse trains were 9.9 sec and 10 msec. In addition, a few exposures were made with 10-μsec pulse trains.

## PRIMATE CARE AND PREPARATION

The San Antonio Laboratory of Technology Incorporated is equipped with a controlled environment vivarium which is used exclusively for housing infrahuman primates to be employed as research subjects. Both temperature and humidity were carefully controlled and the primates individually housed in stainless steel cages. Daily care and feeding were performed by trained personnel. Regular inspections were made by a representative of the U.S. Department of Agriculture, Agricultural Research Service, Animal Health Division, as well as by a company-retained veterinarian.

On the day prior to the retinal irradiations of a primate, atropine sulfate (1% ophthalmic ointment) was introduced into each conjunctival sac to achieve maximum pupillary dilation. Approximately one hour prior to retinal irradiation, each subject was tranquilized with an intra-muscular injection of phencyclidine hydrochloride (Sernylan) 20 mg/cm$^3$ at a dosage of 1 mg/kg of body weight. After onset of tranquilization, a 19-gauge intravenous catheter was introduced into a posterior superficial vein in one leg. To initiate anesthetization, 0.5 cm$^3$ of sodium pentobarbital (50 mg/cm$^3$) was administered by way of the intracatheter. Smaller increments, 0.1 cm$^3$ or less, were injected as necessary to maintain both constant core temperature and deep anesthesia, up to a maximum total dose of 1 cm$^3$/kg of body weight. The eyelids were held open by means of a stainless steel speculum during retinal exposures. Since lacrimation is usually suppressed by anesthesia, the eye was irrigated frequently with sterile, normal saline to preserve corneal transparency. Throughout the course of the experiment, the primate core temperature was monitored with a Yellow Springs Instruments Model 702 Telethermometer equipped with a model 402 rectal probe. The subjects were wrapped securely in a heated blanket, and core temperatures were maintained at 97° ± 2°F (36° ± 1°C).

## APPARATUS AND CALIBRATION

### Experimental Apparatus

A Coherent Radiation model 52 argon-ion laser operating in the $TEM_{00}$ mode and equipped with a prism wavelength selector was used as the radiation source. The 514.5-nm line was used for all experiments reported here. The laser could be operated in either the continuous-wave (CW) or pulsed mode. In the latter case, an intra-cavity Coherent Radiation model 462 acousto-optic shutter (AOS) was used to obtain a pulsed output. With this device, the pulsewidth and the repetition rate were continuously variable over the ranges of 2 μsec to 2 sec and 0.5 Hz to 250 kHz, respectively. However, the maximum laser pulse power was sharply reduced at shorter pulsewidths (<10 μsec). Trains of repetitive pulses were generated by an external 0.5-sec gate pulse from a Systron-Donner Datapulse model 115 pulse generator.

As shown schematically in Figure 1, a constant fraction of the laser output beam was split off and sensed by an EG&G model SGD-100A photodiode, which was coupled to a wide-band oscilloscope (Tektronix type 555 or 7633) for on-line measurements of pulse intensity, width and repetition rate. The photodiode was calibrated against a ballistic thermopile so that its output voltage as read on the oscilloscope could be converted directly into peak pulse power incident on the cornea.

For long (≥5 msec) exposures, the laser was operated in either the CW or pulsed mode, and the respective pulses or pulse trains were delivered by externally gating the beam on and off with a Vincent shutter. The repeatability of this electromechanical device deviated from its set aperture time by less than ±4% as determined from oscilloscope measurements. Pulse powers at the cornea were varied by adjusting the laser tube current and by interposing one or more 5 x 5 cm neutral density filters in the laser beam.

Visual examination of each primate retina was performed with a Zeiss fundus camera rigidly mounted with its optic axis perpendicular to the laser beam (Fig.1). This ophthalmoscopic device was used to view the primate retinae for proper placement of the test exposures and for post-exposure examination to determine which of the irradiated sites incurred damage.

Each primate subject was held in a prone position on a mechanically adjustable table mount adjacent to the fundus camera with ear bars holding the head rigid in an upright position. The pupil of the subject eye was positioned with respect to the camera and laser beam axis by one or more of the five mechanical adjustments on the table mount (x, y, z, azimuth and inclination).

A two-position swing-away mirror was attached to the fundus camera objective barrel to deflect the laser pulses into the eye. In the "in" position, the laser beam was intercepted by the mirror and deflected into the subject eye as shown in Figure 1. When the beam was blocked, the mirror was returned to the "out" position, allowing the eye to be examined through the fundus camera.

With the mirror in place, the distance from the output mirror of the laser to the subject cornea was 90 cm. When required, a corrective lens was inserted in a carefully machined slot placed in front of the cornea.

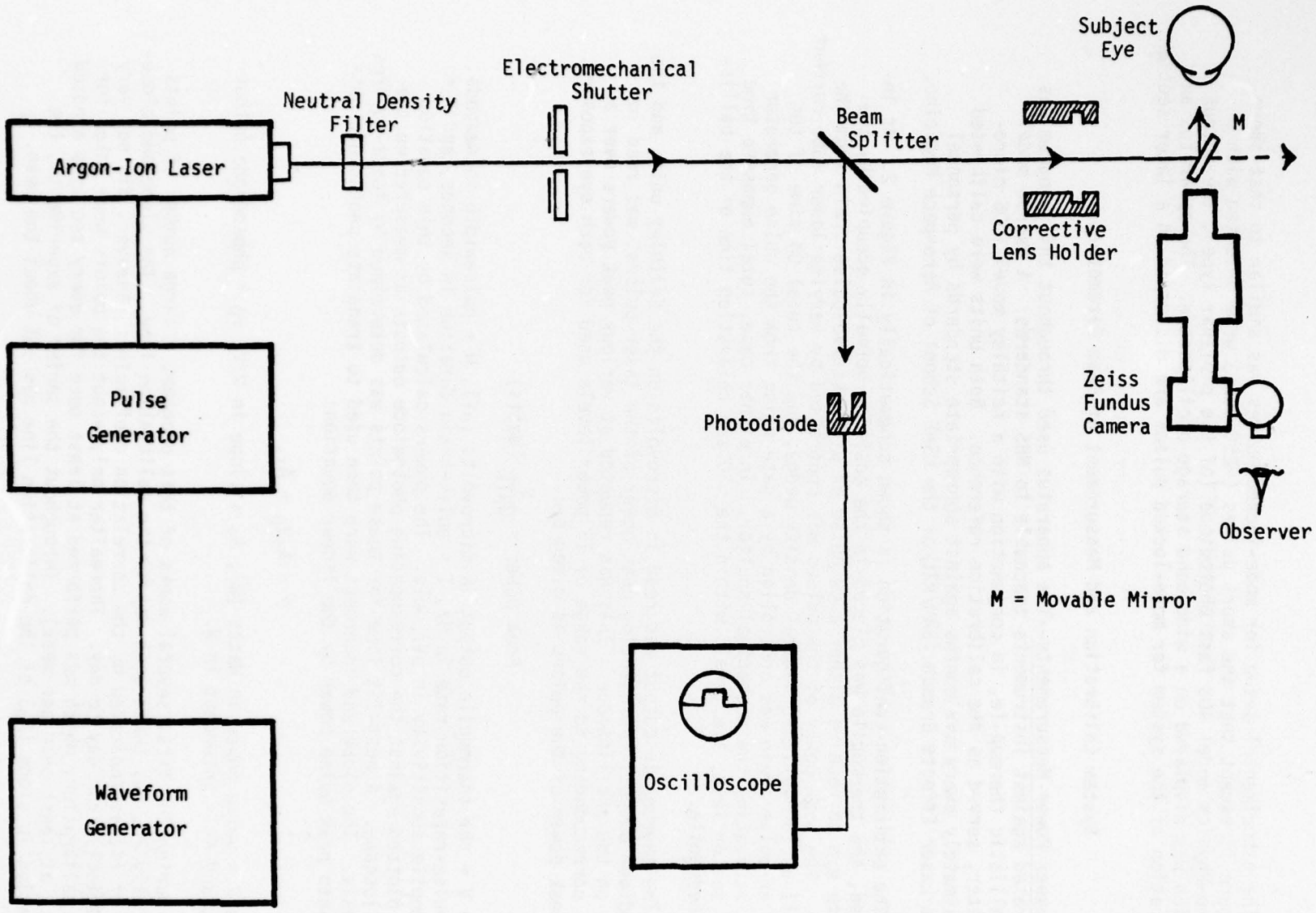


Figure 1. Block diagram of experimental apparatus.

The experimental setup for mode-locked pulses was similar to that shown in Figure 1, except that the short pulses (~250 psec) were detected with a Spectra-Physics model 403 fast photodiode (of the biplanar type), the output of which was displayed on a wide-band storage oscilloscope. The apparatus and calibration of the system for mode-locked pulses are discussed in a later section.

## System Calibration and Measurement of Beam Parameters

Laser Power Measurements--The apparatus used throughout this program was calibrated against instruments traceable to NBS standards. A Hadron model 100 ballistic thermopile, in conjunction with a Keithley model 150B microvoltmeter, served as the calibration reference. Both units were calibrated approximately every six months against appropriate standards by personnel in the Laser Effects Branch (SAM/RZL) of the USAF School of Aerospace Medicine.

The calibration configuration is shown schematically in Figure 2. As indicated, the thermopile was placed in the position normally occupied by the primate eye to receive either a CW pulse or a repetitive-pulse train from the laser. The peak power of the pulses was controlled by varying laser tube current as well as the variable neutral density wedge, and the total ON time of the pulse or pulse train was controlled by a gate pulse from the pulse generator or by activating the mechanical shutter. In either case, total exposure time was 3 sec or less, i.e., well within the ~30 sec relaxation time of the ballistic thermopile.

The thermopile output was read in microvolts on the Keithley unit, and the photodiode output, representing peak power of the laser pulses, was read in volts on the oscilloscope. This was repeated at various peak powers over a range corresponding to the range of 16 power levels used for each eye exposure. The peak power of the pulses is given by:

$$\text{Peak power} = \frac{V}{WRTK} \text{ (Watts)}$$

where V = the thermopile output in microvolts ($\mu$V), W = pulsewidth in seconds, R = pulse-repetition rate in Hz, T = pulse-train duration in seconds, and K = thermopile sensitivity in $\mu$V/joule. The powers calculated by this equation were plotted against the corresponding photodiode outputs as measured on the oscilloscope. A best-fit line for these points was determined by least-squares analysis. The slope and intercept were then used to translate photodiode output into peak pulse power by the linear equation:

$$P = A_0 V_p + A_1,$$

where P = pulse power in Watts (W), $A_0$ = slope in W/V, $V_p$ = photodiode output in V, and $A_1$ = intercept in W.

During the first several weeks of this program, a large number of points, typically 20, was taken each day for the calibration line. The slope and closeness of fit as indicated by the correlation coefficient, however, did not vary appreciably from day to day. Thereafter only about ten points were taken for each calibration, which was performed at least once for every ten eyes exposed (i.e., at least once per week). Throughout the series of experiments, the variation in slope ($A_0$) of the calibration line was ±5% about the mean.

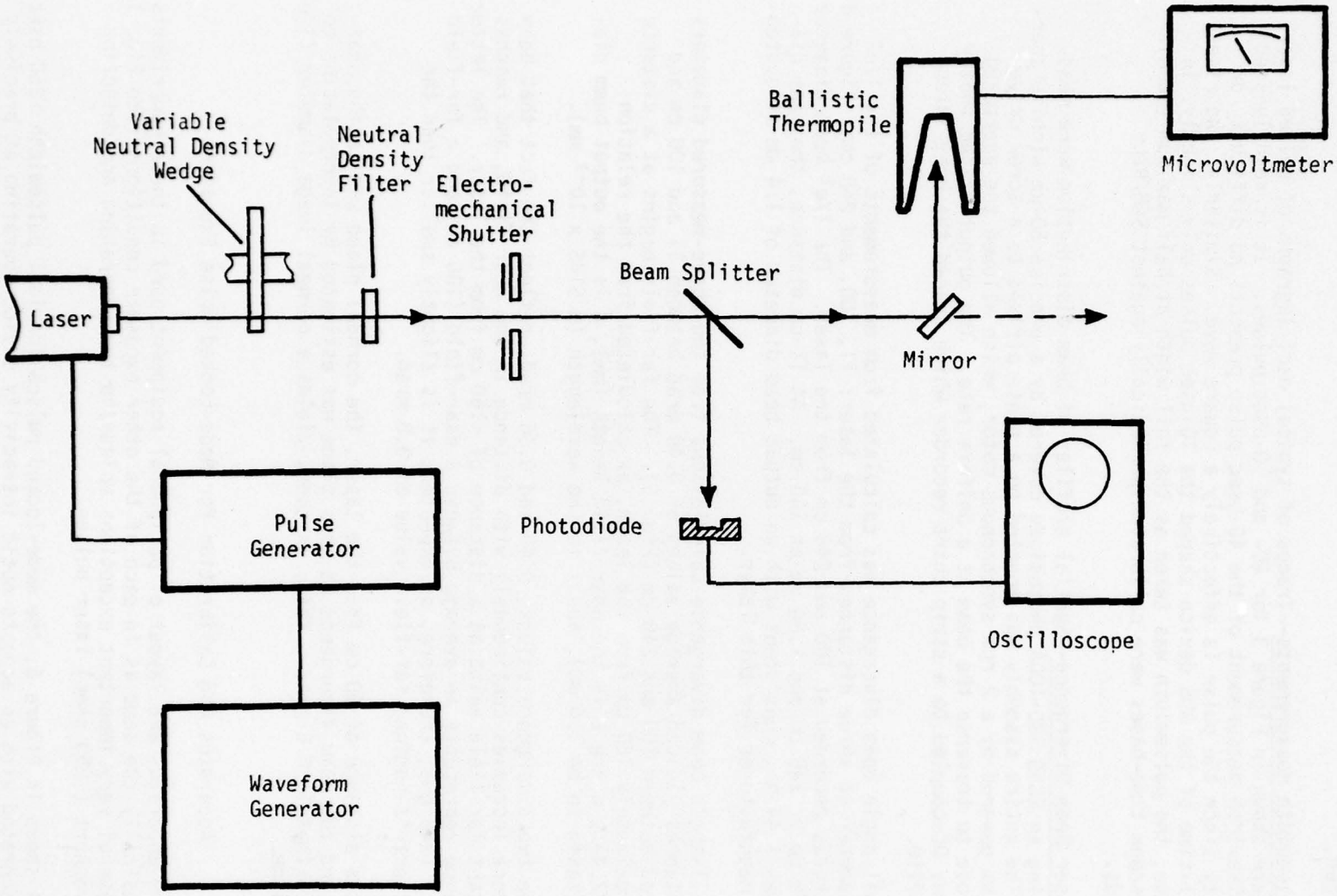


Figure 2. Block diagram of laser power calibration system.

Correlation coefficients for all the least-squares determinations were 0.994 or greater.

Pulsewidth Measurements--Traces of typical oscillographs of pulsed laser output are shown in Figure 3 for 40- and 10-μsec pulses. It is readily seen that pulsewidth measurement of the 40-μsec pulse presents no difficulty or ambiguity since the pulse is effectively a square wave. Similarly, the rise- and fall-time of the AOS device shaped the 10-μsec pulses only slightly. In this case, the pulsewidth was taken as the full width at half maximum (FWHM). Oscilloscope time-bases were calibrated periodically against SAM/RZL standards.

Laser Beam Divergence--Spatial profiles of beam distribution were measured using an EG&G SGD-100A photodiode covered by a precise 50-μm pinhole aperture. The entire assembly was mounted on a plate affixed to a screw drive mechanism powered by a 2 rpm synchronous motor, which allowed the apertured photodiode to traverse the beam at a uniform rate. The output of the photodiode was DC-coupled to a strip chart recorder which traced the beam intensity profile.

Full-angle beam divergence was calculated from measurements of the $1/e^2$ beam diameter at three distances from the laser: 11, 100, and 248 cm. Figure 4 shows traces recorded at 100 and 248 cm from the laser. The $1/e^2$ beam diameter was 2.78 mm at 248 cm and 1.80 mm at 100 cm. At 11-cm distance, the beam diameter was 1.44 mm, consistent with an output beam diameter of 1.4 mm as quoted by the manufacturer for this laser.

Full-angle beam divergence calculations from the above-measured diameters and distances yielded average values of 0.40 mrad between 11 and 100 cm and 0.66 mrad between 100 and 248 cm (Fig. 5). The far-field begins at a distance of approximately 160 cm from the laser, as calculated from the relation: $L = d^2/2.44\lambda$, where L is the near field length (mm), d is the output beam diameter (taken to be 1.4 mm), and $\lambda$ is the wavelength ($0.5145 \times 10^{-3}$ mm).

The two divergence values, 0.40 and 0.66 mrad, reflect the fact that beam divergence increases continuously with distance in the near field, and reaches a constant far field value at a distance of ∿160 cm from the laser. The latter divergence represents an average between a near-field (100 cm) and a far-field distance (248 cm); therefore, as expected, it is slightly smaller than the manufacturer's nominal far-field value of 0.8 mrad.

At a distance of 90 cm from the laser, the corneal plane was in the near-field, and the beam divergence at this plane was estimated by interpolation to be approximately 0.6 mrad. This, in turn, yields a corneal image diameter ($1/e^2$) of 1.74 mm.

## Apparatus and Calibration for Mode-Locked Pulse Exposures

The apparatus and layout of peripheral equipment used in these experiments were basically the same as in each of the other exposure conditions (see Fig. 1) with several very important exceptions unique to the generation and detection of ultrashort (∿250 psec) laser pulses.

As shown in Figure 6, the mode-locked pulses (nominal pulsewidth ∿250 psec) were generated with an acousto-optic intracavity device operating at precisely

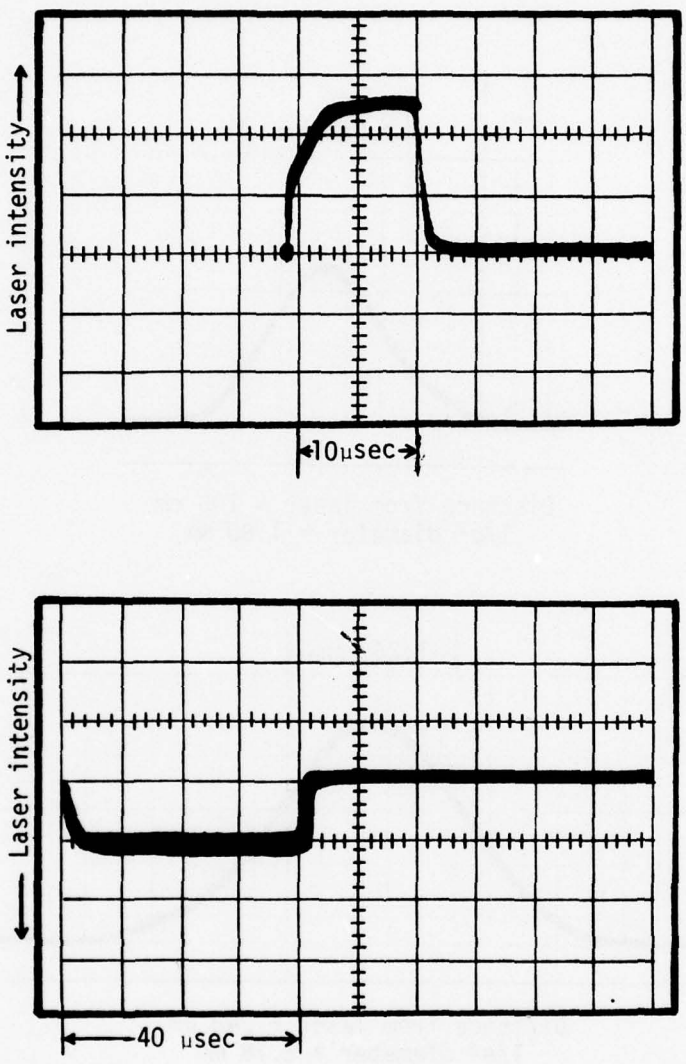


Figure 3. Oscilloscope traces of 514.5-nm laser pulses.

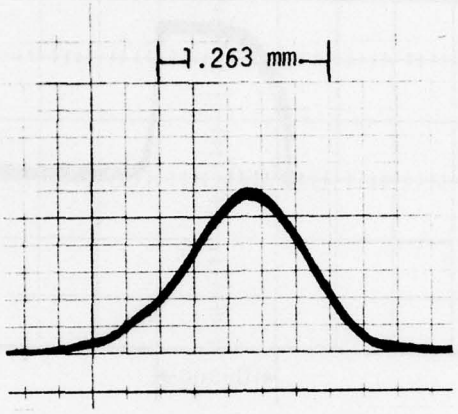


Distance from laser = 100 cm
$1/e^2$ diameter = 1.80 mm

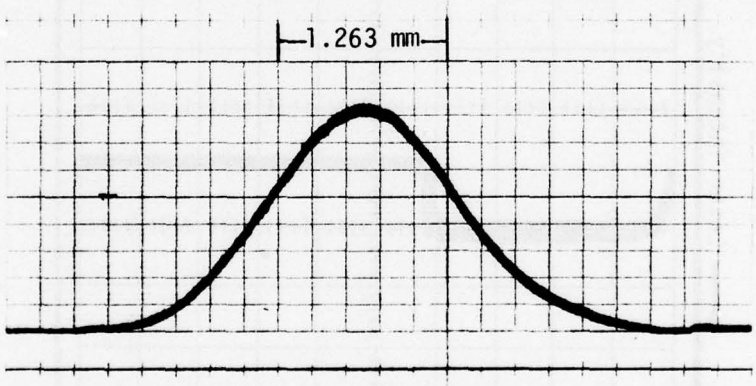


Distance from laser = 248 cm
$1/e^2$ diameter = 2.78 mm

Figure 4. Spatial distribution of CW argon-ion laser beam.

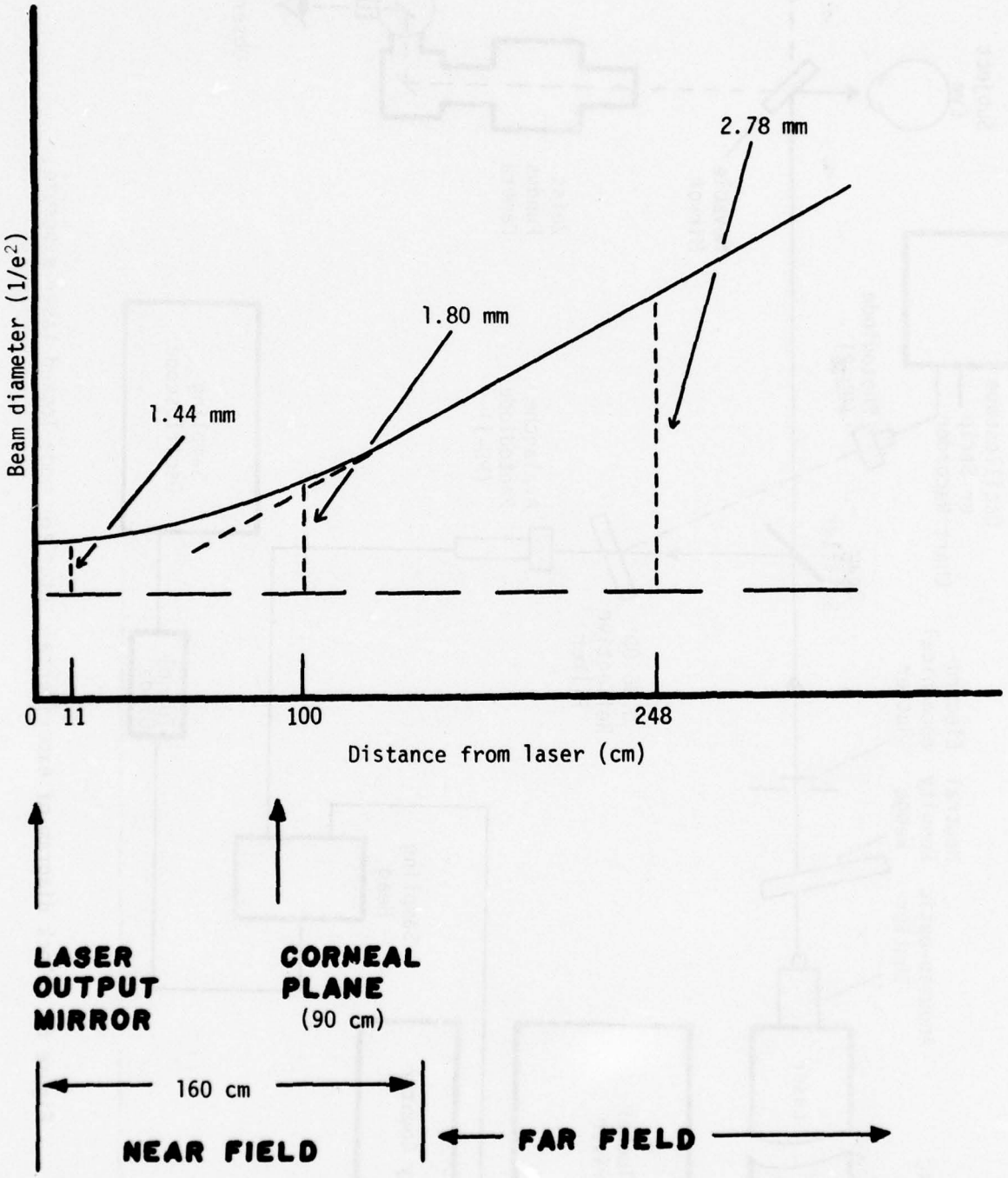


Figure 5. Beam-divergence diagram for argon-ion laser output.

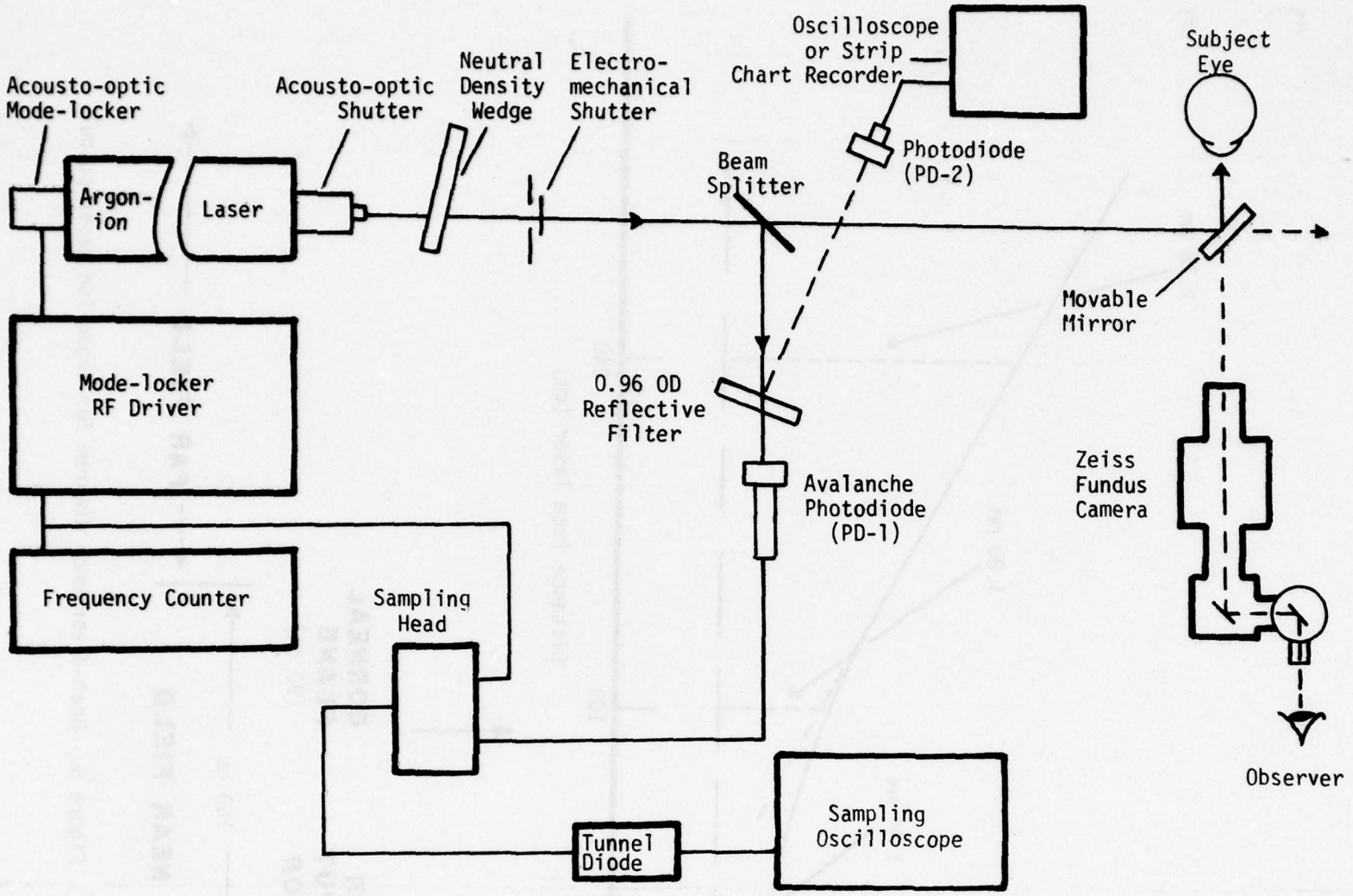


Figure 6. Block diagram of experimental setup for mode-locked laser exposure.

one-half the resonant cavity frequency of the laser. The operating principle and theory of this Coherent Radiation model 467 device are discussed in detail in Appendix B. As shown in the figure, the intracavity acousto-optic shutter at the output end of the laser was left in place for reasons to be made clear.

With this device in place, the cavity length of the laser could be determined by measuring the resonant frequency of the laser operating in the CW mode. This was done by coupling an EG&G SGD 444 photodiode (PH-2 in Fig. 6) to a spectrum analyzer (either a Tektronix 7L13 coupled to a Tektronix 7633 oscilloscope or a Hewlett-Packard 8557A coupled to a Hewlett-Packard 184B storage oscilloscope). This frequency centered at about 103.82 (±0.05) MHz, which translates to a cavity length of 144.38 (±0.05) cm.

The laser power (peak power per pulse) was varied by a suitable combination of the laser tube current setting and the optical density (OD) of the variable neutral density wedge. A fraction of the beam (∿20%) was split off using a microscope slide set at 45° to the laser axis. This portion of the beam was then deflected onto a fast photodiode (PD-1 in Fig. 6) of the avalanche type (Spectra-Physics model 403) which was protected from saturation by interposing a 0.96 OD reflective filter in the deflected beam. The output of PD-1 was then coupled to a Hewlett-Packard 184B storage oscilloscope, equipped with a model 1811A sampling plug-in and 1104A trigger-countdown unit, via a model 1430C sampling unit and 1106B tunnel diode. The sampling unit was triggered in synchrony with the RF signal of the mode-locker driver (monitored by a Hewlett-Packard model 5248M frequency counter), thus producing stable displays of the mode-locked pulses on the sampling oscilloscope.

Figure 7 shows oscillographs of the CW and mode-locked frequency spectra (A and B, respectively) and a typical display of mode-locked pulses in the time domain (C). In each of these cases, the H-P 184B storage oscilloscope was used in conjunction with the H-P 8557A spectrum analyzer (A and B) or the sampling accessories listed above (C).

Calibrations of mode-locked laser output were made essentially as described in the System Calibration system and Figure 2, except that the output of PD-2 (Fig. 6) was coupled to a Clevite Brush Mark 220 strip chart recorder through an RC filter with $\tau = 1/RC \sim 56$ msec (i.e., R = 1 kΩ, C = μ56 fd). This permitted a stable record of each train of mode-locked pulses to be compared against the output of the ballistic thermopile/microvoltmeter assembly (see Fig. 8). Calibration of this unit in SAM/RZL immediately prior to these experiments gave 202.9 μV/J.

Because of the observed power fluctuations of the mode-locked laser during warm-up and the clear possibility of error in the calibration procedures (e.g., a slight misalignment of the beam deflected onto PD-2), power calibrations were run immediately before and immediately after each daily series of exposures. When there was a relatively long hiatus (> 2 hours) between sets of exposures, a power calibration was run during that interval.

As in the case of other short pulses, shuttered exposures of 3 sec were used to activate the ballistic thermopile; thus, the equivalent peak pulse power for a 1-μV deflection of the microvoltmeter (i.e., 1 $\mu V_k$) achieved in 3 sec is given by:

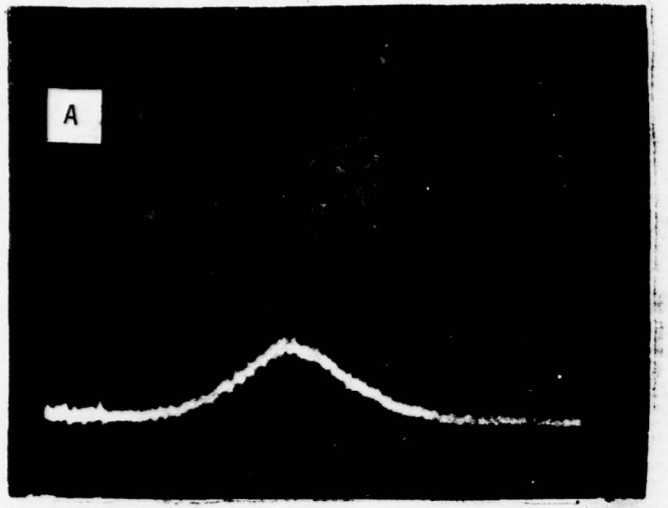


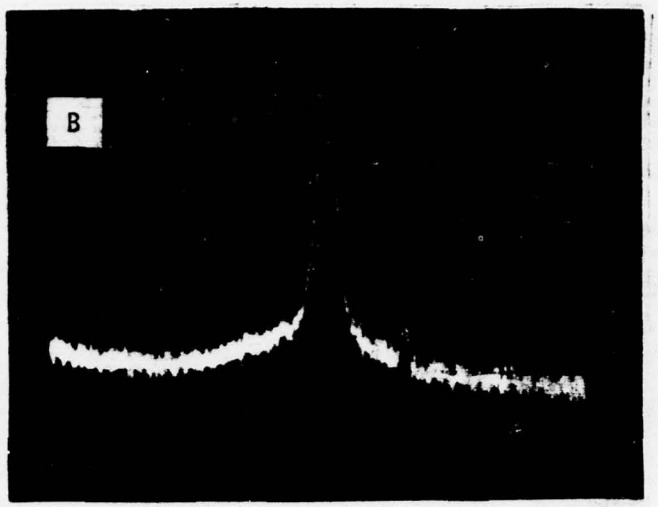


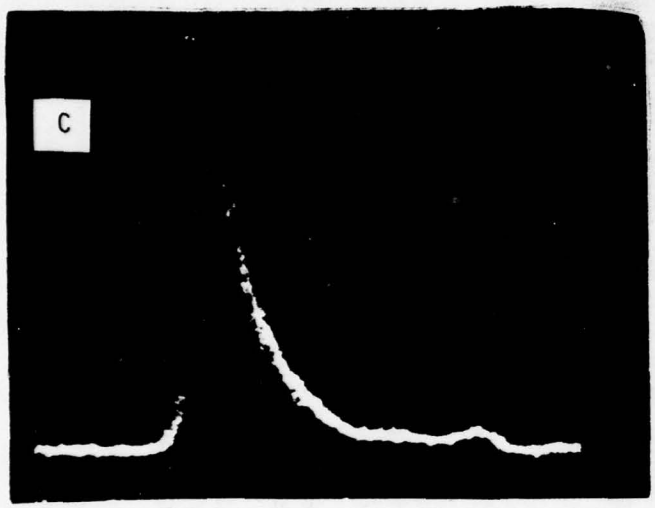


(A) and (B): Frequency spectra of CW and mode-locked laser outputs, respectively, obtained with Hewlett-Packard 8557A spectrum analyzer and H-P 184B storage oscilloscope. Resolution: 10 kHz; bandwidth: 100 kHz/cm; amplitude: 10 dBm/cm (referred to -40 dBm). Peak frequencies both 103.854 MHz.

(C): Sampled output of Spectra-Physics 403 avalanche photodiode showing mode-locked pulses sampled at 51.92 MHz. Vertical deflection: 10 mV/cm; horizontal: 500 psec/cm. The nominal rise- and fall-times of the photodiode are 150 and 200 psec, respectively. Thus the nominal pulsewidth, ~250 psec, can only be inferred.

Figure 7. Oscillographs of CW and mode-locked 514.5-nm laser output in frequency and time domains.

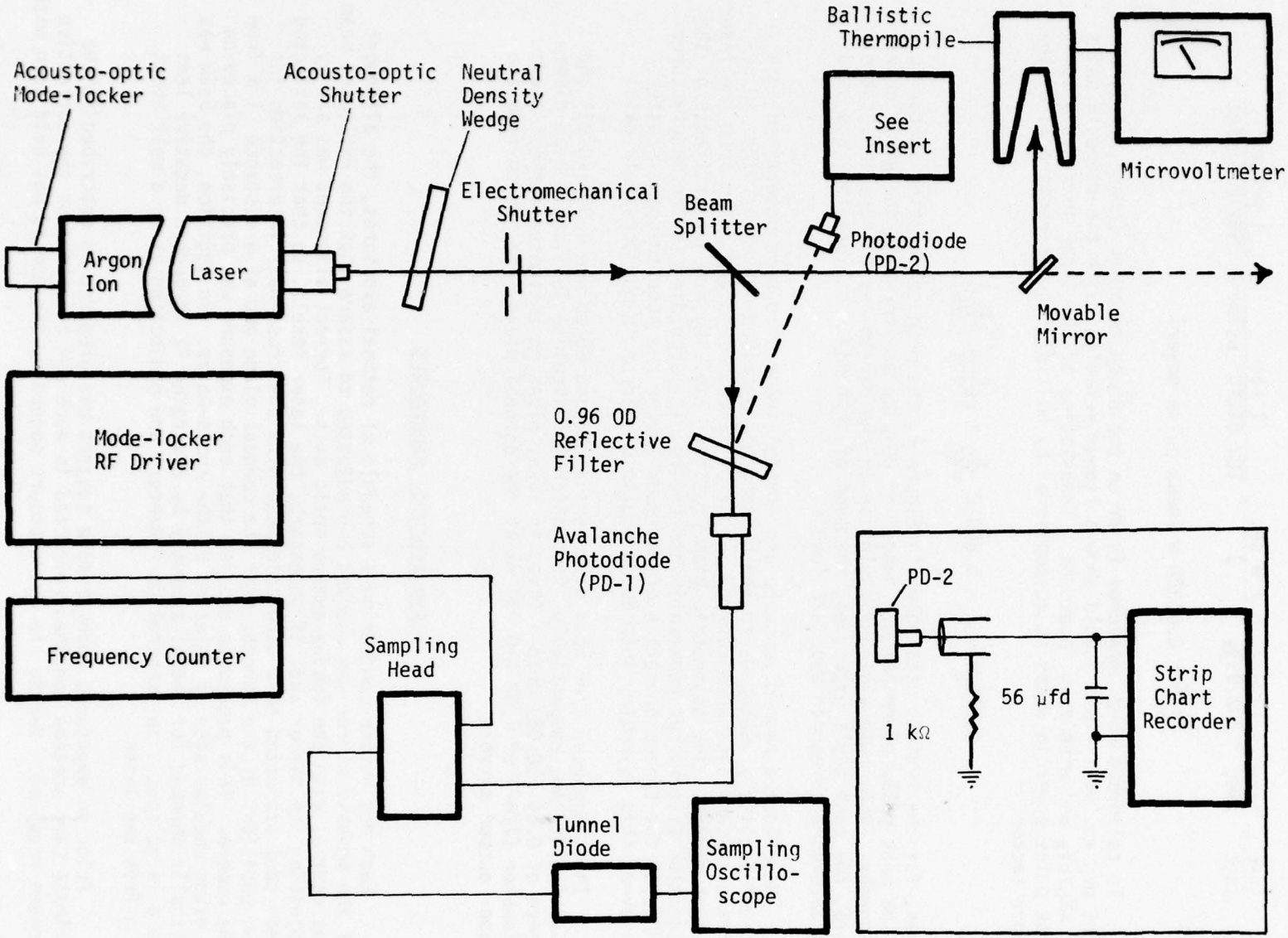


Figure 8. Block diagram of experimental setup for power calibration of mode-locked laser pulses.

$$\frac{1\mu V_k}{3sec} = \frac{1\mu V_k}{3sec} \times \frac{1\ J}{202.9\mu V_k} \times \frac{1\ W\ sec}{J} \times \frac{1\ sec}{103.84\times10^{6}\ pulse} \times \frac{1\ pulse}{250\times10^{-12}\ sec}$$

or:

$$\frac{1\mu V_k}{3sec} = 0.06328\ W\ (peak\ pulse\ power)$$

To calibrate PD-2, measured in mV on the Brush recorder (hence, $mV_b$), we plot $mV_b$ vs. $\mu V_k$. This should show a linear relation, with the slope in units of $mV_b/\mu V_k$ and with zero intercept. Translation of the slope in $mV_b/\mu V_k$ to peak pulse power in watts is accomplished by multiplying its reciprocal by the above factor:

$$\text{Calibration} = 0.06328\ \frac{W}{\mu Vk} \times \frac{1}{\text{Slope}}\ \left(\frac{V_k}{mV_b}\right)$$

Thus, for the typical data shown in Figure 9, the mean calibration factor is ~6 mW peak pulse power per $mV_b$ output of PD-2 as monitored on the strip chart recorder. There was a slight variation in the day-to-day calibration; therefore, for each day's exposures, the mean of that day's calibrations was used to determine threshold exposure levels.

Mode-locked beam-divergence and corneal image size were determined in a manner precisely analogous to the procedures described above for other pulsewidths. Beam scans were carried out at distances of 55 and 80 cm from the laser output mirror. The asymmetric beam profiles (Fig. 10) are not artifacts of the detection system, but apparently are the result, according to the manufacturer (39), of the tandem operation of the mode-locker and acousto-optic shutter. However, this asymmetry introduces negligible error in our threshold data.

Thus, *apparent* $1/e^2$ beam diameters at 55 and 80 cm are 1.30 (±0.02) and 1.46 (±0.02) mm, respectively, from which we calculate full-angle beam divergence of 0.64 (±0.08) mrad. This, in turn, gives an estimated corneal image diameter ($1/e^2$) of 1.52 (±0.03) mm at the corneal plane, viz. 90 cm from the laser output mirror.

## EXPERIMENTAL PROCEDURES

Each day before commencing a schedule of retinal exposures, the alignment of the movable mirror was checked and adjusted to assure that the reflected beam was coaxial with the fundus camera optic axis. Correct alignment was set by adjusting the mirror and, if necessary, the laser itself, so that the reflected beam spot projected on a card coincided with the cross-hair intersection for two positions of the target, near the corneal plane and at a distance 1 m from the camera. This procedure ensured that each exposure was precisely placed on a given macular site as selected by the cross-hairs. In addition, the beam was visually checked for radial symmetry by diverging it through a negative lens to a large spot size (several cm diameter) and projecting it on a wall about 3 m from the laser.

Prior to exposure, each primate subject was prepared as described in the Primate Care section and then refracted in each eye to determine the corrective lenses required. During the eye exposure sequence, the eyelid was held open with

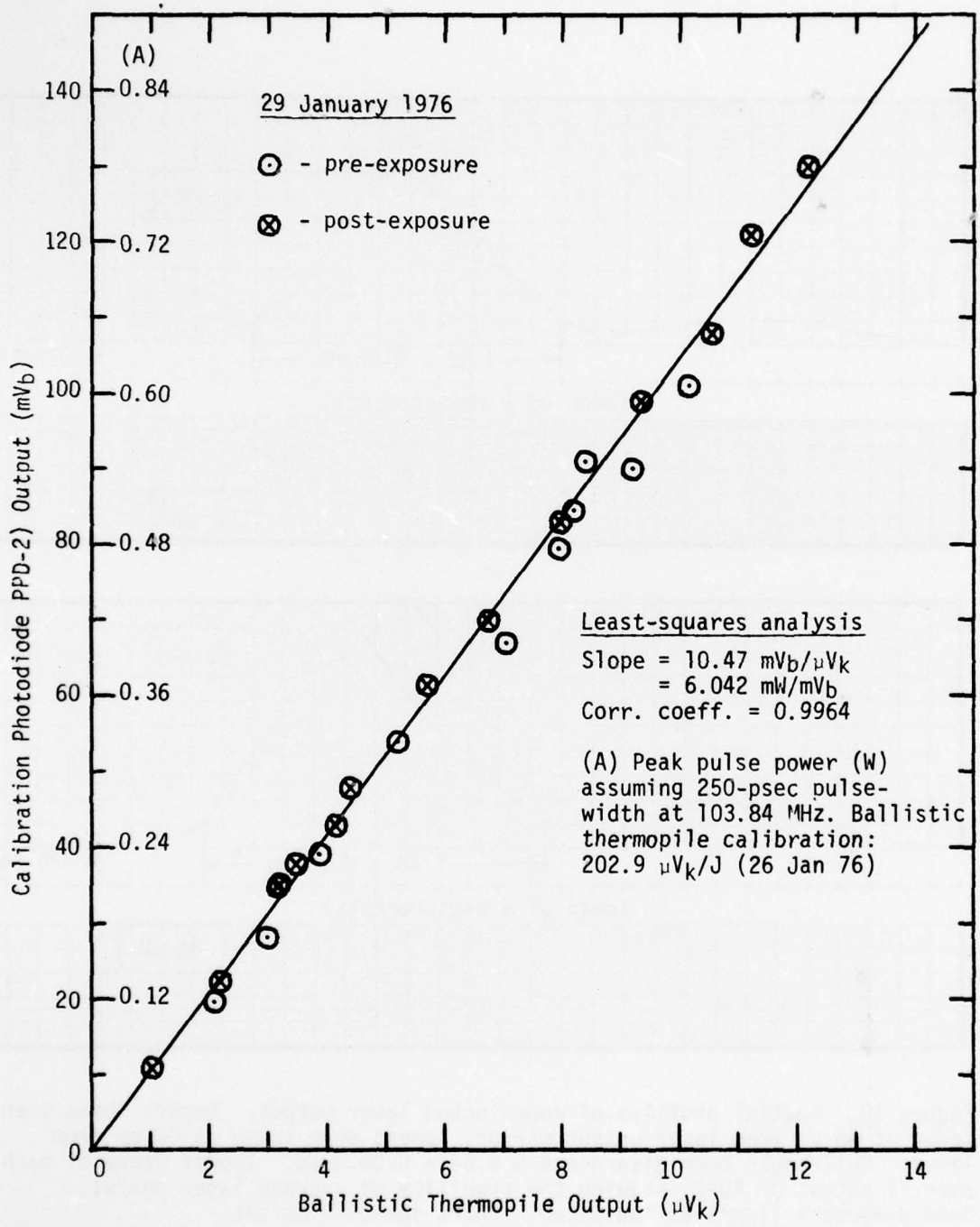


Figure 9. Typical power calibration data for mode-locked laser output.

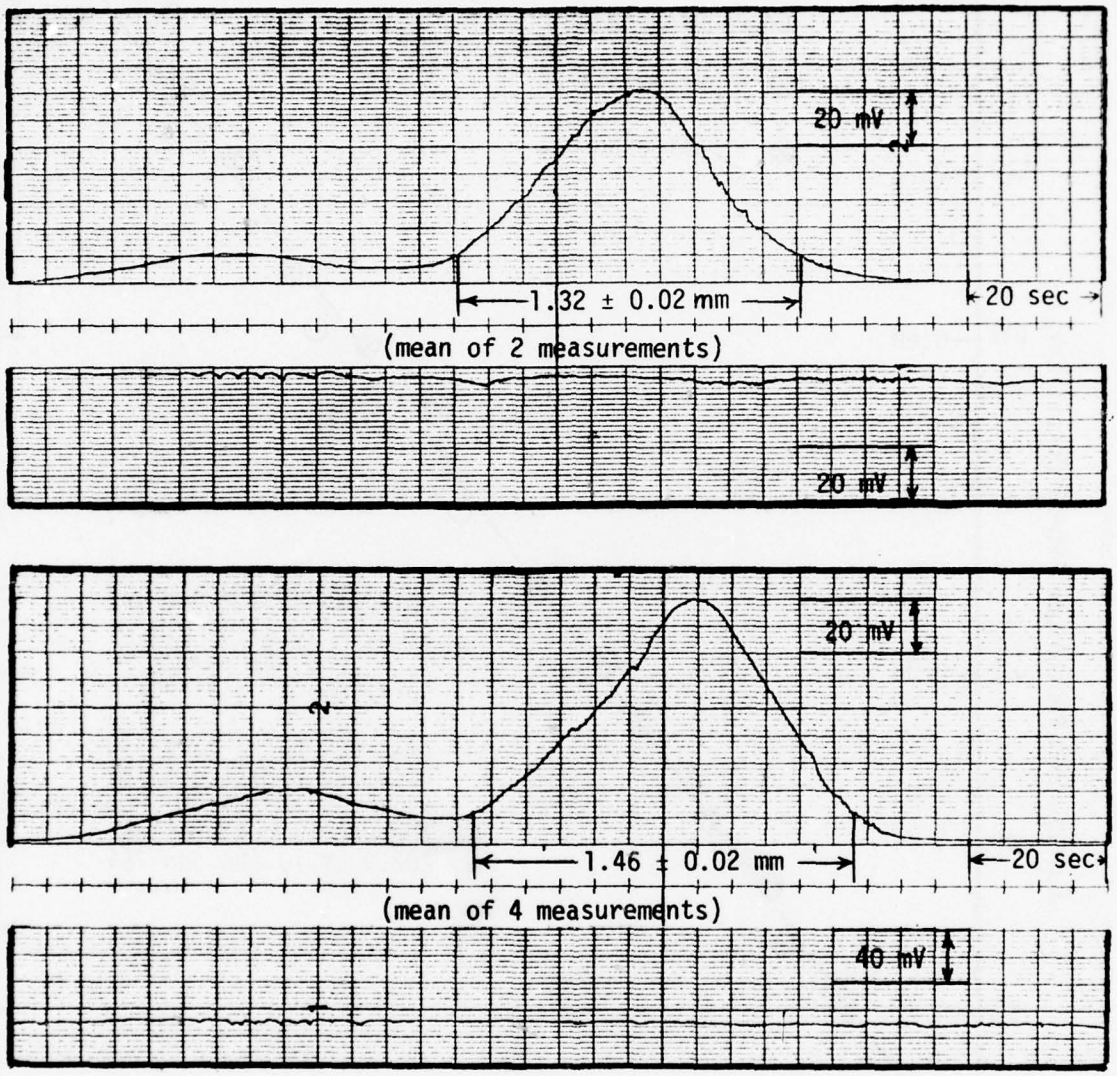


Figure 10. Spatial profiles of mode-locked laser output. Upper: beam scan taken at 55 cm from laser output mirror; lower: scan taken at 80 cm from laser. Full-angle beam divergence $\approx$ 0.64 ± 0.08 mrad. (Lower trace of each pair is output of PD-2, showing the stability of average laser output.) Beam diameters ($1/e^2$) as indicated. Chart speed: 5 mm/sec.

a stainless steel speculum and the cornea was irrigated frequently with normal saline to maintain optical clarity.

Eight marker lesions, four arranged vertically and four horizontally, were placed adjacent to the macula to define the coordinate positions for the 16 test exposures within the macula, as shown in Figure 11. The 16 exposure intensities (peak pulse power) to be used were determined as follows. Based on previous experiments on trial exposures of one or two animals, a preliminary ED50 was estimated for each exposure condition. Then 16 power levels, spaced uniformly on a log dose scale, were tabulated such that the estimated value was half-way down the scale and twice this power was at the top. This normally yielded a range in which the maximum power was about 3.7 times the minimum. The 16 exposures were delivered to the eye in a random sequence, with a different randomization for each eye. The sequence was unknown to the eye examiner so that his lesion evaluations would be unbiased.

Immediately prior to exposure, standard retinoscopy was performed on each eye to find the refractive error in white light. The degree of error in each meridian was measured to the nearest 0.25 diopter. In general, no corrective lens was used if the error was within ±0.5 diopter. Eyes found to have refractive error greater than ±2.5 diopters or any cylindrical error were not used in the experiments.

If the dioptric error was greater than ±0.5, a corrective lens was interposed in the laser beam, in which case an additional correction was applied to compensate for the distance (9 cm) between the corrective lens and the eye. This was computed from the relation $F_y = F/(1 + D_yF)$; where $F_y$ is the corrected power for the lens distance ($D_y$) measured from a plane 1.5 cm in front of the cornea (i.e., $D_y$ = 9-1.5 cm), and F is the lens power uncorrected for distance. This distance correction was very small, and for most eyes, turned out to be less than 0.25 diopter.

In experiments where a corrective lens was required, its transmittance was measured in the laser beam in the CW mode. The transmittance was taken to be the ratio of beam power (as measured by the photodiode) with the lens in place to that without the lens, averaged over a set of 10-15 readings. The exposure energies as determined from the photographs of the oscilloscope traces were corrected by the transmittance factor. Transmission values for all lenses used were found to cluster around 92%.

The time that each exposure was made was recorded to the nearest minute. A photograph or strip chart record of each pulse or pulse train was labeled with the exposure number and the oscilloscope or records scale settings for subsequent computation of laser power and pulsewidth. The designated retinal sites were then examined ophthalmoscopically at 1 hour or 24 hours post-exposure using a simple lesion/no-lesion evaluation. In other words, no attempt was made to quantify retinal damage severity for the purposes of statistical analysis. Preliminary ED50 thresholds were calculated on a Wang 700B programmable calculator using the method of probits, as discussed in Appendix A. Tabular data on each subject eye were submitted to USAFSAM, Biometrics Division for final statistical analysis. The latter values are reported here (See Appendix A).

Normally, thresholds were calculated from observations of at least ten eyes. In some cases, more eyes were exposed and examined, especially if initial

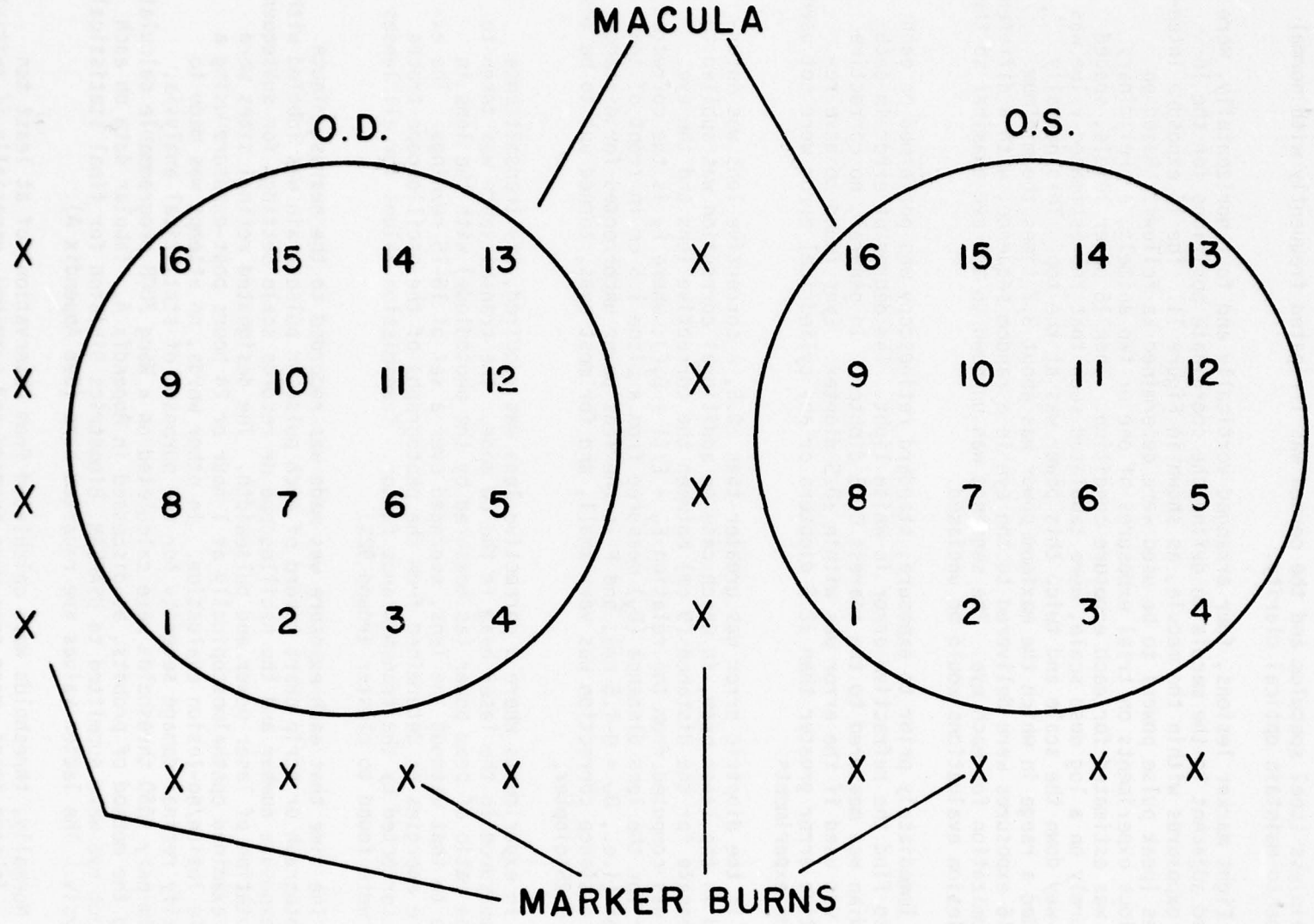


Figure 11. Diagram of macular exposure sites on rhesus retina.

results showed wide variability or were otherwise questionable. In other cases, fewer than ten eyes were used, principally because of time limitations on the total program imposed by nonavailability of needed laser components. These cases are noted in the Results section, and introduced negligible, if any, discrepancies. In fact, we found that highly reproducible threshold data, with good statistical correlations, could be obtained with as few as four eyes.

## RESULTS

### Single-Pulse Experiments

Thresholds (ED50) for retinal exposure to single pulses of 514.5-nm laser radiation were determined for the following pulsewidths: 40 and 10 μsec, and 1, 10, 100, and 500 msec. The results are listed in Table 1 and shown graphically in Figure 12 on a log-log scale. We also report here, for the first time, some limited data obtained at 2 μsec pulsewidth. For comparison, data from previous studies (12, 15, 24, 27, 29) in the visible region are also included in Figure 12. The solid curve represents the empirical relationship (40):

$$ED50(mW) = 7.466t^{-.1502} + 1.030(10)^{-3}t^{-1} \qquad (1)$$

for $t \geq 10^{-5}$ where t is exposure time (pulsewidth) in seconds. For $t \leq 10^{-5}$, a constant energy of 1.89 μJ is used. This is the mean of the three experimental estimates in this region.

The trend of the data is clear: at short pulsewidths (40 μsec or less) the thresholds appear to converge to a constant energy dose of about 2μJ at the cornea; i.e., for pulse widths from about 2 to 40 μsec, the negative slope of log (ED50) vs. log (pulsewidth) approaches unity. For much longer single-pulse exposures (greater than 100 msec), the rate of change of threshold in log, log units appears to be constant; i.e., the rate of decrease in threshold is proportional to the threshold and inversely proportional to the time.

As noted previously by Vassiliadis et al. (25) and Sanders and Hemstreet (31), there is no significant trend among data throughout the visible range included in the figures. However, it should be noted that all of the data shown were obtained using a one-hour post-exposure damage criterion. Recent results obtained by Gibbons and Allen (3,4) and Ham et al. (5,6) suggest that by using a different damage criterion (e.g., 24 hours post-exposure), significantly lower thresholds are obtained. Ham (5,6) has attributed this phenomenon to unspecified photochemical processes. As we shall demonstrate later in this report, photobiological processes, perhaps involving the photoreceptors themselves, can be invoked to explain non-thermal retinal injury observed in the case of certain repetitive-pulse exposures.

### Repetitive-Pulse Experiments

Approximately 350 rhesus eyes were exposed in a series of systematic experiments in which pulsewidth, repetition frequency and pulse-train duration were varied at a fixed wavelength of 514.5 nm. Of this total, about 330 eyes were used for statistical evaluation of threshold data. Table 2 lists the matrix of parameter variations for all repetitive-pulse exposures except mode-locked pulses, which are discussed in a later section.

TABLE 1. SINGLE-PULSE RETINAL DAMAGE THRESHOLDS AT 514.5 nm

| Pulsewidth | ED50 on cornea: Peak pulse power | ED50 on cornea: Energy per pulse | 90% Confidence intervals[a] | No. of eyes | Notes Reference |
|---|---|---|---|---|---|
| 2 µs | 1.15 W | 2.31 µJ | .780-1.70 W | 2 | b |
| 4 | 473 mW | 1.89 | - | - | c |
| 6 | 315 | 1.89 | - | - | c |
| 10 | 161 | 1.61 | 158-165 mW | 5 | b |
| 10 | 176 | 1.76 | 153-202 | 30 | (12)[d] |
| 20 | 89.4 | 1.79 | 74.3-107.7 | - | c |
| 30 | 70.0 | 2.10 | 59.6-82.4 | - | c |
| 40 | 39.9 | 1.60 | 35.8-44.5 | 10 | b |
| 40 | 50.5 | 2.02 | 42.4-60.0 | 18 | (15) |
| 50 | 53.7 | 2.68 | 46.2-62.3 | - | c |
| 100 | 46.7 | 4.67 | 44.1-49.5 | 19 | b |
| 1 ms | 21.3 mW | 21.3 µJ | 20.5-22.1 mW | 20 | b |
| 10 | 18.0 | 180 | 17.4-18.5 | 20 | b |
| 50 | 11.7 | 587 | 10.2-13.4 | - | c |
| 100 | 10.6 | 1.06 mJ | 9.9-11.3 | 19 | b |
| 500 | 6.9 | 3.45 | 6.5-7.3 | 10 | b |
| 500 | 9.4 | 4.71 | 9.0-9.9 | 16 | (3) |
| 5 sec | 6.4 mW | 32 mJ | 6.0-6.8 mW | 20 | (3) |
| 30 | 5.4 | 162 | 4.9-5.9 | 7 | (3) |
| 120 | 4.4 | 526 | 4.1-4.6 | 21 | (3) |
| 1000 | 1.8 | 1818 | 1.7-1.9 | 10 | (3) |

[a]Methods of calculating 90% confidence limits given in Appendix A for experimental and predicted estimates.

[b]This work.

[c]4 - and 6-sec estimates are interpolated, assuming constant energy of 1.89 µJ. All others are calculated from equation 1, p. 27.

[d]Thresholds are from SAM analysis of original data.

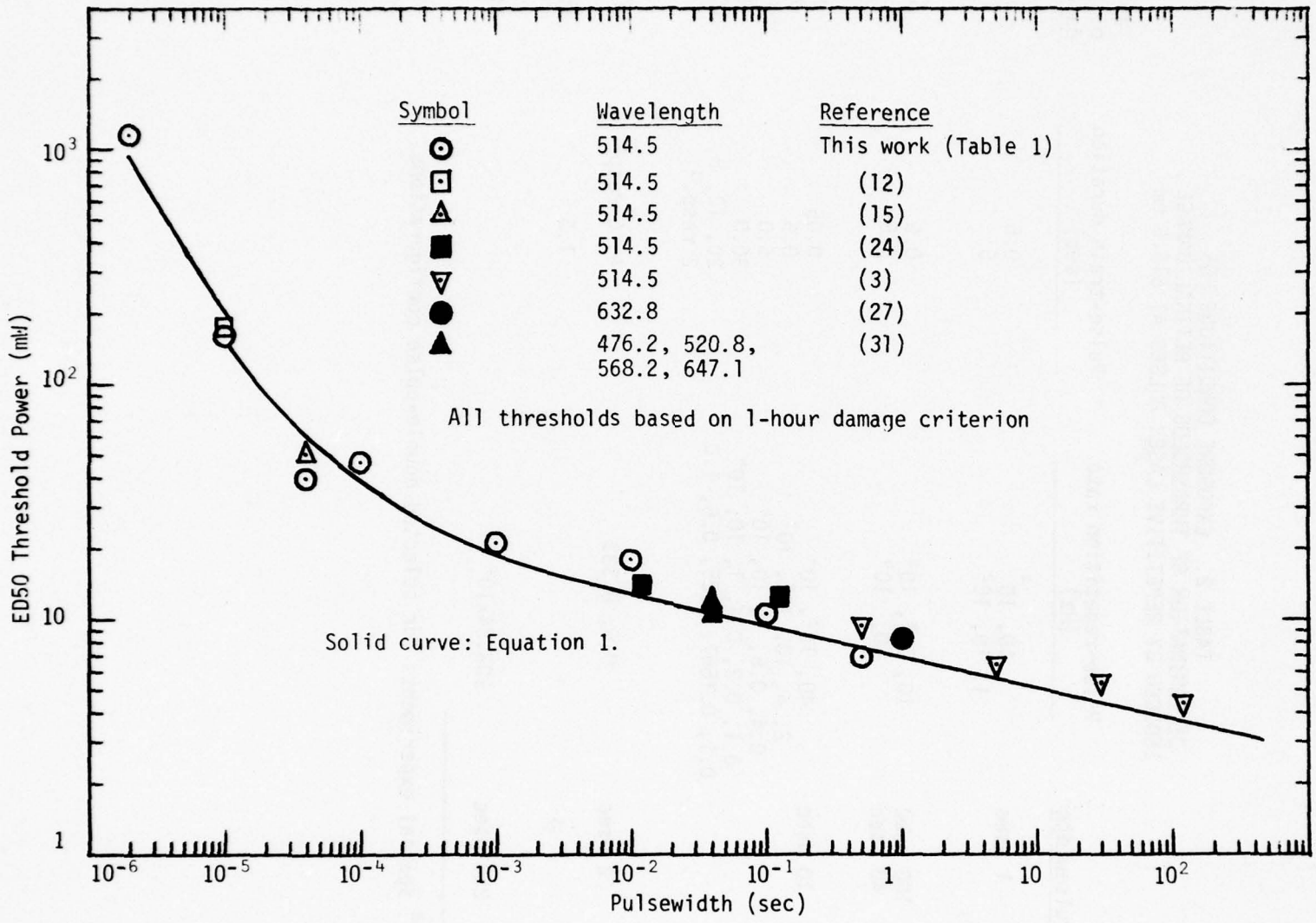


Figure 12. Summary of single-pulse retinal thresholds for visible laser radiation.

TABLE 2. EXPOSURE CONDITIONS FOR DETERMINATION OF THRESHOLDS OF RETINAL DAMAGE INDUCED BY REPETITIVE LASER PULSES AT 514.5 nm

| Pulsewidth | Pulse-repetition rate (Hz) | Pulse-train duration (sec) | Table of data |
|---|---|---|---|
| 1 msec | 10, $10^2$ | 0.5 | 3 |
| | 1, 10, $10^2$ | 5 | 4 |
| 100 µsec | 10, $10^2$, $10^3$ | 0.5 | 5 |
| 40 µsec | 10, $10^4$ | 0.5 | 6 |
| 10 µsec | 40, $10^2$, $10^4$ | 0.05 | 7 |
| | 2, 4, 10, $10^2$, $10^3$ | 0.5 | 7 |
| | 0.4, 0.6, 1, 10, $10^4$ | 5.0 | 8 |
| | 0.1, 0.2, 0.4, 1, 10, $10^4$ | 30.0 | 9 |
| | 0.1, 0.1667, 0.25, 0.6, 1.0 | 20, 12, 8, 3, 2 resp.[a] | 10 |
| 2 µsec | 0.5, 0.333 | 4, 6 resp[a] | 10 |
| | | 1.5 | 10 |
| 250 psec | $103.84 \times 10^6$ | | 11 |

[a] Special experiments for selected double-pulse configurations.

Note that the data points for 2-μsec pulses are included here but must be considered preliminary. It was considered necessary to expose at least ten eyes to obtain valid threshold data. Statistics do tend to improve in proportion to the number of eyes exposed; however, as we shall demonstrate below, reasonably good threshold estimates can be obtained from as few as four eyes. Hence, we tend to place limited confidence in the two-eye exposure data.

Repetitive-pulse data are summarized in tabular and graphical form in the order listed in Table 2. In addition, for each set of exposure conditions for which we have carried out IITRI model (2) calculations, these results are included in the respective figures. Summaries of repetitive-pulse data for 0.5 and 5 sec trains of 1-msec pulses are shown in Table 3 and Figure 13 and in Table 4 and Figure 14, respectively. In each case we include the low- and high-frequency limits (i.e., single-pulse and effective CW limit, respectively) to show the full range of threshold data for each repetitive-pulse configuration. Thus, for 0.5-sec trains of 1-msec pulses, the high-frequency (CW) limit is a single 0.5 sec pulse; the low-frequency end is set by the threshold for single 1-msec pulses. Note that the frequencies of single-pulse data are displayed as the reciprocals of the respective pulse train durations, an artifice which is employed only for convenience.

For both 0.5- and 5.0-sec trains of 1 msec-pulses, the experimental retinal threshold data are completely consistent with computer predictions (2) based solely on thermal damage mechanisms. Evidently, one could achieve agreement between predicted and observed thresholds by adjusting the RIM parameter (i.e., $1/e^2$ retinal image radius) to a suitable value. Thus, in Figure 13, a RIM of $\sim$45 μm would yield complete overlap of computer calculations with actual observations, at least within experimental error. Similarly, in Figure 14, we see that calculations based on an assumed RIM of 25 μm are uniformly low by about a factor of 2, whereas a RIM of 50 μm yields predicted thresholds that are uniformly high by a slightly larger factor ($\sim$2.5). Since retinal temperatures are dependent, to a first approximation, on the square of the retinal image radius, we would have obtained entirely satisfactory agreement with the experimental data for 5.0-sec trains of 1-msec pulses had we chosen a RIM of 40-45 μm for the computer calculations.

In summary, therefore, we find no discrepancy between our threshold data and assumptions of thermal damage mechanisms for repetitive 1-msec laser pulses at frequencies ranging from single pulse to 1 kHz for pulse-train durations of 0.5 and 5 sec.

When we compare experimental data with computer calculations for pulses of shorter duration, however, we begin to see departures from modeled thermal damage estimates. Table 5 and Figure 15 summarize our data for 100-μsec, 514.5-nm laser pulses. In Table 6 and Figure 16, we show the 40-μsec pulsewidth data acquired in this program together with the complementary data of Gibbons and Egbert (14). For 100-μsec pulses in the range of 10 to 100 Hz, there is a departure from the trend predicted by IITRI model calculations (Fig. 15).

Even though model calculations were not carried out for 40-μsec pulses, it can be asserted by extension that departures from thermal behavior appear in about the same frequency range for this pulsewidth. Specifically, the departure from negative curvature seen in the previous displays of IITRI model calculations (Figs. 13-15) is more pronounced when the pulses are separated by 0.1 to 1 sec. Figures 15 and 16 show that 0.5-sec trains of either 100-μsec

TABLE 3. SUMMARY OF ED50 THRESHOLDS
FOR RHESUS MACULAE EXPOSED TO
0.5-sec TRAINS OF 1-msec, 514.5-nm LASER PULSES

| Pulse-repetition rate (Hz) | No. of pulses | ED50 on cornea: Peak pulse power (mW) | ED50 on cornea: Energy per pulse (μJ) | 90% Confidence interval power (mW) | No. of eyes |
|---|---|---|---|---|---|
| (Single 1 msec) | 1 | 21.3 | 21.3 | 20.5 - 22.1 | 20 |
| 10 | 5 | 18.9 | 18.9 | 17.8 - 20.1 | 10 |
| 100 | 50 | 15.0 | 15.0 | 14.4 - 15.7 | 10 |
| $10^3$[a] | 500 | 6.9 | 6.9 | 6.5 - 7.3 | 10 |

[a] CW limit, assumes 500 contiguous 1-msec pulses, or a single 0.5-sec pulse from Table 1.

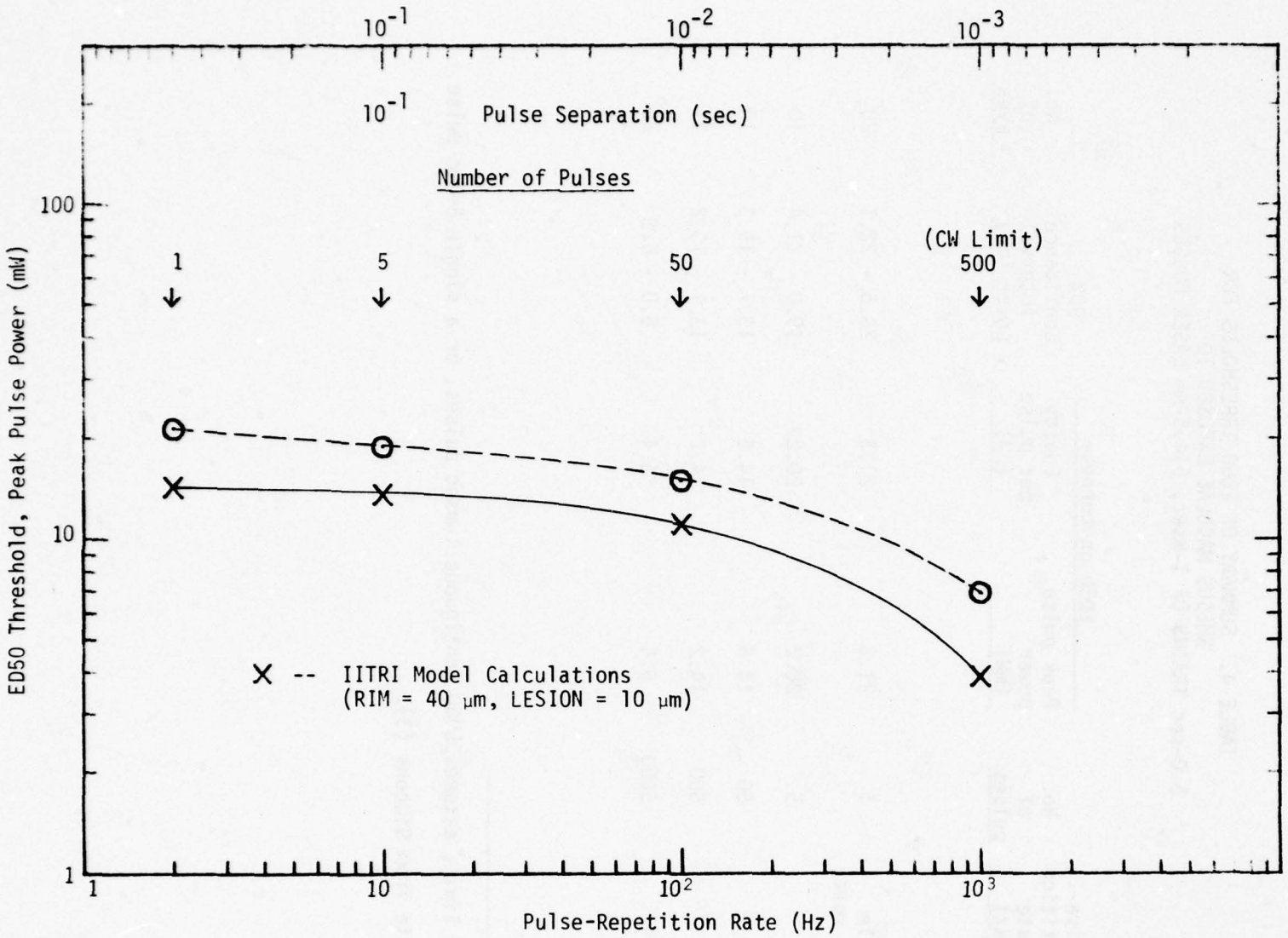


Figure 13. Observed and predicted retinal thresholds for 0.5-sec trains of 1-msec, 514.5-nm laser pulses.

TABLE 4. SUMMARY OF ED50 THRESHOLDS FOR RHESUS MACULAE EXPOSED TO 5.0-sec TRAINS OF 1-msec, 514.5-nm LASER PULSES

| Pulse-repetition rate (Hz) | No. of pulses | ED50 on cornea: Peak pulse power (mW) | ED50 on cornea: Energy per pulse (μJ) | 90% Confidence interval power (mW) | No. of eyes |
|---|---|---|---|---|---|
| Single (1 msec) | 1 | 21.3 | 21.3 | 20.5 - 22.1 | 20 |
| 1 | 5 | 20.2 | 20.2 | 19.0 - 21.4 | 10 |
| 10 | 50 | 14.5 | 14.5 | 13.7 - 15.3 | 10 |
| $10^2$ | 500 | 14.2 | 14.2 | 13.1 - 15.2 | 11 |
| $10^3$[a] | 5000 | 6.4 | 6.4 | 6.0 - 6.8 | 20[b] |

[a] CW limit, assumes 5000 contiguous 1-msec pulses, or a single 5-sec pulse.

[b] Data from Gibbons (3).

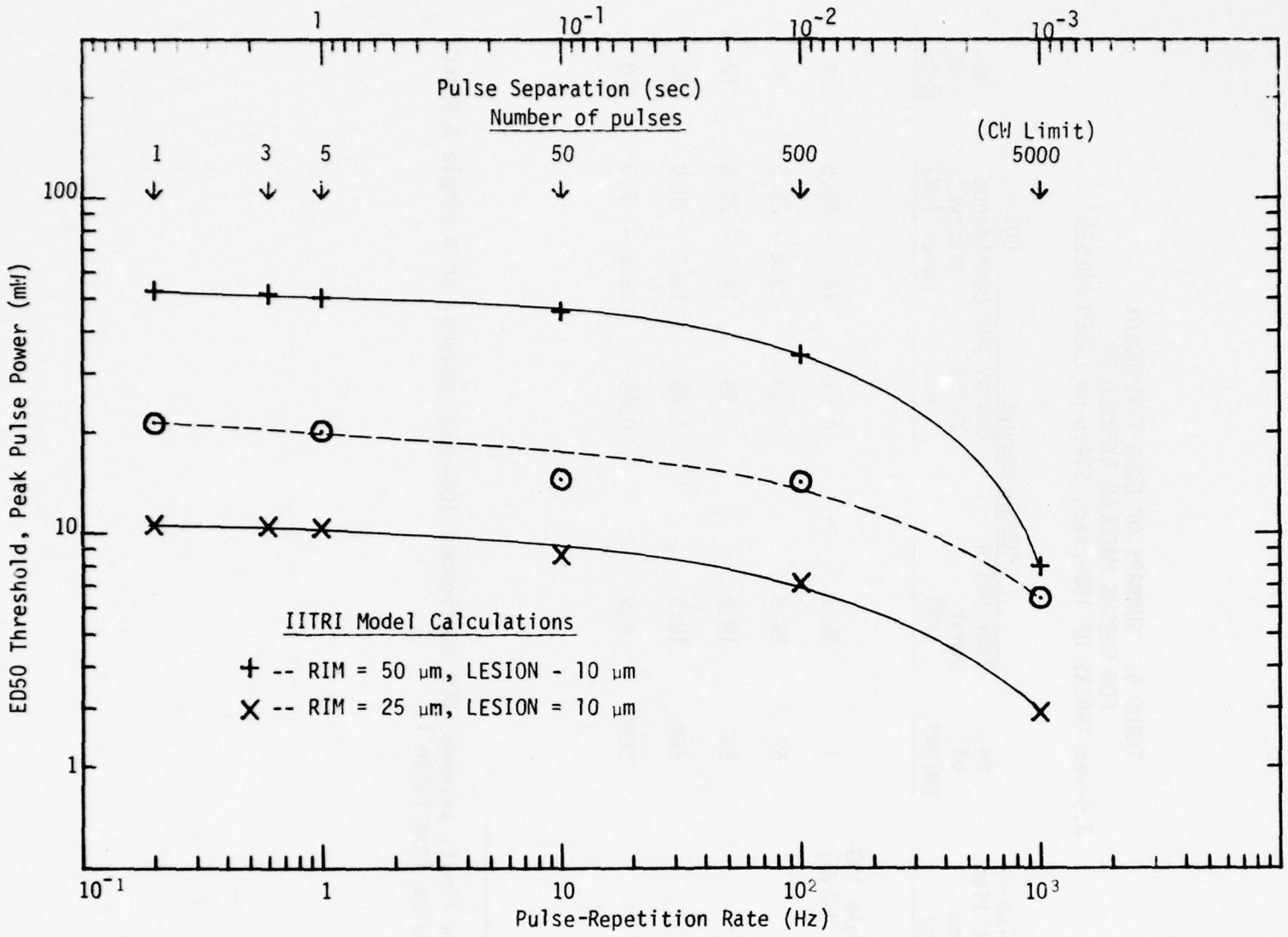


Figure 14. Observed and predicted retinal thresholds for 5-sec trains of 1-msec, 514.5-nm laser pulses.

TABLE 5. SUMMARY OF ED50 THRESHOLDS
FOR RHESUS MACULAE EXPOSED TO
0.5-sec TRAINS OF 100-μsec, 514.5-nm LASER PULSES

| Pulse-repetition rate (Hz) | No. of pulses | ED50 on cornea | | 90% Confidence interval power (mW) | No. of eyes |
|---|---|---|---|---|---|
| | | Peak pulse power (mW) | Energy per pulse (μJ) | | |
| (Single 100-μsec Pulse) | 1 | 46.7 | 4.67 | 44.1 - 49.5 | 19 |
| 10 | 5 | 24.8 | 2.48 | 23.8 - 25.9 | 10 |
| $10^2$ | 50 | 19.9 | 1.99 | 19.1 - 20.8 | 10 |
| $10^3$ | 500 | 19.3 | 1.93 | 18.7 - 20.0 | 10 |
| $10^{4a}$ | 5000 | 6.9 | 0.69 | 6.5 - 7.3 | 10 |

[a]CW limit, assumes 5000 contiguous 100-μsec pulses, or a single 0.5-sec pulse from Table 1.

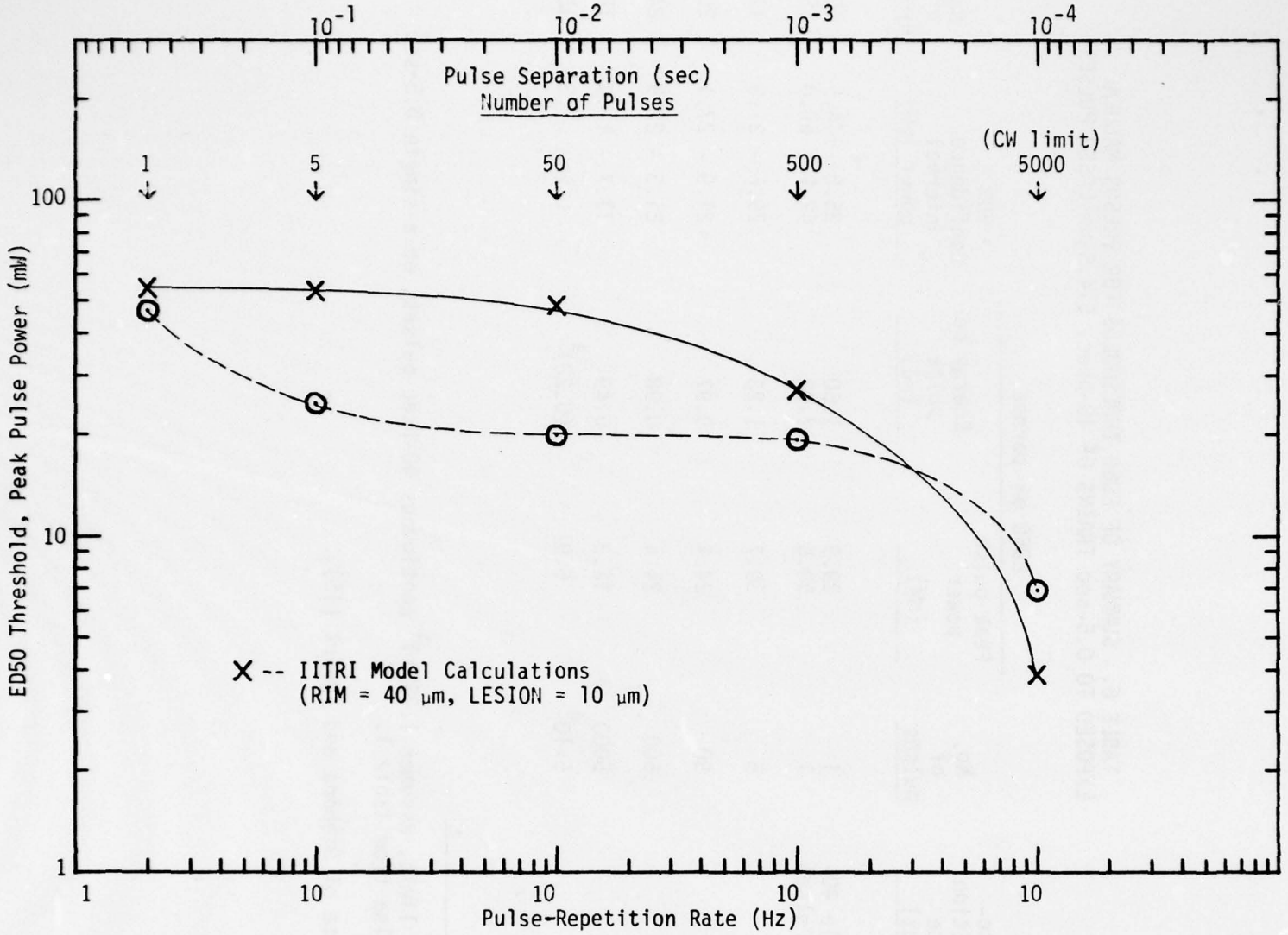


Figure 15. Observed and calculated retinal thresholds for 0.5-sec trains of 100-μsec, 514.5-nm laser pulses.

TABLE 6. SUMMARY OF ED50 THRESHOLDS FOR RHESUS MACULAE EXPOSED TO 0.5-sec TRAINS OF 40-μsec, 514.5-nm LASER PULSES

| Pulse-repetition rate (Hz) | No. of pulses | ED50 on cornea: Peak pulse power (mW) | ED50 on cornea: Energy per pulse (μJ) | 90% Confidence interval power (mW) | No. of eyes |
|---|---|---|---|---|---|
| (Single 40-μsec Pulse) | 1 | 39.9 | 1.60 | 35.8 - 44.5 | 10 |
| | 1 | 50.5 | 2.02 | 42.4 - 60.0 | 18[b] |
| 10 | 5 | 30.7 | 1.23 | 29.6 - 31.9 | 11 |
| $10^2$ | 50 | 24.4 | 0.97 | 21.9 - 27.1 | 20[b] |
| $10^3$ | 500 | 24.4 | 0.98 | 21.3 - 27.9 | 24[b] |
| $10^4$ | 5000 | 12.3 | 0.49 | 11.7 - 13.0 | 10 |
| $10^{5a}$ | $5x10^4$ | 6.9 | (0.28)[a] | 6.5 - 7.3 | 10 |

[a] CW limit, assumes $1.25x10^4$ contiguous 40-μsec pulses, or a single 0.5-sec pulse from Table 1.

[b] Data of Gibbons and Egbert (15).

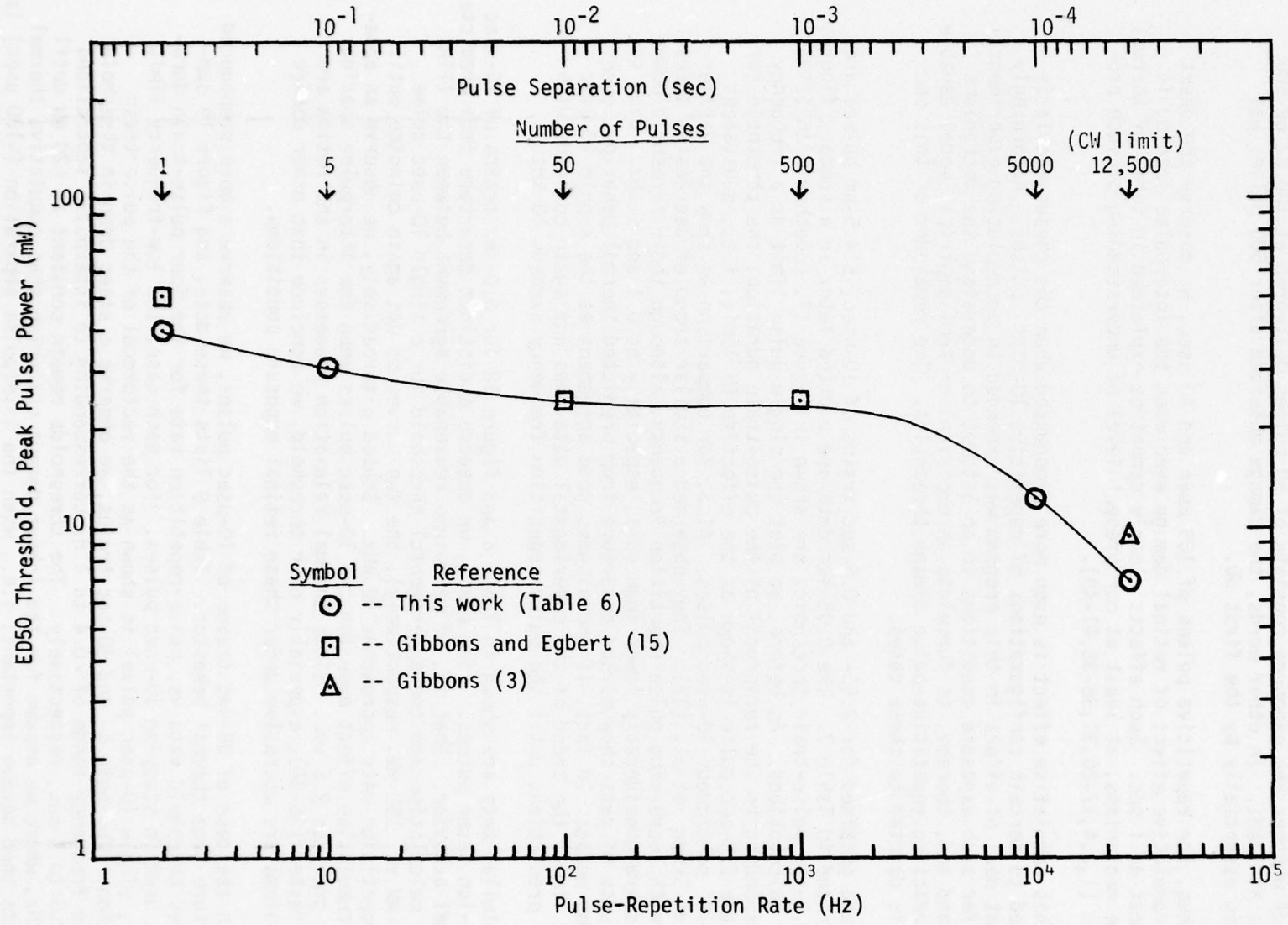


Figure 16. Observed retinal thresholds for 0.5-sec trains of 40-μsec, 514.5-nm laser pulses.

or 40-μsec pulses produce retinal damage at the same peak pulse power regardless of whether the exposure consists of 50 pulses delivered at 100 Hz or 500 pulses at 1 kHz. In other words, the damage observed after 500 pulses was induced essentially by the first 50.

Thus, for repetitive pulses of 100 μsec and 40 μsec, we observe the onset of a cumulative effect of retinal damage even when the interpulse spacing is as great as 1 sec. Such effects clearly cannot be explained in terms of thermal damage mechanisms, at least at our present level of understanding of such processes (1,2,4,17-20,31,36-38,41-49).

This cumulative effect is even more pronounced when the rhesus macula is exposed to certain configurations of repetitive 10-μsec pulses. Accordingly a great deal of effort in this program was expended on accumulating experimental data for such exposure conditions in an attempt to understand the mechanisms involved and, thereby, to formulate an empirical or semi-empirical model capable of predicting repetitive-pulse damage thresholds. The remainder of this section is devoted to these cases.

Data obtained for 0.05- and 0.5-sec trains of 10-μsec, 514.5-nm pulses are summarized in Table 7. The 0.05-sec data are plotted later in a summary figure; the 0.5-sec pulse-train thresholds are shown in Figure 17, together with IITRI model calculations. As before, we plot the single-pulse limit at a frequency corresponding to the reciprocal of the pulse-train duration; the threshold for a single 0.5-sec pulse is shown as the effective CW limit, i.e., equivalent to $5 \times 10^4$ contiguous 10-μsec pulses. Also, for comparison we show the earlier data of Skeen et al. (12). They observed a similar trend of decreasing threshold with increasing pulse-repetition frequency, although their threshold power levels are considerably lower than ours, especially at 0.1 and 1 kHz. Even so, both sets of data show marked departure from predicted thermal behavior, *even for two pulses*. In fact, if one assumes good agreement at the single 10-μsec pulse limit, the trend of the experimental data does not again coincide with model predictions until the pulse-repetition frequency exceeds 10 kHz.

Similar data are shown in Table 8 and Figure 18 for 5.0-sec trains of 10-μsec argon-ion laser pulses. Here again, we observe a distinct departure from predicted thermal behavior. That is, if we assume reasonable agreement between the IITRI model calculation and the experimental threshold for a single 10-μsec pulse ($\leq$200 mW vs. 160 mW, respectively), the two curves do not again coincide until the repetition rate approaches 10 kHz. Stated alternatively, we observe an apparent cumulative effect even for two 10-μsec pulses when the interpulse spacing is as great as 2.5 sec. Since thermal relaxation processes in the retina are much faster (36-38), especially near threshold, we conclude that other damage mechanisms are operative under these retinal exposure conditions.

In the case of 30-sec trains of 10-μsec pulses, we observe a more pronounced departure from thermal behavior. Table 9 lists these data, and Figure 19 summarizes threshold data vs. pulse-repetition rate for the four pulse-train durations used in studying 10-μsec pulses. For each case, the low-frequency limit (i.e., single 10-μsec pulse) is shown as the reciprocal of the pulse-train duration. For both 5- and 30-sec trains, we observe a steep drop in threshold in the frequency range of $\sim$0.4 to 1 Hz corresponding to interpulse separations of $\sim$2.5 to 1 sec, respectively. The thresholds remain constant at $\sim$20 mW until $\sim$10 kHz, where we assume for the 1-hour damage criterion that cumulative thermal effects then become important; i.e., when the interpulse separation ($\sim$100 μsec) is of the same order as thermal relaxation times (36-38). The 24 hour and 1 hour thresholds from Table 9 at 10 Hz for the 30-sec train are significantly different. At 10 kHz, the two thresholds are comparable to the long-term effects reported by Gibbons (3).

TABLE 7. SUMMARY OF ED50 THRESHOLDS FOR RHESUS MACULAE EXPOSED TO 0.05- AND 0.5-sec TRAINS OF 10-μsec, 514.5-nm LASER PULSES

| Pulse-train duration (sec) | Pulse-repetition rate (Hz) | No. of pulses | ED50 on cornea: Peak pulse power (mW) | ED50 on cornea: Energy per pulse (μJ) | 90% Confidence interval power (mW) | No. of eyes |
|---|---|---|---|---|---|---|
| (Single 10-sec pulse) | -- | 1 | 161 | 1.61 | 158 - 165 | 5 |
| | -- | 1 | 176 | 1.76 | 153 - 202 | 30[b] |
| 0.05 | 40 | 2 | 103 | 1.03 | 98.5 - 108 | 10 |
| | 100 | 5 | 79.8 | 0.80 | 77.8 - 81.8 | 10 |
| | $10^4$ | 500 | 40.5 | 0.40 | 38.1 - 42.9 | 11 |
| | $10^{5a}$ | 5000 | $10^c$ | 0.10 | -- | -- |
| 0.5 | 4 | 2 | 113 | 1.13 | 108 - 118 | 9 |
| | 10 | 5 | 67.8 | 0.68 | 66.5 - 69.2 | 6 |
| | | | 67.9 | 0.69 | 62.2 - 74.1 | 30[b] |
| | 100 | 50 | 52.7 | 0.53 | 52.1 - 53.4 | 9 |
| | | | 20.3 | 0.20 | 18.5 - 22.3 | 29[b] |
| | $10^3$ | 500 | 42.5 | 0.43 | 41.2 - 43.8 | 10 |
| | | | 14.7 | 0.15 | 13.7 - 15.8 | 30[b] |
| | $10^4$ ($10^{5c}$) | $5\times10^4$ | 6.9 | 0.07 | 6.5 - 7.3 | 30[b] 10 |

[a]CW limit, assumes 5000 contiguous 10-μsec pulses, or a single 0.05-sec pulse, calculated from equation (1).
[b]Thresholds are from SAM analysis of orginal data of Skeen et al. (12)
[c]CW limit, assumes $5\times10^4$ contiguous 10-μsec pulses, or a single 0.5-sec pulse from Table 1.

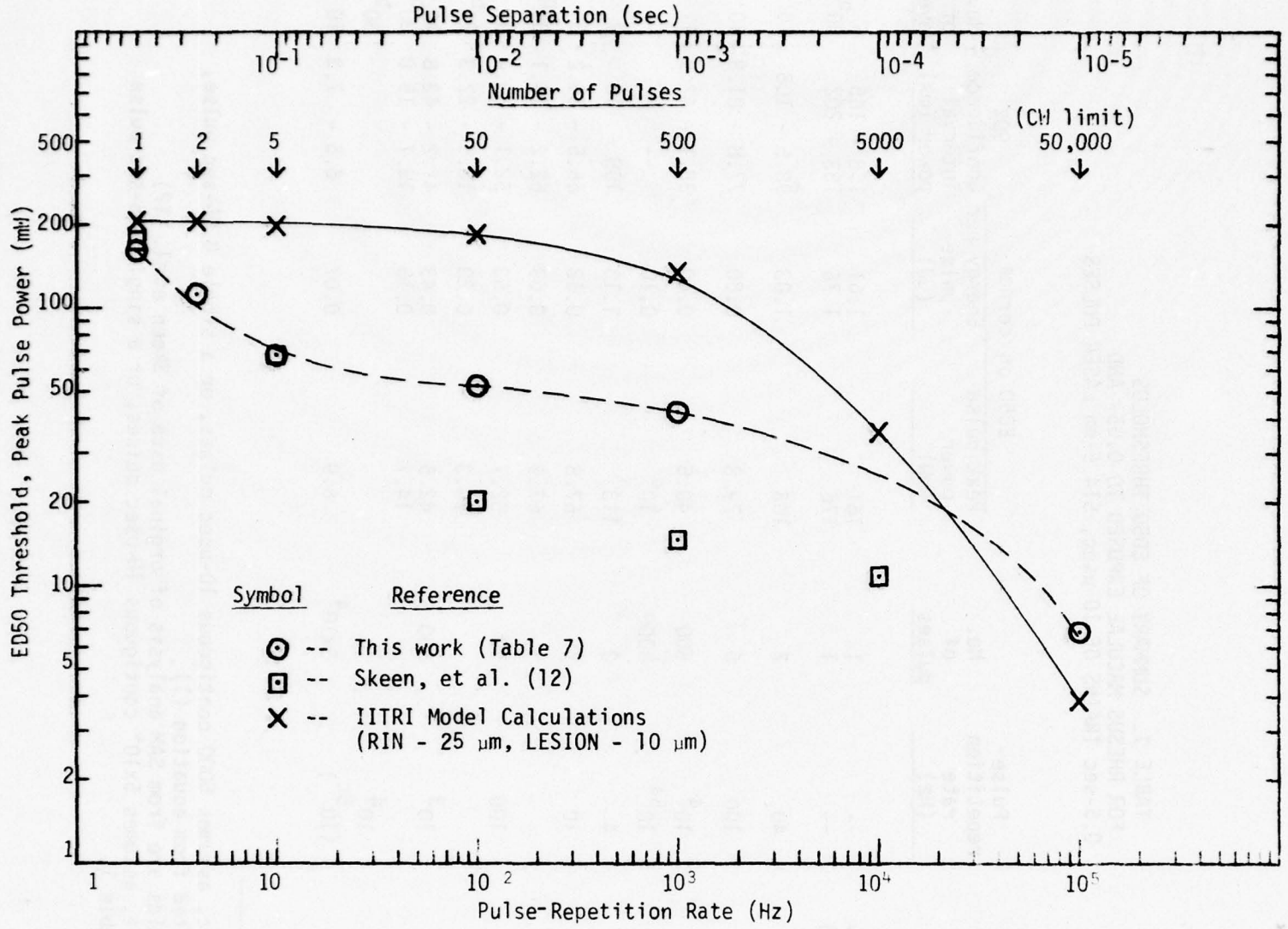


Figure 17. Observed and calculated retinal thresholds for 0.5-sec trains of 10-μsec, 514.5-nm laser pulses.

TABLE 8. SUMMARY OF ED50 THRESHOLDS FOR RHESUS MACULAE EXPOSED TO 5-sec TRAINS OF 10-μsec, 514.5-nm LASER PULSES

| Pulse-repetition rate (Hz) | No. of pulses | ED50 on cornea: Peak pulse power (mW) | ED50 on cornea: Energy per pulse (μJ) | 90% Confidence interval power (mW) | No. of eyes |
|---|---|---|---|---|---|
| (Single 10-μsec pulse) | 1 | 161 | 1.61 | 158 - 165 | 5 |
| 0.4 | 2 | 72.3 | .72 | 69.8 - 74.9 | 11 |
| 0.6 | 3 | 41.3 | .41 | 39.6 - 43.2 | 10 |
| 1 | 5 | 25.0 | .25 | 23.9 - 26.1 | 11 |
| 10 | 50 | 24.9 | .25 | 24.3 - 25.6 | 10 |
| $10^3$ | 5000 | 22.2 | .22 | 21.5 - 22.9 | 10 |
| $10^4$ | $5 \times 10^4$ | 19.2 | .19 | 18.4 - 20.1 | 12 |
| $10^{5a}$ | $5 \times 10^5$ | 6.4 | .06 | 6.0 - 6.8 | 20[b] |

[a] CW limit, assumes $5 \times 10^5$ contiguous 10-μsec pulses, or a single 5-sec pulse.

[b] Data of Gibbons (3).

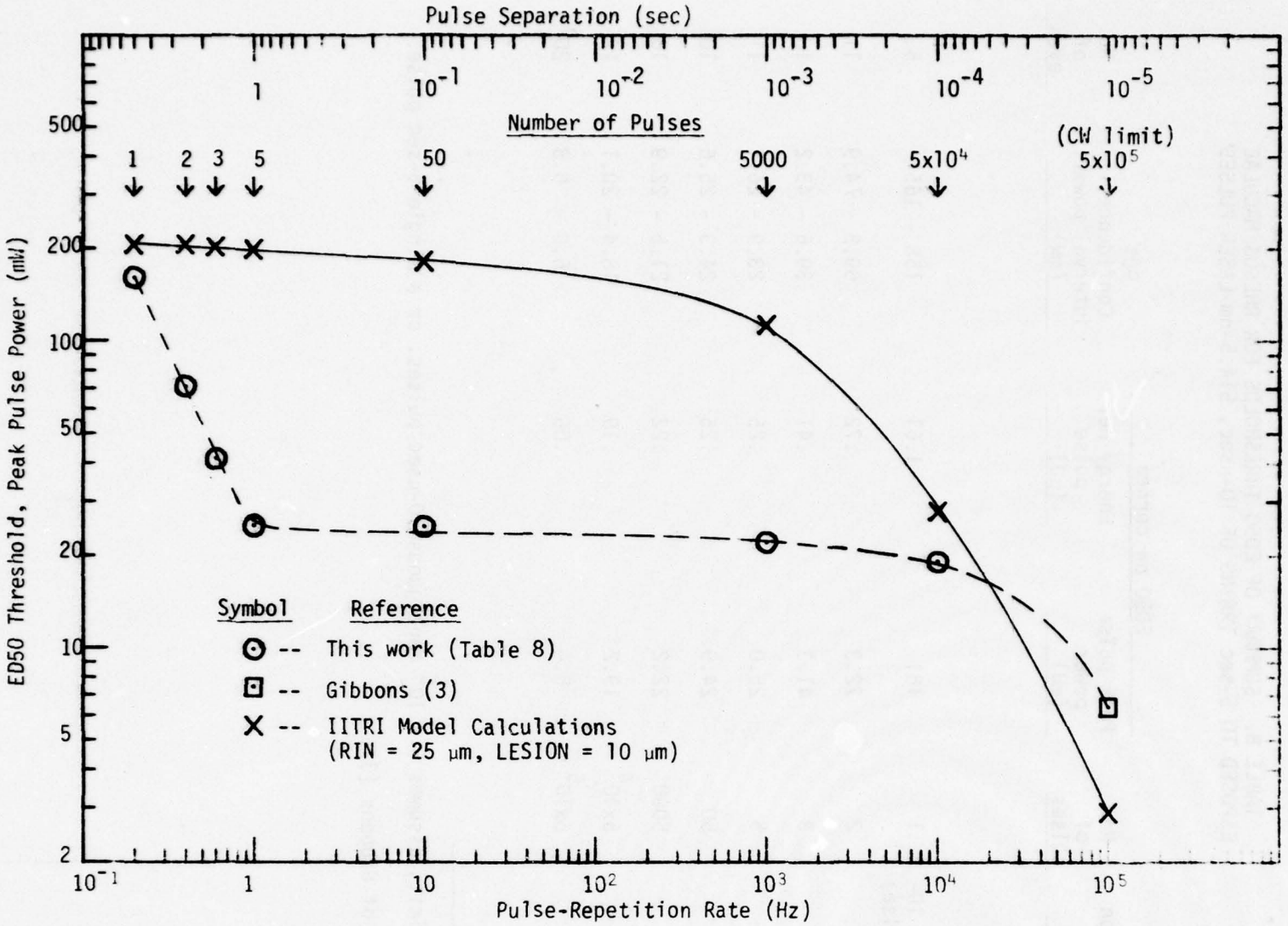


Figure 18. Observed and calculated retinal thresholds for 5-sec trains of 10-μsec, 514.5-nm laser pulses.

TABLE 9. SUMMARY OF ED50 THRESHOLDS FOR RHESUS MACULAE EXPOSED TO 30-sec TRAINS OF 10-μsec, 514.5-nm LASER PULSES

| Pulse-repetition rate (Hz) | No. of pulses | ED50 on cornea: Peak pulse power (mW) | ED50 on cornea: Energy per pulse (μJ) | 90% Confidence interval power (mW) | No. of eyes |
|---|---|---|---|---|---|
| (Single 10-sec pulse) | 1 | 161 | 1.61 | 158-165 | 5 |
| 0.1 | 3 | 150 | 1.50 | 144-158 | 10 |
| 0.2 | 6 | 138 | 1.38 | 130-146 | 10 |
| 0.4 | 12 | 73.0 | 0.73 | 71.2-74.8 | 10 |
| 1 | 30 | 26.4 | 0.26 | 25.4-27.4 | 10 |
| | | 23.9 | 0.24 | 22.4-25.6 | 9[c] |
| 10 | 300 | 22.0 | 0.22 | 21.5-22.5 | 10 |
| | | 17.1 | 0.17 | 15.9-18.4 | 8[c] |
| $10^4$ | $3x10^5$ | 11.0 | 0.11 | 10.1-11.8 | 10 |
| | | 5.0 | 0.05 | 4.5-5.5 | 9[c] |
| $10^5$[a] | $3x10^6$ | 5.4 | 0.05 | 4.9-6.0 | 7[b] |
| | | 2.5 | 0.025 | 2.1-2.8 | 7[b,c] |

[a] CW limit, assumes $3x10^6$ contiguous 10-μsec pulses, or a single 30-sec pulse.

[b] Data of Gibbons (3).

[c] 24-hour damage criterion.

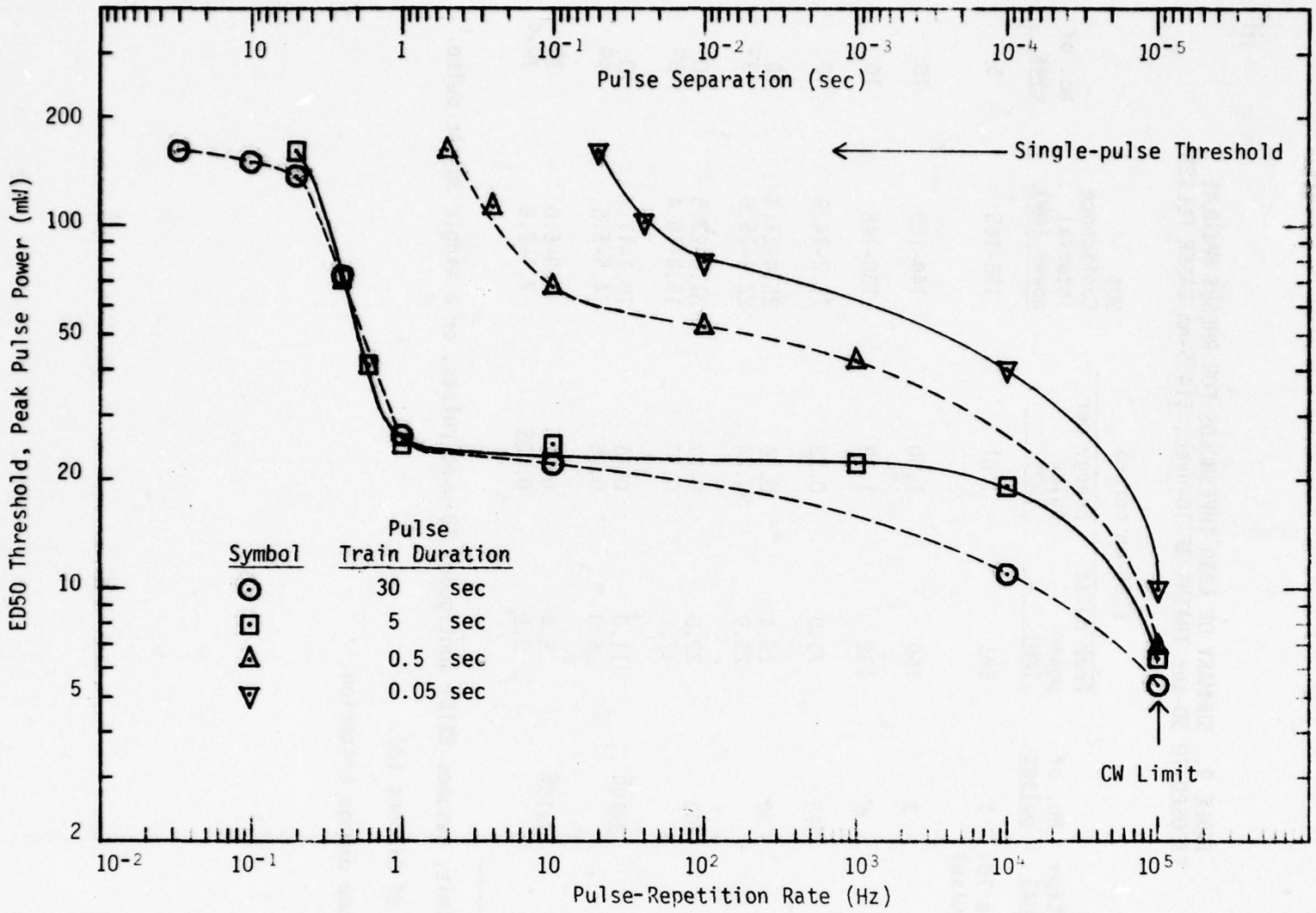


Figure 19. Observed retinal thresholds vs. repetition rate for 0.05-30-sec trains of 10-μsec, 514.5-nm laser pulses for 1-hour damage criterion.

Clearly, each point in the figure represents a discrete number of pulses. Thus for the 30-sec curve, the first six points (left to right) correspond to 1, 3, 6, 12, 30, and 300 pulses. Similarly on the 5-sec curve, the first five points represent retinal thresholds for 1, 2, 3, 5, and 50 pulses. Thus, within experimental error, there is no difference between the thresholds for 50 and 300 pulses at 10 Hz. We conclude, therefore, that the damage observed after 300 pulses was induced by the first 50. Similarly, thresholds obtained at 1 Hz for 5 (25.0 mW) and 30 pulses (26.4 mW) are the same, within experimental error, indicating that the damage observed in the latter case was induced by the first 5 pulses.

For double-pulse configurations, the minimum threshold appears to be in the neighborhood of repetition frequencies of 0.1 to 2 Hz, corresponding to an interpulse spacing of 10 to 0.5 sec, respectively. To determine the optimum spacing, we undertook a series of double-pulse experiments at interpulse separations of 1, 1.67, 4, 6, and 10 sec, in each case exposing 16 sites in each of 3-5 eyes to determine ED50 thresholds. Results of these experiments, together with all threshold data acquired for fixed configurations of two, three, five, and ten pulses, are listed in Table 10. Where required, threshold values can be interpolated from Figure 19 since the trend for each pulse train duration is clear and the precision of the experimental data is high (i.e., the upper and lower 95% confidence limits generally span less than ±5% of the ED50).

The 10-μsec pulsewidths listed in Table 10 are shown in Figure 20. This figure is equivalent to Figure 19 with the profiles defined for fixed numbers of pulses rather than for fixed pulse-train durations. For multiple-pulse configurations (at constant peak power) there is an obvious cumulative effect of the pulses in the rhesus macula. Thus for double-pulse configurations, the minimum threshold appears at an interpulse spacing of ∿2.5 sec, with the minimum progressing to closer separations for exposures of more pulses. Although more data are needed, especially for 10-pulse configurations, it is clear that the cumulative effect of repetitive pulses tends to "saturate", so to say, at a peak corneal power of ∿20-25 mW. That is, for no combination of repetition rate and train duration for 10-μsec visible laser pulses do we observe a lower threshold value.

In the Discussion section, the implications of these results are discussed in terms of mechanisms involving nonthermal processes, possibly of photobiological origin. We shall also discuss the elements of a semi-empirical model which appears to account satisfactorily for the repetitive-pulse data acquired to date.

## Retinal Effects of Mode-Locked Visible Laser Pulses

Rhesus maculae were exposed to 9.9-sec and 10-msec trains of mode-locked 514.5-nm pulses from the argon-ion laser. As discussed previously and in Appendix B, the nominal pulsewidth was fixed at ∿250 psec and the pulse-repetition frequency (103.84 MHz) was determined by the round-trip transit time of the laser cavity. The acousto-optic shutter (AOS) was left in place when the mode-locking unit was installed in the hope that pulse-train durations of 100 μsec and 10 μsec might also be used.

Because of a delay in receiving the mode-locking device from the manufacturer, and also in its installation in the laser, we had less than three weeks

TABLE 10. RETINAL THRESHOLDS FOR FIXED NUMBERS OF REPETITIVE 2- and 10-μsec, 514.5-nm LASER PULSES

| No. of pulses | Pulse separation (sec) | Pulse repetition rate (Hz) | ED50 on cornea: Peak pulse power (mW) | ED50 on cornea: Energy per pulse (μJ) | 90% Confidence interval pwr(mW) | No. of eyes | Notes |
|---|---|---|---|---|---|---|---|
| | 2-μsec Pulses: | | | | | | |
| >1 | →∞ | →0 | 1150 | 2.31 | 780-1705 | 2 | a |
| 2 | 3 | 0.33 | 438 | 0.87 | 77-2490 | 2 | - |
| | 2 | 0.5 | 537 | 1.07 | 462-624 | 2 | - |
| | 0 | $5x10^5$ | 474 | 0.95 | - | - | a |
| 3 | 2 | 0.5 | 436 | 0.88 | 369-515 | 2 | - |
| | 0 | $5x10^5$ | 326 | 0.69 | - | - | a |
| | 10-μsec Pulses: | | | | | | |
| >1 | →∞ | →0 | 161 | 1.61 | 158-165 | 5 | a |
| 2 | 15 | 0.067 | 146 | 1.46 | - | - | c |
| | 10 | 0.10 | 143 | 1.43 | 133-155 | 4 | - |
| | 6 | 0.167 | 114 | 1.14 | 105-128 | 4 | - |
| | 4 | 0.25 | 102 | 1.02 | 97.0-107 | 4 | - |
| | 2.5 | 0.4 | 72.3 | 0.72 | 69.8-74.9 | 11 | b |
| | 1.667 | 0.6 | 77.3 | 0.77 | 67.8-88.1 | 3 | - |
| | 1.0 | 1.0 | 90.5 | 0.90 | 83.7-98.0 | 5 | - |
| | 0.25 | 4.0 | 113 | 1.13 | 108-118 | 9 | b |
| | 0.025 | 40 | 103 | 1.03 | 98.5-108 | 10 | b |
| | 0 | $10^5$ | 116 | 1.16 | - | - | a |
| 3 | 10 | 0.1 | 150 | 1.50 | 144-158 | 10 | b |
| | 1.667 | 0.6 | 41.3 | 0.41 | 39.6-43.1 | 10 | b |
| | 0.167 | 6 | 82 | 0.82 | - | - | c |
| | 0.017 | 60 | 90 | 0.90 | - | - | c |
| | 0 | $10^5$ | 86 | 0.86 | - | - | a |
| 5 | 6 | 0.167 | 130 | 1.3 | - | - | c |
| | 1 | 1 | 25.0 | 0.25 | 23.9-26.1 | 11 | b |
| | 0.10 | 10 | 67.8 | 0.68 | 66.5-69.2 | 6 | b |
| | 0.01 | 100 | 79.8 | 0.80 | 77.8-81.8 | 10 | b |
| | 0 | $10^5$ | 60 | 0.60 | - | - | a |
| 10 | 3 | 0.333 | 87 | 0.87 | - | - | c |
| | 0.5 | 2 | 23 | 0.23 | - | - | c |
| | 0.05 | 20 | 58 | 0.58 | - | - | c |
| | 0.005 | 200 | 74 | 0.74 | - | - | c |
| | 0 | $10^5$ | 46.7 | 0.47 | 44.1-49.5 | 19 | a |

a. CW limits (pulse separation = 0) and single-pulse limits (pulse separation →∞) are from single-pulse data-Table 1.

b. Data from Tables 7, 8, or 9.

c. Interpolated (Fig. 19).

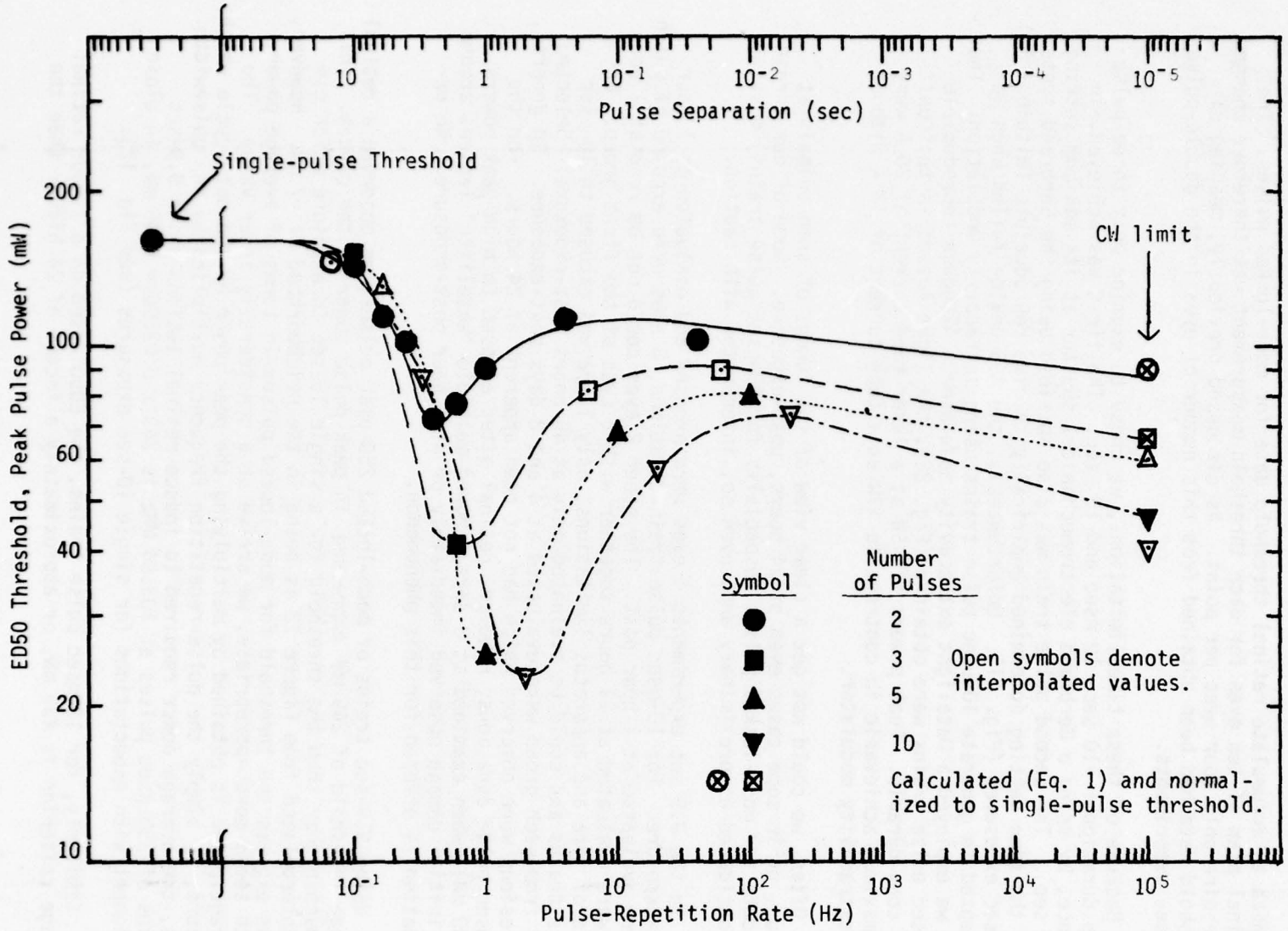


Figure 20. Retinal threshold vs. pulse separation for fixed numbers of repetitive 10-μsec, 514.5-nm laser pulses.

in which to accumulate retinal threshold data for mode-locked pulses. The original plan of ten eyes for each threshold measurement was therefore changed to require only four eyes per point. As discussed previously, meaningful threshold data had been obtained from this number of eyes in the double-pulse 10-μsec experiments.

Because of these time limitations, we chose to examine only three pulse-train durations: ≈10 sec, 10 msec and 10 μsec. The first was achieved, in essence, by using a Gerbrand electromechanical shutter at its maximum setting (9.9 sec). The second pulse train was also obtained using the Gerbrand system with the time setting determined empirically to give reproducible (within ± 5%) 10-msec exposures (Fig. 21). Unfortunately, the AOS device failed when we attempted to generate 10-μsec pulse trains using intracavity modulation. Therefore we employed a Datalight extracavity modulator. Although reproducible 10-μsec pulse trains were obtained (Fig. 22), the light losses in this unit were considerable. Peak powers of ≤5W at a laser tube current of 20 A were the maximum achievable in contrast to ≥7W at a tube current of 18 A without the extracavity modulator.

Often, we could not get a clear view of the fundus of some animals at 1 hour, or in some cases even at 24 hours, post-exposure. Some of our threshold data for mode-locked pulses (especially for 10-μsec pulse trains) must be considered as preliminary and, even so, interpreted with caution.

In the 9.9 sec experiments 4 eyes were exposed and evaluated at 1 hour post-exposure. For 10-msec pulse-train durations, 8 eyes were exposed of which 6 were evaluated at 1 hour post. The other 2 eyes could not be read at 1 hour but were evaluated at 24 hours together with 2 eyes of the first group. Because of time and apparatus limitations, only 1 eye was exposed to 10-μsec pulse trains and could be evaluated only at 48 hours post-exposure. Selected eyes from each group were evaluated at 4 and 8 days post-exposure. In general, no lesions were observed which had not been apparent at 24 hours. For the 10-msec pulse durations, however, retinal sites exposed to high peak powers (≳600 mW), when examined at 8 days, showed multiple "satellite" lesions around the initial damage observed immediately or at 1 hour post-exposure. No explanation is offered for this phenomenon.

Using 9.9-sec trains of mode-locked 250-psec pulses, we observed a retinal damage threshold of 249 mW expressed in peak pulse power at the cornea. This is much higher than the threshold for a single 10-sec CW exposure which can be interpolated from Figure 12 as being in the neighborhood of ≈7 mW. However, if we express the threshold for mode-locked pulses in terms of average power, which seems more appropriate, we arrive at a considerably lower value. The average power is obtained by multiplying the peak power by the duty cycle which, in turn, is simply the pulse-repetition frequency multiplied by the pulsewidth. Thus, the average power required to induce retinal lesions using 9.9-sec trains of 250-psec pulses at 103.84 MHz is 249 x 0.02596 = 6.46 mW, in close agreement with expectations for single 10-sec exposures (see Fig. 12).

Similarly, for 10-msec pulse trains, the ED50 based on a 1-hour retinal damage criterion is 439 mW, or approximately a factor of 24 higher than the

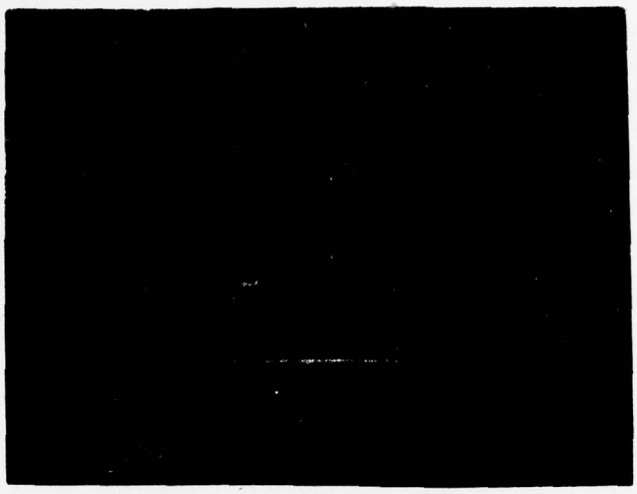

Figure 21. Oscilloscope photograph of calibration photodiode showing 10-msec train of mode-locked pulses of argon-ion laser. Photodiode (PD-2) was terminated at 50 Ω to a wide-band preamplifier. (See text and Fig. 6).


Figure 22. Oscilloscope photograph of calibration photodiode showing 10-μsec train of extracavity-modulated, mode-locked pulses of argon-ion laser. Photodiode (PD-2) was terminated at 50 Ω to a wideband oscilloscope with a rise-time sufficiently fast to detect the sharp rise and fall of the mode-locked train, the modulation of which (at 103.84 MHz) is reflected by the width of the trace. (See text and Fig. 6.)

threshold for single 1-msec, 514.5-nm pulses reported above (Table 1 and Fig. 12). Again, if we calculate the average power, we see that the threshold for mode-locked pulses delivered in a 10-msec exposure is 11.4 mW, i.e., only somewhat lower than the 17.9 mW value found for 10-msec CW exposures.

In contrast, using a 24-hour retinal damage criterion, the ED50 for these mode-locked pulses is 207 mW peak power or 5.36 mW average power. Thus, by this criterion, mode-locked pulses appear to constitute a more severe retinal hazard by at least a factor of 3, compared to 10-msec exposures of unmodulated 514.5 nm laser radiation (see Table 1). Unfortunately, we do not have a similar basis for comparison, since the threshold for the latter case using a 24-hour damage criterion is not known. However, we also observed lower thresholds for 30-sec trains of 10-μsec, 514.5-nm pulses using a 24-hour retinal evaluation rather than the usual 1-hour damage criterion, as discussed in the following section.

From our very limited data for 10-μsec trains of 250-psec pulses, we can say only that the threshold appears to be close to the value observed for single 10-μsec pulses of CW laser output. Specifically, of the 16 macular sites exposed, only two showed damage 48 hours later. There was a sharp transition from "no-lesion" to "lesion" at an average corneal power of 138 mW (5.31 W peak). Hence, the term "ED50" is inapplicable to this case. All we can say is that the *apparent* threshold for 10-μsec trains of mode-locked pulses is quite close to that for unmodulated exposures of the same duration (161 mW, Table 1).

The entire set of threshold data for mode-locked 514.5-nm pulses is listed in Table 11. As noted previously, these data must be considered preliminary, especially for 10-μsec pulse trains. Clearly, more experiments are needed to define the retinal hazards of mode-locked visible laser pulses. In particular, more attention must be paid to long-term damage criteria, e.g., 24 hours post-exposure.

## DISCUSSION

### General Observations

As in the case of Nd:YAG exposures (Vol. I), we observed marked differences in the size and appearance of laser-induced retinal lesions depending on exposure conditions. Thus, lesions induced by single pulses tended to be relatively large in diameter and diffuse in appearance, whereas the lesions produced by repetitive pulses (especially at 10-μsec pulsewidth) were smaller and more sharply defined and appeared to be not as deep in the retina. In contrast, lesions produced by mode-locked pulses with train durations of 10 msec or 10 μsec appeared as diffuse, lightly pigmented "puffs", as opposed to well-defined light spots surrounded by a dark area. In addition, several macular sites showed dark pigmentation immediately after the exposure (i.e., within 1-2 min) or, at lower energies, at 1 hour post-exposure. These sometimes developed into well-defined lesions when observed later (1 to 8 days). In several cases of trains for 10-μsec or 250-psec pulses, we observed a distinct transition from "lesion to "no lesion".

On the basis of these observations, it appears that there may be a difference between the nature of chorioretinal damage produced by single CW pulses and that induced by trains of repetitive pulses, especially in the case of the

TABLE 11. SUMMARY OF RETINAL THRESHOLD DATA
FOR TRAINS OF MODE-LOCKED ARGON-ION LASER PULSES

Wavelength: 514.5 nm; pulsewidth: ≃250 psec;
Repetition frequency: 103.84 MHz

| Pulse-train duration | ED50 on cornea[a] | | | | 90% Confidence interval power (mW) | No. of eyes |
|---|---|---|---|---|---|---|
| | Peak pulse power | Average power (mW) | Energy per pulse (nJ) | Total energy (J) | | |
| 9.9 sec | 249 mW | 6.46 | 0.062 | $6.40 \times 10^{-2}$ | 225-276 | 4[b] |
| 10 msec | 439 mW | 11.4 | 0.110 | $1.14 \times 10^{-4}$ | 406-476 | 6[b] |
| | 207 | 5.37 | 0.052 | $5.37 \times 10^{-5}$ | 181-235 | 4[c] |
| 10 µsec | 5.2 W | 135 | ≃1.3 | $\simeq 1.35 \times 10^{-6}$ | | 1[d] |

[a] Average power = peak power x duty cycle (0.026).

[b] 1-hour damage criterion.

[c] 24-hour damage criterion.

[d] 48-hour damage criterion, there was no immediate observable damage. Mean of highest power "no-lesion" and lowest power "lesion" equals ED50.

10-μsec and 250-psec pulsewidths. As in the Nd:YAG experiments, these differences may reflect mechanism: for relatively long (≥100 sec) single-pulse exposures, strictly thermal processes appear to predominate; whereas in the case of the repetitive pulses at repetition frequencies of 0.1 to 10 Hz, photobiological processes may predominate.

We noted earlier that 30-sec trains of 10-μsec repetitive pulses showed lower thresholds when a 24-hour damage criterion was used than when the retina was examined only at 1-hour post-exposure. These differences are depicted graphically in Figure 23. There is little or no difference between thresholds determined using the two criteria until the pulse-repetition rate exceeds 1 Hz. Interestingly enough, the magnitude of the disparity increases with repetition frequency and is not maximal in the same frequency region as the short-term cumulative effect (1-10 Hz). If this reflects a change in mechanism as suggested by Gibbons and Allen (4) and also by Ham et al. (5), then we are apparently dealing with three, rather than two, types of retinal damage mechanisms. That is, for relatively short (<5 sec) single-pulse exposures, observed thresholds appear to be consistent with thermal damage mechanisms. Likewise, long single-pulse exposures induce thermal damage as observed at one hour post. However, if the damage criterion is based on retinal examination at 24 hours post-exposure, a lower threshold is observed for visible laser pulses, but not for near-IR wavelengths (4). This suggests involvement of photochemical or photobiological mechanisms, the distinction between which is unclear in this case.

As discussed in greater detail below, our repetitive-pulse data also suggest that photobiological processes are involved in producing retinal damage, particularly in the range of repetition frequencies of ∿0.1 - 10 Hz. It is conceivable, of course, that the long-term visible exposure data (3,4) reflect a combination of photobiological and thermal processes. However, at present it appears unlikely that the same photo-processes are operable in both the short-pulse repetitive exposures and the long-term experiments. In any case, our repetitive-pulse data indicate a critical need for further refinement of theoretical models to account for the decidedly anomalous behavior of threshold pulse power as a function of repetition rate, both for argon-ion and Nd:YAG laser exposures.

In cases where damage is induced by repetitive visible-laser pulses of pulsewidth ≥100 μsec, we find generally good agreement between experimental results and theoretical calculations predicted exclusively on thermal damage mechanisms. This indicates that thermal processes (high temperature gradients), possibly unaided by any photobiological processes, are chiefly responsible for producing damage (e.g., through the mechanisms of protein denaturation or enzyme inactivation).

However, for threshold damage induced by repetitive, visible pulses of shorter pulsewidths and higher intensities, especially pulses shorter than 10 μsec, we find serious disparities between experiment and theory. Considered in terms of double-pulse exposures, we hypothesize that even if the energy of the initial pulse is insufficient to induce thermal damage, its intensity (power) may react a level sufficient to trigger a photochemical reaction, possibly involving one or more intermediate stages of the photopigment cycle, e.g., production of excess opsin in the photoreceptors, accumulation of excess retinol in the pigment epithelium, or production of high, localized $Na^+$ or $Ca^{++}$ concentrations in the outer segments (49). Whatever the initial reaction or its products, the cumulative effects appear to be maximal within a few seconds after photic stimulation

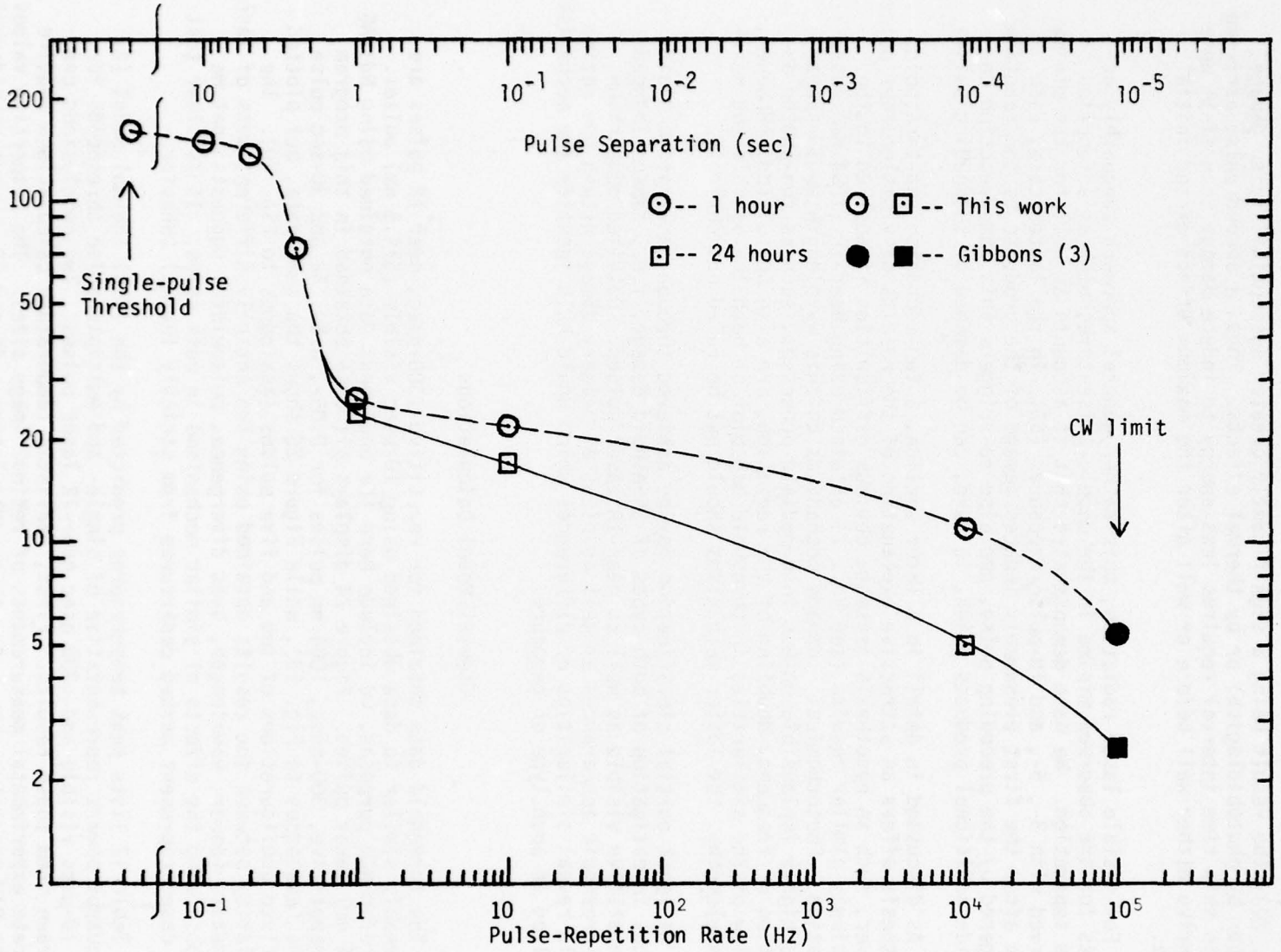


Figure 23. Comparative retinal damage thresholds for 30-sec trains of 10-μsec, 514.5-nm laser pulses using 1-hour and 24-hour post-exposure evaluation criteria.

(Fig. 20), the result being a significantly greater susceptibility to damage, whether by photobiological or by thermal effects. Thus, a second pulse arriving within this time interval requires less energy to induce damage than if it were to arrive either well before or well after the maximum effect of the initial pulse.

For visible laser radiation, this rather general approach adequately accounts for the observed minima in the double-pulse thresholds as a function of pulse separation. We have demonstrated that it accounts as well for the minima observed with 3-, 5-, and 10-pulse exposures (50). In the latter case, each pulse after the first presumably induces damage of the products of the reaction triggered by the preceding pulse, and also re-triggers this same reaction to provide additional products which, in turn, can be damaged by succeeding pulses.

As discussed in detail in a later section, a two-mechanism/two-threshold hypothesis offers an attractive explanation of the results of visible laser pulses. However, such an hypothesis presents obvious difficulties if applied to the strikingly similar results (see Vol. I) obtained using near-IR (1064 nm) laser radiation. Photochemical damage mechanisms at this wavelength would appear to be highly implausible unless intermediate processes, such as two-photon absorption or frequency-doubling of the radiation, are also postulated. However, in view of the similarities in threshold behavior at both the visible and near-IR wavelengths, the latter mechanisms should not be ruled out entirely.

At least partial clarification may be achieved through comparative histological investigation of both types of threshold damage, i.e., damage induced by repetitive visible as well as near-IR laser pulses. Detailed comparison of microscopic appearances as well as sites of primary damage within the retina should reveal similarities or differences which would help identify the mechanisms involved in each type of exposure.

## Thermal Model Calculations

The threshold data obtained for repetitive ~300-nsec, near IR pulses are remarkably similar to data obtained using 10-μsec visible (514.5 nm) pulses. For reference purposes, we include here the analogous data obtained using Nd:YAG (1064 nm) laser pulses. Figure 24 displays all data obtained in this program for repetitive, 300-nsec, 1064-nm pulses for 0.05-, 0.5-, 5- and 30-sec pulse trains (analogous to Fig. 19), while Figure 25 shows the same data, but plotted for fixed configurations of two and five pulses (analogous to Fig. 20). The similarity between the results obtained using two entirely different sets of laser parameters (power, wavelength, beam divergence, pulsewidth) suggests that we are observing the effects of similar mechanisms in both cases. It is clear that both cases represent marked departures from strictly thermal behavior.

Table 12 lists peak temperatures predicted by the IITRI thermal model (2) for output powers representative of single- and multiple-pulse thresholds for both 10-μsec visible and ~300 nsec near-IR laser pulses. Two conclusions can be drawn from these results. First, realistic temperature calculations require accurate experimental measurements of retinal image sizes. The respective values of the RIM parameter chosen for these calculations, 25 and 50 μm, are considerably larger than retinal image radii calculated by ray-trace techniques (51), although the ratio is approximately correct for beam divergence angles of 0.6 mrad (514.5 nm) and 1.2 mrad (1064 nm). However, smaller retinal spot sizes will yield

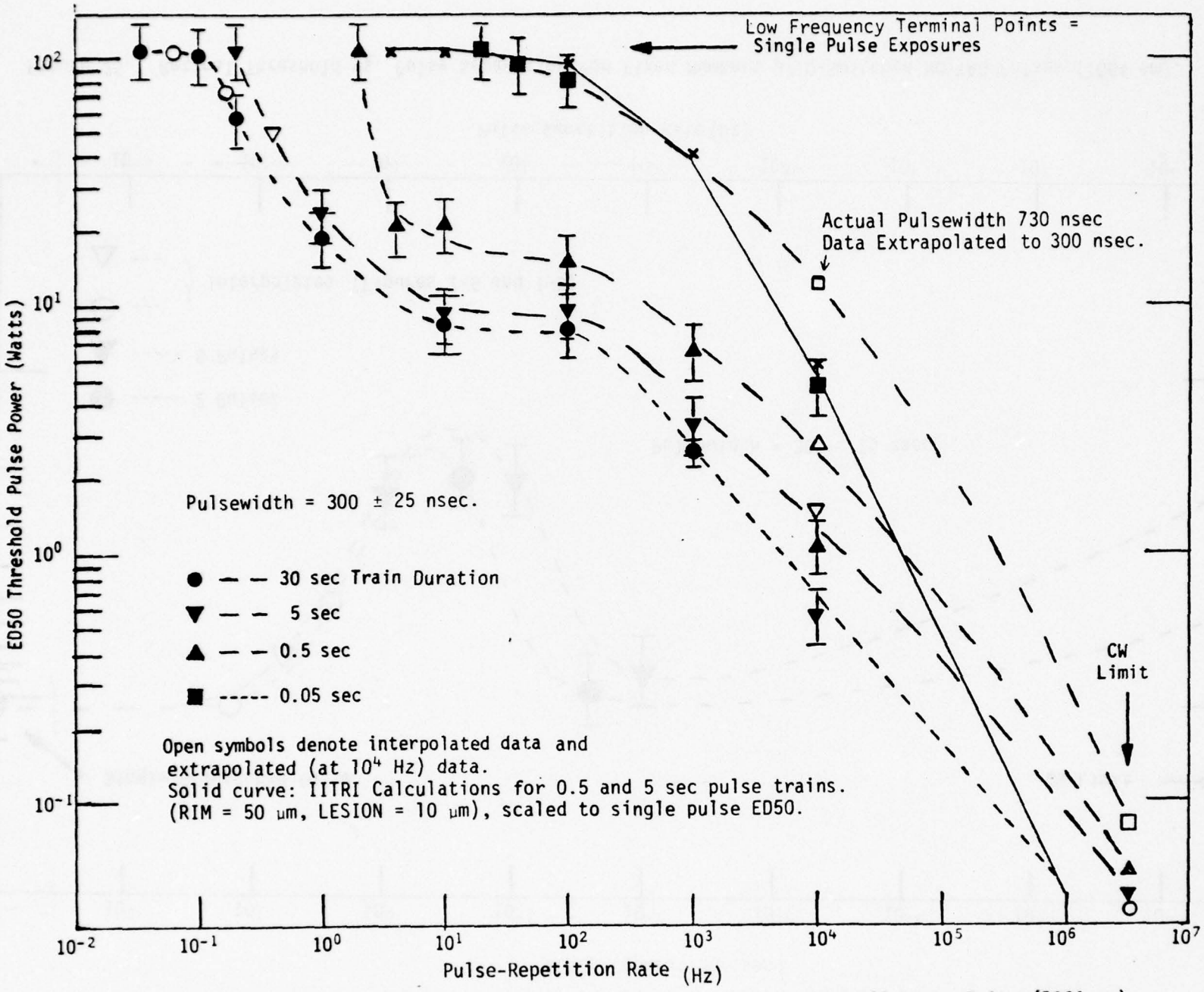


Figure 24. Summary of Retinal Thresholds for Q-Switched Nd:YAG Laser Pulse (1064 nm).

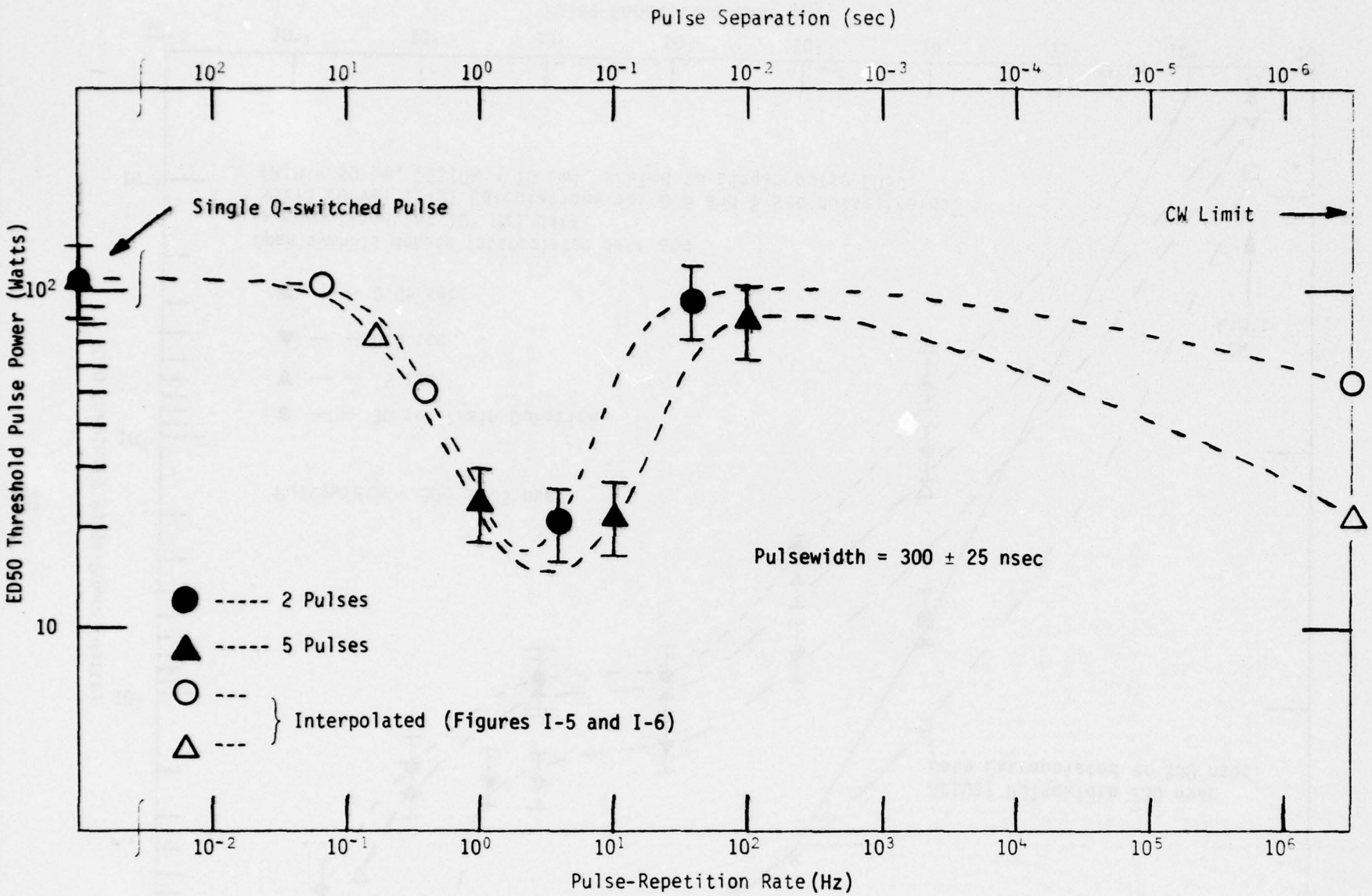


Figure 25. Retinal Threshold vs. Pulse Separation for Fixed Numbers of Q-Switched Nd:YAG Pulses (1064 nm).

TABLE 12. COMPARATIVE PEAK RETINAL TEMPERATURES PREDICTED BY IITRI THERMAL MODEL AT THRESHOLD POWERS FOR 514.5- AND 1064-nm LASER PULSES

| Wavelength (nm) | Pulse width | RIM[a] (μm) | LESION (μm) | No. of pulses | Pulse separation (sec) | ED50[b] peak pulse power | ΔT (°C)[c] |
|---|---|---|---|---|---|---|---|
| | | | | | | (mW) | |
| 514.5 | 10 μsec | 25 | 10 | 1 | --- | 161 | 38.6 |
| | | 25 | 10 | 2 | 2.5 | 72.3 | 17.3 |
| | | 25 | 10 | 3 | 1.7 | 41.3 | 9.9 |
| | | 25 | 10 | 5 | 1.0 | 25.0 | 6.0 |
| | | | | | | (W) | |
| 1064 | 300 nsec | 25 | 10 | 1 | --- | 96.7 | 190 |
| | | 50 | 10 | 1 | --- | 96.7 | 30.0 |
| | | 50 | 10 | 2 | 0.25 | 18.8 | 5.3 |
| | | 50 | 10 | 5 | 0.1 | 19.1 | 5.4 |

---

a Retinal image radius ($1/e^2$ intensity).

b Powers indicated are minimum thresholds observed for the number of pulses indicated assuming the respective pulsewidths.

c Temperatures are peak values calculated at the end of a single pulse at the center of the retinal image (R = 0) at a depth of 1.2 μm in the pigment epithelium.

even higher, and probably unrealistic, calculated temperatures, as shown in Table 12 by the comparative values for 1064-nm laser pulses.

Second, the 514.5 nm calculations show that strictly thermal damage mechanisms cannot account for the multiple-pulse thresholds, even if one assumes that the single-pulse threshold (161 mW) is representative of such mechanisms. Thus, if a peak temperature increase of ∿38° C is required to induce thermal damage, then irreversible damage would not be anticipated at the proportionately lower temperatures predicted for the laser powers observed for minimum repetitive-pulse thresholds.

In this connection, it must be borne in mind that thermal relaxation processes in retinal tissues are very fast relative to the optimal interpulse spacings (1-2 sec) shown in Figures 20 and 25. For example, IITRI model calculations indicate that a peak temperature increase of ∿17°C (representative of a single ∿70 mW, 10-μsec, 514.5-nm laser pulse) will subside to less than 2°C within ∿0.5 msec after the end of the pulse. This may be compared with the microthermocouple measurements of Welch and co-workers (36-38) who observed thermal relaxation times (1/e) of ∿100 msec following 10-msec, sub-threshold exposures of much larger retinal areas (≥150 m radius).

## Working Hypotheses to Explain Cumulative Effects of Repetitive Laser Pulses

Since purely thermal mechanisms cannot explain the repetitive-pulse experimental threshold data (Figs. 19, 20, 24, and 25), we are compelled to invoke other processes. The most likely alternative appears to be involvement of photochemical or photobiological damage mechanisms, although contributions of thermal effects are not necessarily excluded.

For the moment, we shall consider only the visible-wavelength threshold data (Figs. 19 and 20). We have shown (see Results section) that departures from apparent thermal behavior do not become distinct until the pulse duration is decreased well below 1 msec. Thus, for 100- and 40-μsec pulses, slight departures from predicted thermal behavior are observed (Figs. 15 and 16), but the effect does not become pronounced until 10-μsec laser pulses are used. This suggests that the minima in Figure 20, and by extension in Figure 25 as well, represent an intensity- rather than an energy-dependent phenomenon.

This is borne out by 514.5 nm threshold data for widely disparate pulsewidths of 1 msec and 10 μsec. At a pulse separation of 1 sec, the threshold (in terms of peak power per pulse) for five 1-msec pulses is ∿20 mW (Table 4 and Fig. 14); for five 10-μsec pulses at the same separation, the threshold is ∿25 mW (Tables 8 and 10, Figs. 18-20). Thus, in the case of 1-msec pulses, the energy per pulse at threshold is nearly 100-fold greater than for 10-μsec pulses, but the intensity (watts ∝ photons/sec) is about the same. For a single 1-msec pulse the threshold, 21 mW (Table 1), is within experimental error of the five-pulse threshold (Figs. 13 and 14), indicating no additivity of effects for consecutive 1-msec pulses. In contrast, the threshold for a single 10-μsec pulse (161 mW) is some 6.4 times higher than the minimum threshold for five pulses, a factor which indicates the magnitude of additive effects of optimally separated, 10-μsec visible-laser pulses.

For the special case of double-pulse exposures, the effect of the first pulse appears to be primarily photochemical (or photobiological), whereas the

second pulse may initiate either thermal or photochemical processes, or both. At present, we do not completely rule out the possibility of both pulses acting thermally, although based on our present understanding of thermal processes in the retina, this seems improbable. Therefore, we must consider four working hypotheses based on the principal effects of the first and second pulses, respectively: A--photochemical + thermal; B--photochemical + photochemical; C--thermal + photochemical; and D--thermal + thermal. In all cases, combinations of thermal and photochemical effects from a given individual pulse must also be kept in mind.

According to hypothesis A, the effect of the first pulse (photochemical) should be intensity (i.e., power) dependent, whereas the effect of the second pulse (thermal) should also be power dependent, but along the lines analogous to the IITRI (2) model. To the extent that this hypothesis is valid, one would expect the threshold obtained in a mixed-pulsewidth experiment (e.g., 10 μsec followed by 1 msec at optimum spacing) to be lower than the threshold for reverse pulse configuration. Results to the contrary would strongly indicate predominately thermal effects arising from the first pulse. However, based on present data and the considerations discussed previously, we tend to rule out thermal effects of the initial pulse, at least for the time-being. Hence we are left with two alternative working hypotheses.

In both cases, we consider that the effect of the first pulse involves quantum conversion of the incident laser pulse; whether this involves photochemical processes (i.e., relatively rapid molecular changes due to chemical reactions of excited electronic states) or photobiological processes (e.g., alteration, possibly longer term, of biological activity) remains to be determined. In either case, it is apparent that the effect of the first pulse is reversible: a single pulse at the minimum threshold power for double pulses (∿70 mW) does not by itself induce observable damage.

The effect of the second pulse may be either thermal or photic. In the former case, we suggest that thermal denaturation of free opsin, the protein moiety of the visual pigment rhodopsin, may be involved in the damage mechanism. Light intensities typical of those used in these experiments induce high concentrations (52-54) of this protein which has been shown to be more thermally labile when in the free state (55) than when bound either to the chromophore or to outer-segment membranes. Moreover, *in vivo* thermal denaturation of free opsin has been implicated in electron microscope studies of light-induced retinal dystrophy in rats (53-55) under conditions such that retinal temperature increases were as low as 3°C.

The alternative hypothesis invokes photic effects for both pulses. From Figure 20, it can be seen that at the optimum spacing for five visible pulses (∿1 sec), the minimum threshold is in the neighborhood of 20-25 mW per pulse. This appears to be a "saturating" value, so to speak, since even for ten pulses, the threshold does not change significantly. In other words, whatever damage is observed after ten pulses was induced by the first five.

Accordingly, the effect of the first pulse can be considered to be a reversible photo-trigger, for which the threshold power is about 20-25 mW (at the cornea). This trigger pulse is assumed to induce formation of either a transient intermediate (i.e., molecular) species or an increased retinal sensitivity, neither of which, by itself, gives rise to ophthalmoscopically visible damage.

If the effect of subsequent pulses is primarily photochemical, the reciprocity relationship should hold; i.e., the effects of subsequent pulses should depend more on the total energy of these pulses than on the peak power per pulse. The data listed in Table 13 show that this appears to be the case. The interpretation is as follows: The threshold energy for the second pulse is ∿0.7 μJ (at the cornea), since for double 10-μsec pulses, the minimum threshold observed at optimum spacing is ∿70 mW. When the effects of subsequent pulses are distributed over time, the system is no longer at its maximum sensitivity at the time these pulses are delivered. For example, for two pulses, the optimum and maximum sensitivity occur simultaneously at 2.5 sec. However, for 3-pulse configurations, the optimum interpulse spacing is 1.67 sec, but the last pulse arrives some 3.33 sec after the first. Similarly, for 5-pulse exposures, the optimum interpulse separation is ∿1 sec but the last pulse evidently arrives ∿4 sec after the first, i.e., an additional ∿1.5 sec after the maximum effect of the first pulse is realized. Thus, for time-symmetric multiple pulses of equal intensity, the apparent total energy requirement increases slightly with increasing numbers of pulses.

Our two remaining working hypotheses may be abbreviated as photo + thermal (A) and photo + photo (B). Double-pulse experiments at visible wavelengths should be undertaken to test these two general mechanisms. One such experiment involves independent variation of the power levels of the two pulses and the results should provide a clear preference between these two alternatives.

Specifically, hypothesis A predicts that the concentration of free opsin (or other thermally labile species) will be proportional to the intensity of the initial pulse (at least up to a saturating value). Since the effect of the second pulse is considered to be essentially thermal, only the temperature change induced by that pulse *in the labile molecules* is important. We assume a normal (i.e., Boltzmann) distribution of temperatures among the molecules in the irradiated area and that a minimum number of labile molecules (e.g., opsin) must be denatured to induce an observable lesion within one hour after exposure. Thus, hypothesis A predicts a smoothly varying dependence of the threshold power of the second pulse ($I_2$) as a function of the intensity of the initial pulse ($I_1$). This is shown in Figure 26 (A), which may be summarized as follows: the lower the concentration of free opsin (at low $I_1$), the higher the local temperature change required in order to damage the critical number of free opsin molecules in the irradiated volume element. Conversely, at high $I_1$, higher concentrations of free opsin will be formed and thus lower peak temperatures will be required to damage the critical number of labile intermediates.

In contrast, hypothesis B predicts a threshold of ∿25 mW for the first pulse and ∿70 mW for the second pulse as shown in Figure 26(B). Thus, to induce retinal damage, the intensity of both pulses must be at or above their respective thresholds; if $I_1$ is less than ∿25 mW or $I_2$ is less than ∿70 mW, no damage will occur.

In addition to providing more quantifiable predictions, hypothesis B has the advantage that it is more amenable than its alternate to experimental verification of predictions for other N-pulse (N > 2) configurations. Both hypotheses, however, can be tested under a variety of double-pulse conditions, such as variation of the width of the second pulse. For example, both hypotheses predict that a 10-μsec pulse followed at optimum spacing by a sufficiently energetic pulse of any other duration should cause observable damage. A clear preference between the two mechanisms can be made on the basis of: A--constancy of observed

TABLE 13. THRESHOLD POWERS AND ENERGIES FOR REPETITIVE 10-μsec, 514.5-nm LASER PULSES AT OPTIMUM SPACING

| No. of pulses (N) | Interpulse spacing (sec) | ED50 on cornea | | Total energy N pulses (μJ) | Total energy (N-1) pulses (μJ) |
|---|---|---|---|---|---|
| | | Peak pulse power (mW) | Energy per pulse (μJ) | | |
| 2 | 2.5 | 72 | 0.72 | 1.44 | 0.72 |
| 3 | 1.67 | 41 | 0.41 | 1.23 | 0.82 |
| 5 | 1.0 | 25 | 0.25 | 1.25 | 1.00 |
| 10 | 0.5 | 23 | 0.23 | 2.30 | 2.07 |

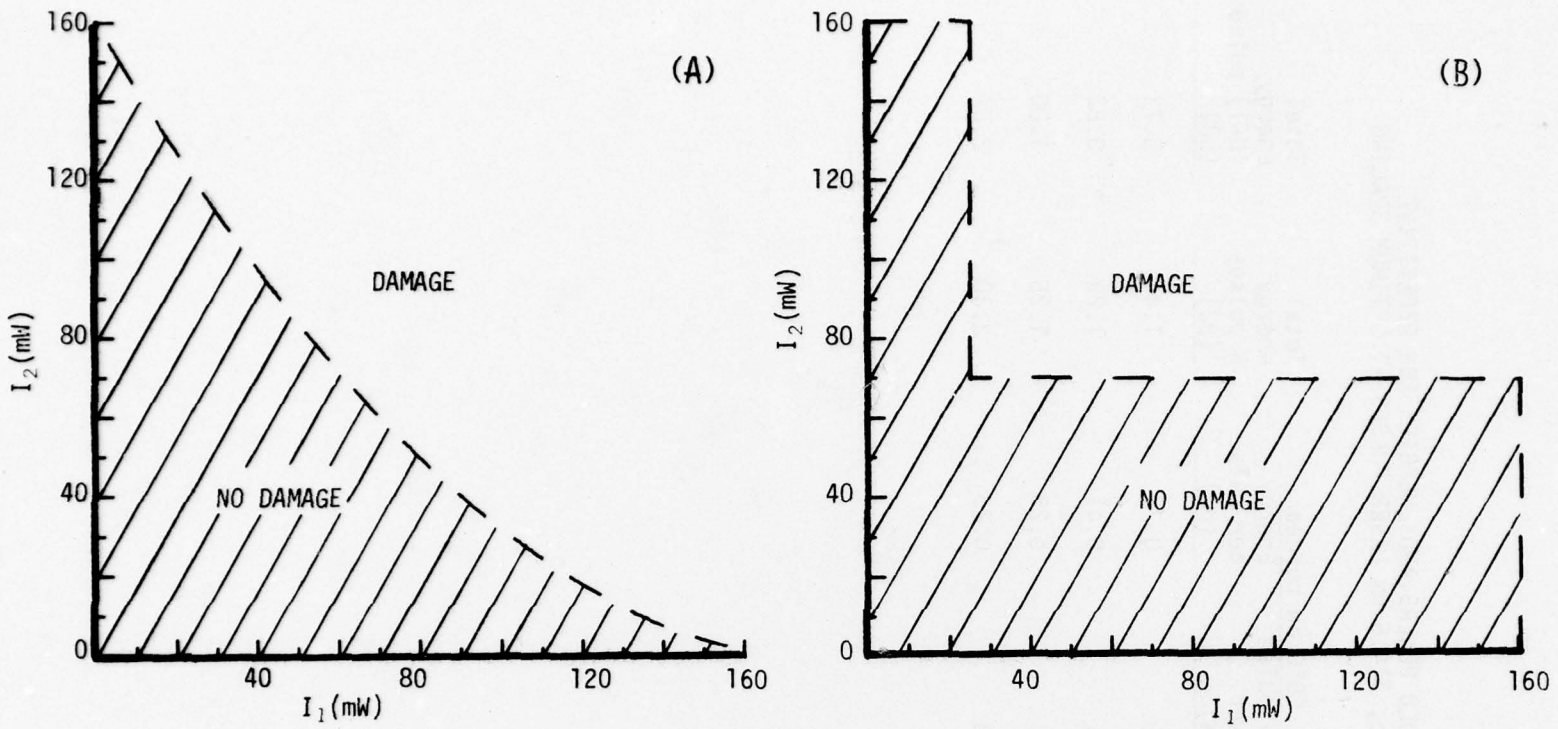


Figure 26. Idealized interpulse power dependencies predicted by working hypotheses for double-pulse threshold experiments. (A) Effects of the two pulses are assumed to be photic and thermal, respectively. Increasing concentrations of a thermally labile intermediate at higher initial pulse intensities ($I_1$) require lower peak temperatures induced by the second pulse ($I_2$). (B) The effects of both pulses are assumed to be photic: the reversible trigger ($I_1$) requires a threshold of ∿25 mW after which the second pulse has a threshold of ∿70 mW for irreversible photochemical damage. Both cases assume double 10-μsec, 514.5-nm pulses separated by ∿2.5 sec.

(or calculated) retinal temperatures, or B--constancy of total energy of the second-pulse threshold.

Another important, but extremely difficult, double-pulse experiment to test these hypotheses involves measuring the action spectra for retinal damage; i.e., using identical pulsewidths, with the power and wavelength fixed for one pulse and varied for the other. In a photo + thermal mechanism (hypothesis A), the wavelength dependence could very well be the same for both pulses. With hypothesis B, however, a different wavelength specificity can be anticipated for the two pulses; i.e., the action spectrum for the second pulse should follow the absorption spectrum of the presumed photo-induced, labile intermediate(s).

In either case, it is essential that several wavelengths ($\geq$10) be used in such a study. Even so, the action spectra for both pulses will most probably be broad and structureless unless either the visual pigment, rhodopsin, or the macular pigment, xanthophyll (35), is involved. Thus, in addition to the experimental difficulties imposed by the requirements of careful coalignment and sequential triggering of two separate laser systems, one must be prepared for inconclusive results.

Although the preceding discussion is relatively straightforward in the case of visible laser pulses, hypotheses invoking photochemical or photobiological processes are presented with obvious difficulties if the strikingly similar near-IR data (Figs. 24 and 25) are to be understood on the same basis. However, plausible mechanisms other than direct, single-photon absorption processes exist which permit us to consider the repetitive-pulse 1064-nm retinal threshold data in parallel with data obtained using visible laser radiation. Doubling of the fundamental frequency of ruby laser pulses (694.3 nm) has been observed experimentally in excised corneal tissues, albeit at extremely low conversion efficiencies (59). This phenomenon almost certainly occurs in the stroma, behaving as a nonlinear optical medium, possibly with higher doubling efficiencies than in the corneal epithelium because of greater thickness of the stroma.

Efficiency of second harmonic generation (SHG) is strongly dependent upon both the power density and mode purity of the incident laser beam. In the Nd:YAG experiments cited here and discussed in detail in Volume I, precautions were taken to assure that only the $TEM_{00}$ mode was incident on the subject eye. Furthermore, the repetitive-pulse intensities for near-IR damage thresholds were on the order of tens of watts as opposed to tens of milliwatts for visible wavelength thresholds.

On a more quantitative basis, the double-pulse threshold at 1064 nm is about 20 W at optimum spacing ($\sim$0.5 sec). This power, incident on a $\sim$1.5-mm diameter corneal spot, yields a power density of $\sim 10^4$ W/cm$^2$, as compared with $\sim$1 W/cm$^2$ for 25 mW of 514.5-nm radiation incident on a corneal spot of 1.8 mm. Thus, a frequency-doubling efficiency of less than 0.1% for 1064-nm radiation could give rise to the power required for the reversible photo-trigger invoked in hypothesis B. We suggest, therefore, that an experimental search for frequency doubling in the anterior media should be undertaken.

In addition to its possible importance in explaining our repetitive pulse Nd:YAG data, observation of frequency doubling of 1064-nm radiation

would go far toward explaining the interesting and rather curious observations reported recently (60) in the Russian literature. A series of experiments was carried out in which human subjects were presented the task of comparing their subjective observations of the colors perceived emanating from various near-IR laser sources with noncoherent monochromatic light. In all cases, the subjects perceived the laser radiation at twice the fundamental frequency. It seems safe to assume that the power levels used in that experiment were considerably lower than those used in the damage threshold studies reported here.

In any case, these subjective observations neither prove nor require actual SHG of laser radiation in the anterior media. Simultaneous two-photon absorption by the visual photoreceptors would give rise to the same observations. Moreover, considering the low laser powers employed in the subjective experiments, this mechanism could well be more efficient than SHG.

Using experimental values for two-photon absorption cross-sections of aromatic hydrocarbons (61), we have estimated (11) the relative intensities of 500- and 1000-nm light required to pump the $S_0 \rightarrow S_1$ transition of rhodopsin at the same rate by one- and two-photon processes, respectively. These calculations indicate that for assumed retinal image diameters of 50 μm, a 20-W, 300-nsec pulse of near-IR radiation could be as effective in bleaching rhodopsin as a 25-mW, 10-μsec pulse of visible light. This estimate (11) must be considered an upper limit until such time as rigorous quantum mechanical calculations can be carried out. In the meantime, an obvious experiment suggests itself: the molecule in question, rhodopsin, should be studied by laser flash photolysis (62) using both extracted pigments and whole disc preparations and Nd:YAG or Nd:glass as the laser source. Photobleaching, if observed, will depend linearly on the square of the incident light intensity.

## Empirical Model of Effects of Repetitive Laser Pulses

We assume that in the case of double 10-μsec visible laser pulses, the first pulse sensitizes the irradiated retinal area and the second pulse induces irreversible photochemical or photobiological damage by interacting with a transient intermediate formed by the initial pulse.

In Figure 27, the double-pulse data are displayed in terms of relative damage thresholds as a function of linear interpulse separation. For this purpose we define "relative sensitivity" of the retina as the ratio of the single-pulse ED50, 161 mW, (Table 1) to the ED50 determined for two pulses at a given pulse separation. As shown in the figure, it appears that the retina is ∿2.2 times more sensitive at a pulse separation of ∿2.5 sec than it is to a single pulse. This can be understood (11) in terms of a set of transient intermediates, formed by the first pulse, in which the concentration of one of these species is maximal at ∿2.5 sec.

The solid line in this figure is the computed (relative) population of species C in the simple reaction scheme:

$$A \xrightarrow{k_1} B \xrightarrow{k_2} C \xrightarrow{k_3} D \qquad (2)$$

The solutions for the set of differential equations representing the appropriate rate expressions can be found in any standard text (63):

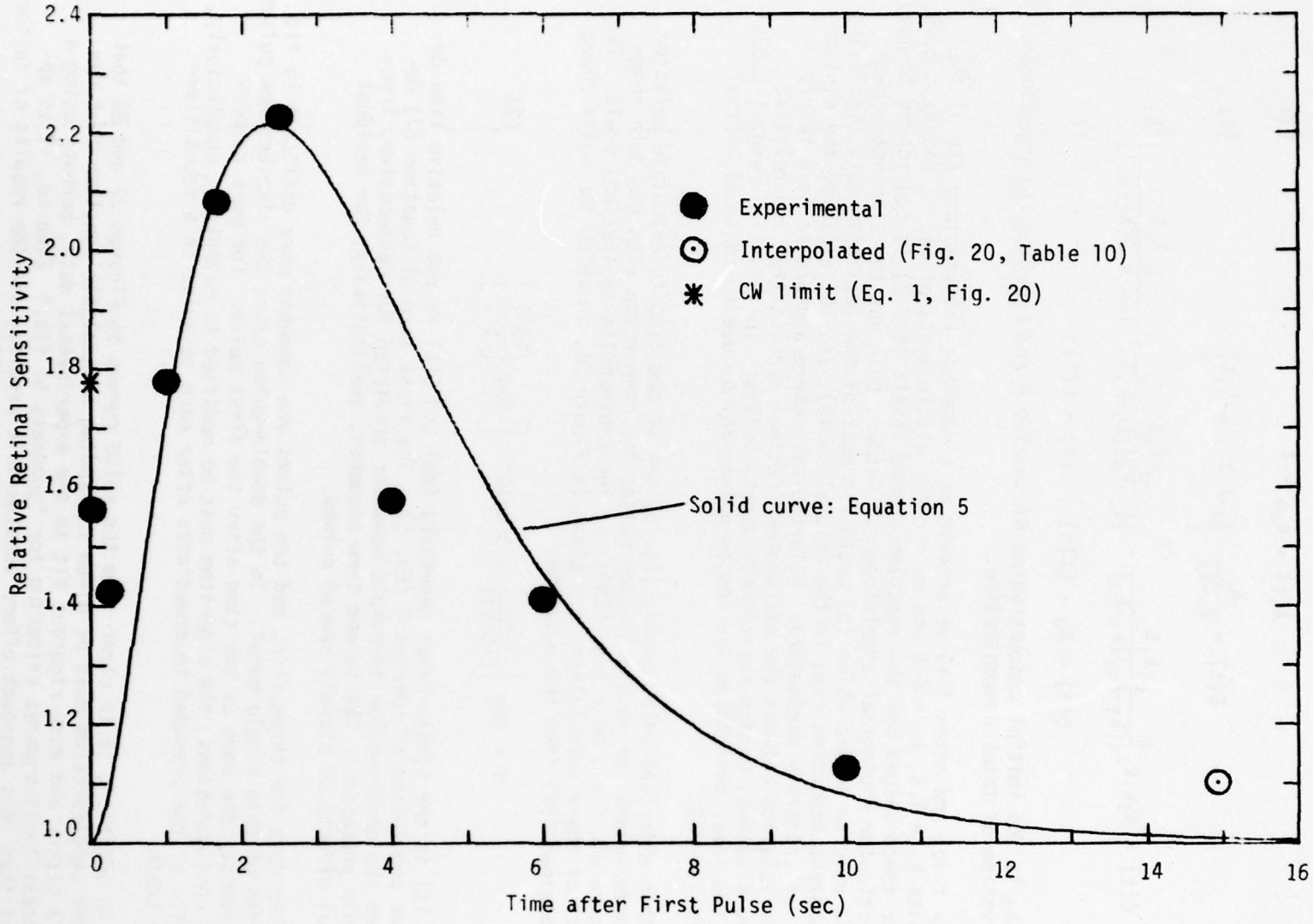


Figure 27. Empirical fit of relative retinal sensitivity as a function of pulse separation. (The sensitivity is defined as the ratio of single- to double-pulse thresholds.)

$$A(t) = A_0 e^{-k_1 t} \tag{3}$$

$$B(t) = \frac{A_0}{k_1 - k_2} \left( e^{-k_2 t} - e^{-k_1 t} \right) \tag{4}$$

$$C(t) = A_0 k_1 k_2 \left( \frac{e^{-k_1 t}}{(k_1 - k_2)(k_1 - k_3)} - \frac{e^{-k_2 t}}{(k_1 - k_2)(k_2 - k_3)} + \frac{e^{-k_3 t}}{(k_2 - k_3)(k_1 - k_3)} \right) \tag{5}$$

$$D(t) = A_0 - [A(t) + B(T) + C(T)] \tag{6}$$

where $A_0$ is the initial concentration of species A and Equation (6) represents conservation of total concentration.

By trial and error (11) we arrived at a somewhat satisfactory fit of the data with $k_1 = 1.6$, $k_2 = 0.8$ and $k_3 = 0.48$, all in units of $sec^{-1}$, and $A_0 = 2.85$. Neither these values nor the reaction scheme itself (Eq. 2) is considered to have any particular biological significance. Rather, this was the simplest scheme we were able to devise which (a) could fit most of the available data (including the apparent induction time in the initial phase), and (b) employed the minimum number of arbitrary parameters. Nevertheless, there appears to be a fairly good correlation between the calculated "retinal sensitivity" and relative threshold values, except for closely spaced pulses. In this time range (<0.025 sec), the lower thresholds for double pulses may be due to residual thermal effects (36-38).

This empirical relationship (Eq. 5) can be modified to calculate relative threshold values for double 10-μsec pulses for comparison with the data shown in Figure 20, i.e., on a log (ED50) vs. log (interpulse separation) scale. The results of these calculations are shown in Figure 28, in which the solid curve was obtained (50) from the equation:

$$Y = \log \left( \frac{161}{1+C(t)} \right) - 3.9 \times 10^{-3} \left[ \log \left( \frac{10^3}{t} \right) \right] \tag{7}$$

where 161 is the single-pulse threshold (mW) and C(t) is the relative time-dependent population of species C (Eq. 5). The first term of Equation (7) describes the double-pulse threshold behavior predicted for consecutive, irreversible processes. The second term accounts, qualitatively, for residual thermal effects of closely spaced pulses.

The data for three, five, and ten pulses are somewhat more difficult to fit in terms of this simple model. In the double-pulse case, the time between pulses is evidently the same as the time after the first pulse. For more complex pulse configurations, the algorithm must be modified to calculate, cumulatively, the kinetics of the presumed intermediates after each stimulus in a repetitive-pulse train.

In addition, it is clear from the solid curves in Figures 27 and 28 that further consideration must be given to finding an analytic function that can give a better and more rigorous fit to the experimental data, perhaps using a nonlinear least-squares criterion for "goodness of fit." Even so, it is apparent that this approach offers considerable promise, and the results of further research in this area will be reported elsewhere (11).

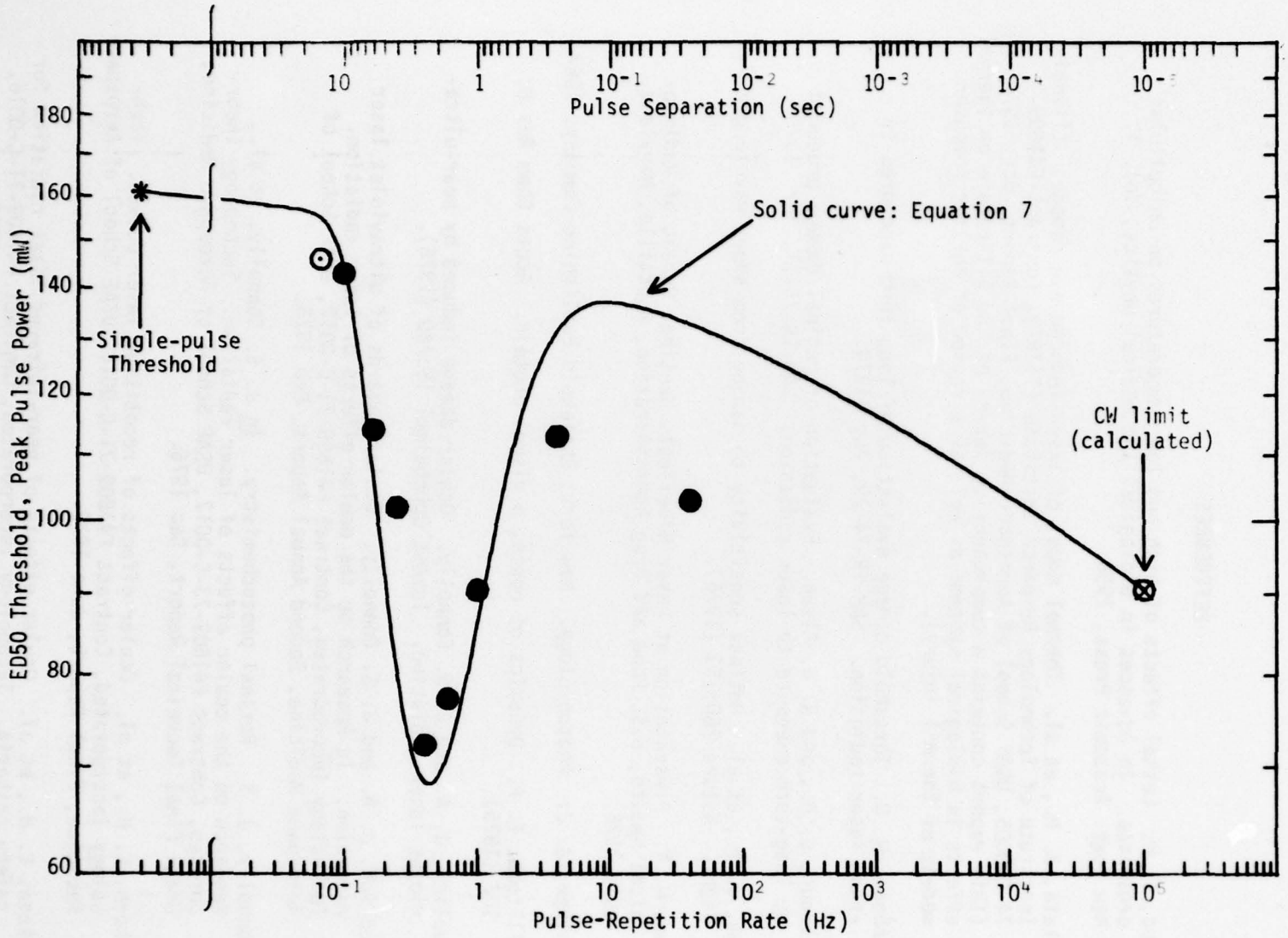


Figure 28. Empirical fit of threshold vs. pulse separation for double 10-μsec, 514.5-nm laser pulses.

## REFERENCES


1. Wood, T. H. Lethal effects of high and low temperatures on unicellular organisms. In Advances in biological and medical physics, Vol. IV. New York: Academic Press, 1956.

2. Takata, A. M., et al. Thermal model of laser-induced eye damage. Illinois Institute of Technology Research Institute (IITRI), Contract F41609-74-C-0005, USAF School of Aerospace Medicine, Final Report, Oct 1974. (This report contains a comprehensive survey of the literature on thermal effects in biological systems as well as a review of earlier computer models of thermal injury).

3. Gibbons, W. D. Threshold damage evaluation of long-term exposures to argon laser radiation. SAM-TR-74-29, Aug 1974.

4. Gibbons, W. D., and R. G. Allen. Evaluation of retinal damage produced by long-term exposure to laser radiation. SAM-TR-75-11, Apr 1975.

5. Ham, W. T., et al. Retinal sensitivity to damage from short wavelength light. Nature 260:153 (1976).

6. Ham, W. T. Presentation at Laser Bioeffects Meeting, Bureau of Radiological Health, U.S. Food and Drug Administration, Rockville, Maryland, July 1976.

7. Wolken, J. J. Photobiology. New York: Rheinhold Publishing Company, 1967.

8. Williams, T. P. Dynamics of opsin, a visual protein. Accts Chem Res 8: 107 (1975).

9. Zuclich, J. A. and J. S. Connolly. Ocular damage induced by near-ultraviolet laser radiation. Invest Ophthalmol 15:760 (1976).

10. Zuclich, J. A. and J. S. Connolly. Ocular hazards of ultraviolet laser radiation. In Research on the ocular effects of laser radiation. Technology Incorporated, Contract F41609-73-C-0017, USAF School of Aerospace Medicine, Second Annual Report, Feb 1975.

11. Connolly, J. S. Retinal photochemistry. In J. S. Connolly, et al., Research on the ocular effects of laser radiation. Technology Incorporated, Contract F41609-73-C-0017, USAF School of Aerospace Medicine, Draft Final Technical Report, Dec 1976.

12. Skeen, C. H., et al. Ocular effects of repetitive laser pulses. Technology Incorporated, Contract F41609-71-C-0018, USAF School of Aerospace Medicine, Final Report, June 1972.

13. Skeen, C. H., et al. Ocular effects of near-infrared laser radiation for safety criteria. Technology Incorporated, Contract F41609-71-C-0016, USAF School of Aerospace Medicine, Final Report, June 1972.

14. Ebbers, R. W., and I. L. Dunsky. Retinal damage thresholds for multiple pulse lasers. Aerosp Med 44:317 (1973).

15. Gibbons, W. D., and D. E. Egbert. Ocular damage thresholds for repetitive pulse argon laser exposures. SAM-TR-74-1, Feb 1974.

16. Gibbons, W. D. Retinal burn thresholds for exposure to a frequency-doubled neodymium laser. SAM-TR-73-45, Nov 1973.

17. Allen, R. G., et al. Research to obtain eye effects data and develop a mathematical model for eye effects predictions. Technology Incorporated, Contract F41609-70-C-0007, USAF School of Aerospace Medicine, Final Report, Dec 1970.

18. Allen, R. G., et al. Research on ocular effects produced by thermal radiation. Technology Incorporated, Contract AF 41(609)-3099, USAF School of Aerospace Medicine, Final Report, July 1967.

19. Mainster, M. A., T. J. White, and R. G. Allen. Spectral dependence of retinal damage produced by intense light sources. J Opt Soc Am 60: 848 (1970).

20. Miller, N. D., and T. J. White. Retinal burns and flashblindness. Technology Incorporated, Contract F41609-68-C-0023, USAF School of Aerospace Medicine, Final Report, Vol. 1, Nov 1969.

21. Dunsky, I. L., and P. W. Lappin. Evaluation of retinal thresholds for CW laser radiation. Vision Res 11:733 (1971).

22. Bresnick, G. H., et al. Ocular effects of argon laser radiation. Invest Ophthalmol 9:901 (1970).

23. Ham, W. T., et al. Helium-neon laser in the rhesus monkey. Arch Ophthalmol 84:798 (1970).

24. Frisch, G. D., E. S. Beatrice, and R. C. Holsen. Comparative study of argon and ruby retinal damage thresholds. Invest Ophthalmol 10:911 (1971).

25. Vassiliadis, A., H. C. Zweng, and K. G. Dedrick. Ocular laser threshold investigations. Stanford Research Institute, Contract F41609-70-C-0002, USAF School of Aerospace Medicine, Final Report, Jan 1971.

26. Ebbers, R. W. Retinal effects from multiple pulse gallium arsenide lasers. SAM-TR-72-25, Nov 1972.

27. Lappin, P. W., and P. S. Coogan. Relative sensitivity of various areas of the retina to laser radiation. Arch Ophthalmol 84:350 (1970).

28. Vassiliadis, A., R. C. Rosan, and H. C. Zweng. Research on ocular laser thresholds. Stanford Research Institute, Contract F41609-68-C-0041, USAF School of Aerospace Medicine, Final Report, Aug 1969.

29. Adams, D. O., D. J. Lund, and P. D. Shawaluk. The nature of chorioretinal lesions produced by the gallium arsenide laser. Invest Ophthalmol 13: 471 (1974).

30. Gibson, G. L. M. Retinal damage from repeated subthreshold exposures using a ruby laser photocoagulator. SAM-TR-70-59, Oct 1970.

31. Sanders, V. E., and H. W. Hemstreet, Jr. Wavelength dependence of retinal damage induced by visible laser radiation. In J. S. Connolly, et al. (ed.). Research on the ocular effects of laser radiation. Technology Incorporated, Contract F41609-73-C-0017, USAF School of Aerospace Medicine, Second Annual Report, Feb 1975.

32. Boettner, E. A., and J. R. Wolter. Transmission of the ocular media. Invest Ophthalmol 1:776 (1962).

33. Boettner, E. A. Spectral transmission of the eye. University of Michigan, Contract AF Y1(609)-2996, USAF School of Aerospace Medicine, Final Report, July 1967.

34. Boettner, E. A., and D. Dankovic. Ocular absorption of laser radiation for calculating personnel hazards. University of Michigan, Contract F41609-74-C-0008, USAF School of Aerospace Medicine, Final Report, Oct 1974.

35. Coogan, P. S., W. G. Hughes, and J. A. Mollsen. Histologic and spectrophotometric comparisons of the human and rhesus retina and pigmented ocular fundus. Chicago Presbyterian Hospital, Contract F41609-71-C-0006, USAF School of Aerospace Medicine, Final Report, Jan 1974.

36. Welch, A. J., C. P. Cain, and L. A. Priebe. Investigation of temperature rise in the fundus exposed to laser radiation. University of Texas at Austin, USAF Contract F41609-73-C-0031, Final Report, May 1974.

37. Priebe, L. A., C. P. Cain, and A. J. Welch. Temperature rise required for production of minimal lesions in the *Macaca mulatta* retina. Am J Ophthalmol 79:405 (1975).

38. Welch, A. J., et al. Limits of applicability of thermal injury. The University of Texas at Austin, Contract F41609-76-C-0005, USAF School of Aerospace Medicine, Interim Technical Report, May 1976.

39. Reed, C. Coherent Radiation, Palo Alto, California. Personal communication to J. S. Connolly, 1976.

40. McNee, R. C. Prediction of a single-pulse ED50. Unpublished report, USAF School of Aerospace Medicine (SAM/BRD), May 1975.

41. Mainster, M. A., et al. Retinal temperature increases produced by intense light sources. J Opt Soc Am 60:264 (1970).

42. White, T. J., et al. Chorioretinal thermal behavior. Bull Math Biophys 32:315 (1970).

43. Technology Incorporated. A study of retinal temperature predictions for high altitude weapon detonations. DASA Contract 01-09-C-0121, Quarterly Progress Report, Feb 1970.

44. Mainster, M. A. Destructive light adaptation. Ann Ophthalmol 2:44 (1970).

45. Fahs, J. H. A model for the study of retinal damage due to laser radiation. Technical Report 3678, Picatinny Arsenal, Feb 1968.

46. Hayes, J. R., and M. L. Wolbarsht. Thermal model for retinal damage induced by pulsed lasers. Aerosp Med 39:474 (1968).

47. Sliney, D. H. The development of laser safety criteria--biological considerations. In Laser applications in medicine and biology, Vol. I. M. L. Wolbarsht (ed.). New York:Plenum Press, 1971.

48. Investigation of keratitis in primates. Unpublished report, USAF School of Aerospace Medicine (SAM/EP), June 1976.

49. Robinson, G. W. Rhodopsin cooperativity in visual response. Vision Res 15:35 (1975).

50. Connolly, J. S. Retinal Photochemistry. In J. S. Connolly, et al. (ed.). Research on the ocular effects of laser radiation. Technology Incorporated, Contract F41609-73-C-0017, USAF School of Aerospace Medicine, Twelfth Interim Technical Report, Mar 1976.

51. Nawrocki, A. D., and R. Lemberger. Unpublished results, 1975. (It should be noted that ray-tracing does not consider diffraction.)

52. Abrahamson, E. W., and J. R. Weisenfeld. The chemistry of visual pigments. Ch 3 In H. J. A. Dartnall (ed.). Handbook of sensory physiology. Vol. VII/1, Berlin: Springer-Verlag, 1972. (and references cited therein).

53. Menger, E. L. (ed.). Special issue on the chemistry of vision. Accts Chem Res 8:March (1974).

54. Cone, R. A., and W. H. Cobbs, III. Rhodopsin cycle in the living eye of the rat. Nature 221:820 (1969).

55. Kuwabara, T., and R. A. Gorn. Retinal damage by visible light: an electron microscope study. Arch Ophthalmol 79:69 (1968).

56. Noell, W. K., et al. Retinal damage by light in rats. Invest Ophthalmol 5:450 (1966).

57. Friedman, E., and T. Kuwabara. The retinal pigment epithelium: IV - The damaging effects of radiant energy. Arch Ophthalmol 80:265 (1968).

58. Dowling, J. E., and R. L. Sidman. Inherited retinal dystrophy in the rat. J Cell Biol 14:73 (1962).

59. Fine, S., and W. P. Hansen. Optical second harmonic generation in biological systems. Appl Opt 10:2350 (1971).

60. Visilenko, L. S., V. P. Chabotaev, and Yu. V. Troitskii. Visual observation of infrared laser emission. Sov Phys JETP (English translation) 21: 513 (1975).

61. Birks, J. B. Photophysics of aromatic molecules. pp. 62-83, London: Wiley-Interscience, 1970.

62. Connolly, J. S., D. S. Gorman, and G. R. Seely. Laser flash photolysis of chlorin and porphyrin systems. Ann N Y Acad Sci 206:649 (1973).

63. Rodiguin, N. M., and E. N. Rodiguina. Consecutive chemical reactions, mathematical analysis and development. (English translation), New York: D. van Nostrand and Co., 1964. pp. 6-10.

## BIBLIOGRAPHY

Arden, G. B. The excitation of photoreceptors. Prog Biophys Mol Biol 19(2): 373 (1969).

Bonting, S. J. The mechanism of the visual process. In D. R. Sanadi (ed.). Current topics in bioenergetics 3:351 (1969).

Bridges, C. D. B. Biochemistry of vision. In C. N. Graymore (ed.). Biochemistry of the eye, Ch. 9, London: Academic Press, 1970.

Cone, R. A. Early receptor potential: photoreversible charge displacement of rhodopsin. Science 155:1128 (1967).

Dartnall, H. J. A. (ed.). Handbook of sensory physiology. Berlin: Springer-Verlag, 1972.

Vol. VII/1, Photochemistry of vision. See especially:

Ch. 2, The chemistry of the visual pigments, R. A. Morton.
Ch. 3. The structure spectra and reactivity of visual pigments, E. W. Abrahamson and J. R. Weisenfeld.
Ch. 5. The behavior of visual pigments at low temperatures, T. Yoshizawa.
Ch. 7. Physical changes induced by light in the rod outer segments of vertebrates, G. Falk and P. Fatt.
Ch. 9. Visual pigments in man, W. A. H. Rushton.
Ch. 10. The regeneration and renewal of visual pigments in vertebrates, Charles Baumann.

Vol. VII/2, Physiology of Photoreceptor organs. See especially:
Ch. 5. The structure and reaction of visual pigments, A. Kropf.
Ch. 16. Light and dark adaptation, P. Gouras.

Kuwabara, T. Surface structure of eye tissue. Proc 3d Ann Scanning Electron Microscopy Symposium, IITRI, Chicago (1970).

Mainster, M. A. Retinal transport and regeneration of human cone photopigment. Nature (New Biol) 238:223 (1972).

Mainster, M. A., J. J. White, and C. C. Stevens. Mathematical analysis of rhodopsin kinetics. Vision Res 11:435 (1971).

Moses, R. A. (ed.). Adler's physiology of the eye, 5th ed., Ch. 15, Photochemistry of vision. St. Louis: C. V. Mosby Co., 1970.

Noell, W. K. Cellular physiology of the retina. J Opt Soc Am 53:36 (1963).

Rushton, W. A. H. Vision as a photic process, pp. 123-162. In A. C. Giese (ed.). Photophysiology, Vol. II. New York: Academic Press, 1964.

Wald, G. Molecular basis of visual excitation. Science 162:230 (1968).

Weale, R. A. Photochemistry and vision. pp. 1-45. In A. C. Griese (ed.). Photophysiology, Vol. IV. New York: Academic Press, 1968.

APPENDIX A

# DATA ANALYSIS

Statistical analyses of the data were performed using the method of probits[1]. Preliminary probit calculations were carried out on a Wang 700B programmable calculator as described previously [2], and final analyses were conducted in the Biometrics Division, USAF School of Aerospace Medicine (SAM/BRD). The latter values are reported here.

For the 16 exposure sites in each eye, the powers (or energies) were equally spaced on a logarithmic scale from about half to twice the estimated threshold. The latter was obtained from prior experiments or, if necessary, from preliminary exposures, usually on one to four eyes. A log-normal distribution of dose was assumed because otherwise, on a linear scale the distribution curve of the experimental thresholds would be skewed; i.e., the probability is nil that an individual threshold will be zero, whereas there is a finite probability that a given threshold will be several times higher than the mean. Thus, by transforming the experimental laser powers (or energies) to a logarithmic scale, the probit analysis could be carried out assuming a Gaussian distribution function.

Because of general differences in pigmentation, age, and overall health of the subjects, we assume that the variability from eye to eye is greater than the variability among sites within a given macula. We further assume that the sensitivity levels (i.e., the threshold level for a burn) for all exposure sites in a given eye are randomly distributed across the macula, regardless of the specific location. Accordingly, a probit analysis was carried out for each eye, using a binary lesion/no-lesion determination for each of the 16 exposure sites. The result of each calculation is an ED50 which is defined as the laser power (or energy), incident on the cornea, that has a 50% probability of inducing macular damage at any site selected at random in the macula.

Each ED50 reported here is the geometric mean (i.e., arithmetic mean on a log scale) of the individual values for a given set of exposure parameters. The mean ED50, therefore, represents the 50% probability point for macular damage induced in any eye taken at random from the population. The upper and lower 95% confidence levels (UCL, LCL) are computed as standard 90% confidence limits on the mean (on a log scale) and then converted to dose units. Thus, UCL and LCL represent the 90% confidence interval for the ED50; i.e., the interval that should contain the true ED50 with 90% probability.

Preliminary probit analyses were carried out on all exposure sites, in all eyes exposed to a given set of conditions (pulsewidth, pulse-repetition rate, pulse-train duration). Implicit in this combined-probit approach is the more restrictive assumption that the variability from eye to eye is no greater than the variability among sites within a given macula. There does not appear to be any *a priori* reason that this assumption should be valid. Nevertheless, we

---

1. Finney, D.J. Probit analysis, 2d ed. New York: Cambridge University Press, 1952.

2. Skeen, C.H., et al. Ocular effects of repetitive laser pulses. Technology Incorporated, Contract F41609-71-C-0018, USAF School of Aerospace Medicine, Final Report, June 1972.

found good agreement between the two sets of ED50's as well as their respective 90% Confidence Intervals, especially for large ($\geq$ 10 eyes) sample populations.

The 90% Confidence Intervals reported here on experimentally determined ED50's are in general, within 5% of the respective ED50's. This narrow range of variation indicates only the precision of our data and not the accuracy. The reproducibility of retinal damage thresholds among different laboratories depends on factors such as equipment setup, system calibration, experimental procedures, animal care, and most importantly, the relative abilities of different observers to detect retinal lesions ophthalmoscopically. Thus, it is not unexpected that results of closely similar experiments, performed independently, have shown significant differences.

A more realistic estimate of the variability of retinal thresholds was obtained by fitting[3] 15 experimental ED50's for a wavelength of 514.5 nm with a pulsewidth not less than 10 μsec. The equation empirically fitted was:

$$ED50(mW) = 7.466t^{-.1502} + 1.030(10)^{-3}\ t^{-1}$$

where t is pulsewidth in seconds. The errors were assumed proportional, so that fitting was done taking logarithms of both sides of the equation as a first order approximation. The standard error thus obtained was 0.0945, which related approximately to an error rate of 24%. This estimate of standard error provides a more reasonable basis for computing confidence intervals than using the estimate of standard error from a single experimentally determined ED50. There is no adjustment for sample size when using this more realistic estimate of error.

This standard error is quite close to our estimated error of $\pm$ 20% which is based on additivity of the possible sources of error in our measurements. It includes the biological variability from subject to subject, as expressed by the 90% Confidence Interval, which ranges from about $\pm$ 1% to $\pm$ 7%. Taking the larger of these two as an upper limit, we add $\pm$ 10% for calibration error and about $\pm$ 3% for operational error. The calibration error contains the absolute error ($\pm$ 5%) of the energy measuring device (ballistic thermopile) and can also be considered an upper limit.

In summary, we believe the threshold values reported here to be accurate within a factor of about 25% and possibly within 20% of the stated value. As noted in the text, the agreement of our values with results reported by other investigators is, in general, quite satisfactory. A similar curve was obtained for neodymium based on seven experimental values. These two equations have been used to obtain predicted values at certain points where no experimental data exists. The tabled 90% Confidence Limits for these values are based on the estimates of the standard errors of predicted values from the fitted curves and are only approximate because of the nonlinearity of the equations.

3. McNee, R. C. Prediction of a single-pulse ED50. Unpublished report, USAF School of Aerospace Medicine (SAM/BRD), Jun 1977.

## APPENDIX B

## MODE-LOCKED LASER: THEORY AND CHARACTERISTICS*

### GENERAL

Briefly stated, there are three requirements for producing mode locking:

1. The mode locker must be producing a significant modulation of the cavity losses (e.g., 5%-25% fractional power loss per pass).
2. The frequency of this modulation must be accurately tuned (e.g., within 5 kHz) to the laser's longitudinal mode spacing frequency.
3. Other cavity losses including output coupling losses as well as scattering, etc., should not be so large as to overpower the effect of the mode locker.

The modulator will satisfy the first condition provided that it is in the correct vertical position with respect to the optical beam and that it is being operated at a frequency coincident with an acoustic resonance.

The vertical alignment can be confirmed by observing the beam position through the viewing port of the mode-locker. The mode spacing frequency can be made coincident with an acoustic resonance by changing the laser cavity length using the length adjustment ring on the mode locker mount.

Cavity Length Adjustment -- Using a fast detection system, the amplitude and duration of the mode-locked pulses are monitored while turning the length adjustment ring. Since the frequency of an acoustic resonance is dependent upon the temperature of the modulator, the modulator should be allowed to reach a stable temperature before any adjustments are made. The adjustment ring should be turned in steps of one or two full turns accompanied by MODE LOCKING FREQUENCY and cavity mirror realignment. Adjustments in the correct direction will result in increases in the pulse amplitude, decreases in duration, and a decrease in the noisiness of the pulse. When the tuning is nearly correct, smaller steps of 1/4 to 1/2 turns are used until optimum performance is achieved.

The laser should be fairly clean in order to achieve good mode locking. Residual losses of 2-3% plus output coupling losses will probably fail to satisfy requirement 3 and will cause broad and possibly noisy pulses.

Effect of Laser Tube Current on Mode Locking -- In the argon-ion laser, lower-state lifetime considerations appear to limit the amount of peak power that can be concentrated into a mode-locked pulse. The quality of the pulses shows a strong dependence of laser tube current. Usually very short pulses, whose durations are near the theoretical limit, can be produced only within a tube current range of 11 to 20 amps. Increases in tube current beyond the optimum value will result in the appearance of a trailing pulse about 1 nsec

---

* Taken from "467 Mode Locker Instruction Manual" © 1975, Coherent Radiation. Reprinted here with permission.

after the short pulse. This trailing pulse is broader and at high currents (>30 amps) can be larger in amplitude than the original pulse.

## SYSTEM THEORY

Acousto-Optic Interactions -- When a sound wave passes through a material, the change in density associated with regions of condensation and rarefaction causes a periodic change in the index of refraction. These sound waves can be produced by a piezoelectric transducer, which converts an electrical signal into acoustic energy. A light beam passing through such a pattern or periodic index changes will be partially diffracted. When the angle of incidence of the light beam is optimized, the fraction of the incident light that is diffracted is given by:

$$\frac{P_D}{P_0} = \pi^2 M_2 \cdot \frac{\ell^2}{2\lambda_0^2} \cdot \frac{P_a}{A} \qquad \text{(B-1)}$$

where,

$\frac{P_D}{P_0}$ = fractional power diffracted

$M_2$ = acousto-optic figure of merit

$\ell$ = dimension of transducer parallel to propagation direction of the optical beam

$\lambda_0$ = light wavelength

$\frac{P_a}{A}$ = acoustic power density.

Mode Locking -- When the longitudinal cavity modes of the laser area caused to maintain a fixed phase relationship with one another, the laser is said to be mode-locked. In this condition, the amplitudes of the cavity modes add constructively at a particular point. This has the effect of converting the continuous beam circulating within the laser to a small intense bundle of light which bounces back and forth between the mirrors.

Mode locking may be produced in the laser by modulating the cavity losses at a frequency equal to the frequency difference between adjacent longitudinal modes. These modes are separated by a frequency, $\Delta\nu$, given by

$$\Delta\nu = \frac{c}{2L} \qquad \text{(B-2)}$$

where c = spread of light and L = laser cavity length.

An acousto-optic modulator can be used to produce the required loss modulation. The modulator is constructed so that a good acoustic standing wave is generated transverse to the optical beam. The standing wave will grow and collapse at a rate equal to twice the drive frequency. Thus, the cell is driven by a piezoelectric transducer at a frequency of d/4L. In effect, the modulator acts as a shutter that opens and closes once during a

round trip transit time of the laser. The light within the laser tends to adjust itself so that a bundle of light is at the shutter when the shutter is open and no light exists elsewhere in the cavity.

In order to produce the correct modulation the length (L) of the laser cavity is adjusted so that the c/2L frequency of the laser is matched to one of the standing wave resonances of the acoustic cell. To be more specific, one must consider the modulation effect on the laser light of the standing waves in the acoustic cell as a function of frequency.

The frequency of a particular acoustic resonance is determined by the dimensions of the acoustic cell and the velocity of sound:

$$f = \frac{nv}{2L} \tag{B-3}$$

where

f = center frequency of the acoustic resonance
n = number of acoustic wavelengths in one round trip through the acoustic resonator
v = acoustic velocity
L = dimension of the acoustic resonator parallel to the direction of propagation of the acoustic wave.

Thus, the mode locking modulator exhibits good response only over the relatively narrow bandwidth of each acoustic resonance whose center frequency (f) is given by Equation B-3. The laser, on the other hand, can be mode locked only by a frequency nearly equal to $\Delta\nu/2$ given in Equation B-2. Thus, a condition for optimum mode locking is that

$$f = \Delta\nu/2 \tag{B-4}$$

within approximately one part of $10^4$. Since the acoustic velocity is temperature dependent, the modulator is contained within a temperature stabilizing oven. The match required by Equation B-4 is achieved by using the length adjustment feature of the mode locker mount in order to vary the laser length (L).

An aspect of the argon-ion laser that must be taken into account during mode locking experiments is the short lifetime of the upper state of the lasing transition. Because this lifetime ($\sim$2.5 nsec) is shorter than the round trip transit time of a light pulse within the optical resonator ($\sim$7 nsec), the ratio of the light lost by spontaneous emission to the light contributed to the stored cavity energy by stimulated emission increases when the laser is mode locked. This occurs because the light pulse is in the vicinity of a particular argon-ion for only a fraction of a nanosecond. The rest of the time, which on the average will be about 5 nsec, the ion is free to undergo spontaneous emission. Because of this extra loss due to spontaneous emission and some other losses associated with the lower state lifetime and with the modulator extinction ratio, the average power obtained from a mode locked, argon-ion laser can be reduced to as little as 30% of the free-running power.